NEW TECHNIQUES FOR SENSITIVITY IMPROVEMENT IN FOURIER TRANSFORM N.M.R.

A thesis submitted to the

University of Manchester

for the degree of

DOCTOR OF PHILOSOPHY

in the Faculty of Science

by

KENNETH STUART LEE

Department of Chemistry,
University of Manchester,
Manchester,
M13 9PL

OCTOBER, 1987

ABSTRACT

Techniques are presented for the enhancement of sensitivity in N.M.R. spectroscopy. For the measurement of the homonuclear scalar coupling between ^{13}C nuclei in the rare spin systems $^{13}CH_n$ $^{13}C_{(unprotonated)}$ sensitivity is enhanced by polarization transfer from protons. Optimum sensitivity is obtained by carrying out a unidirectional relay of magnetization to the non-protonated ^{13}C. Unwanted long-range polarization transfer signals are removed by high pass J filtration. A two-dimensional extension of the HCC relay sequence produces an enhanced ^{13}C-^{13}C COSY experiment which can be used as an alternative to the 2D INADEQUATE experiment.

A theoretical treatment of the sensitivity advantage of indirect detection methods in 2D N.M.R. spectroscopy is compared with the experimental measurement of this advantage. Instrumental requirements for the implementation of existing indirect detection experiments are discussed. These experiments suffer from dynamic range problems, particularly where protonated solvents are used; they also require a very high level of spectrometer stability. A general method for attenuating such problems is proposed, relying on the randomization of coherences involving protons while the signal polarization is stored as X nucleus longitudinal magnetization. Extensions of this technique, to obtain heteronuclear relay and long-range correlation spectra are introduced; indirect measurement of T_1's is also discussed.

The author graduated from the Victoria University of Manchester in 1984 with a first class honours degree in Chemistry. From October 1984 to September 1987 he carried out research in the Chemistry Department of this University under the supervision of Dr. G.A. Morris.

DECLARATION

No portion of the work referred to in this thesis has been submitted in support of an application for another degree of this or any other university or other institution of learning.

To

My Parents

ACKNOWLEDGEMENTS

I would like to acknowledge the following people who have assisted in this research.

Dr. G.A. Morris for his supervision, helpful suggestions and for the provision of research facilities and spectrometer time.

Dr. J.M. Bruce for his assistance in the synthesis of isotopically enriched compounds.

The spectroscopy and electronics technicians of the University of Manchester Chemistry Department.

Mrs. A. Roberts for typing the manuscript.

I would also like to thank the SERC for the provision of a research studentship.

The spectrometer used in the experimental work was purchased with the aid of grants from the Science and Engineering Research Council, the University of Manchester, and the University of Manchester Institute of Science and Technology.

CONTENTS

CHAPTER 1

INTRODUCTION

Nuclear magnetic resonance (N.M.R.) spectroscopy is concerned with the study of the interaction of the magnetic moment of atomic nuclei with electromagnetic radiation. The first descriptions of N.M.R. were given in 1946 by Bloch (1) and Purcell (2). As will be shown below, the resonance frequency associated with a nucleus is dependent upon its chemical environment; it is this effect, called the chemical shift, which allows N.M.R. to be used to study the structure of molecules. This information is accessed by measurement of the energy differences between spin states of the nuclei.

The spin angular momentum $\underline{P}$ of a nucleus of angular momentum quantum number I is given by

$$|\underline{P}| = \hbar[I(I+1)]^{\frac{1}{2}} \qquad .....[1.1]$$

Space quantisation requires that the component P_z of $\underline{P}$ along a specified z axis (which in N.M.R. is usually taken to be parallel to the direction of a strong magnetic field Bo) is restricted to the values

$$P_z = \hbar m_I \quad , \quad \text{where } m_I = I,\ I-1,\ I-2,\ \ldots,-1 \qquad ...[1.2]$$

The value of I for a nucleus depends on its atomic number and its mass number. Nuclei of even mass number and even atomic number have I values of zero and so do not show N.M.R. effects. Nuclei of even mass number and odd atomic number have integral values of I; all nuclei of odd mass number have half integral values of I. Nuclei of spin greater than $\frac{1}{2}$ have an electric quadrupole moment; interaction of electric field gradients at the nucleus with the quadrupole moment can lead to a shortening of the lifetime of the

spin states and so result in a broadening of the N.M.R. absorption lines.

The magnetogyric ratio γ of a nuclear species relates its magnetic moment $\underline{\mu}$ to its spin angular momentum $\underline{P}$.

$$\underline{\mu} = \gamma \underline{P}$$

$$|\underline{\mu}| = |\gamma|\hbar[I(I+1)]^{\frac{1}{2}} \qquad .....[1.3]$$

For a nucleus of magnetic moment $\underline{\mu}$ placed in a magnetic field $\underline{Bo}$, the energy of interaction U is,

$$U = -\underline{\mu}.\underline{Bo}$$

$$= -\mu_z Bo$$

$$= -\gamma\hbar m_I Bo \qquad .....[1.4]$$

The nucleus therefore has 2I+1 energy levels; for spin-$\frac{1}{2}$ nuclei such as ^{1}H, ^{13}C, ^{15}N, m_I has two possible values, $m_I = \pm\frac{1}{2}$ and so there are two energy levels. The two spin states of a spin-$\frac{1}{2}$ nucleus are denoted as α and β. The selection rule for magnetic dipole allowed transitions between levels is $\Delta m_I = \pm 1$, so the energy ΔE required to excite a transition is $\gamma\hbar Bo$, the energy difference between successive levels. For this excitation to be achieved in a spectroscopic experiment the Bohr frequency condition must be satisfied $\Delta E = h\nu$.

The condition for resonance is therefore

$$h\nu = |\gamma\hbar| Bo$$

$$\nu = \left|\frac{\gamma}{2\pi}\right| Bo \qquad .....[1.5]$$

The values of ν required to satisfy equation [1.5] are typically in the radio frequency (R.F.) range of the electromagnetic spectrum.

In liquid state N.M.R. the exact resonance frequency associated with a nucleus is mainly dependent on its chemical shift, which is dependent upon the chemical environment of the nucleus. The chemical shift effect arises from the electrons in a molecule shielding nuclei from the external field. Shielding is the result of the formation of a 'current loop' by the circulation of electrons about the direction of the applied field; a secondary field B' is therefore produced, which by Lenz's law opposes the applied field. The magnitude of this secondary field is proportional to the applied field:

$B' = \sigma Bo$ where σ (strictly a tensor rather than a scalar) is the 'shielding constant'.

Replacing Bo in equation [1.5] by the true field at the nucleus gives the equation

$$\nu = \left|\left(\frac{\gamma}{2\pi}\right)\right|(1-\sigma)Bo \qquad .....[1.6]$$

The value of σ for a nucleus is determined by the electron density at that site in the molecule and is therefore dependent on the chemical environment of the nucleus. In order to allow comparison between spectra run at different field strengths, chemical shifts are quoted with respect to a reference standard measured in the same field as the sample. Referencing spectra in this way avoids any problems concerned with the measurement of absolute values of Bo. For proton N.M.R. this standard is tetramethylsilane (T.M.S.) and shifts are quoted on the δ scale

$$\delta = 10^6 (\nu_{TMS} - \nu_{Sample})ppm \qquad .....[1.7]$$

Additional information to aid assignment may be obtained from the form of each of the resonances. Indirect interaction of the observed nuclei with other nuclei can result in the observed resonance being split into a number of components. The interaction of two spin-$\frac{1}{2}$ nuclei in this way results in each of their resonances being split into two components which constitute a doublet. The frequency splitting of these two peaks is dependent on the size of the interaction between the nuclei. This is quoted in terms of the magnitude of the spin-spin coupling constant J (usually just referred to as the coupling constant). Since J is independent of the magnitude of the static magnetic field it is quoted in Hertz. The interactions occur via the bonding electrons of the molecule; the size of the effect falls off rapidly as the number of bonds separating the interacting nuclei increases. For a nucleus coupled to n non-equivalent spin-$\frac{1}{2}$ nuclei the resonance is split into 2^n lines which constitute a multiplet (these may however overlap depending on the values of the coupling constants involved). For a nucleus coupled to n equivalent spin-$\frac{1}{2}$ nuclei a multiplet consisting of n+1 lines is produced, the relative intensities of the components of the multiplet are given by the values in the $(n+1)^{th}$ line of Pascal's triangle. To improve sensitivity the effects of spin-spin couplings may be removed by irradiation of the coupling partners. For example a ^{13}C multiplet may be collapsed to a singlet by application of ^1H irradiation. This process is termed heteronuclear decoupling; irradiation of nuclei of the same species as the detected nucleus is termed homonuclear decoupling.

Detection of the N.M.R. signal

In an N.M.R. experiment the signal arises from the net molar magnetic moment of a sample. The size of this magnetic moment is dependent upon the product of the nuclear magnetic moment and the population difference (polarization), ΔN, between the spin states of the nucleus. The signal is detected by measuring the E.M.F. which is induced in a detection coil surrounding the sample. When irradiated on resonance, the magnetic moment of the sample can give rise to an induced E.M.F. in the coil. In early N.M.R. spectrometers the exact resonance condition of equation [1.6] was achieved by varying either Bo (field sweep), or ν (frequency sweep), the sample being irradiated continuously. Such continuous wave (CW) experiments are time-consuming due to the requirement that the sweep rate be low. The introduction of pulse Fourier transform (F.T.) techniques to N.M.R. (3), (see section 2.2) greatly decreased the time required to obtain a spectrum and so increased the obtainable sensitivity per unit time.

In a pulse F.T. N.M.R. experiment a short radio frequency pulse is applied to the sample, at a frequency in the centre of the expected spectral width; this has the effect of exciting all of the resonances in the sample simultaneously. The signal detected as a function of time at the end of the pulse is termed the free induction decay (F.I.D.); it contains the frequencies of all of the excited resonances, the amplitude of each frequency component decaying as the sample relaxes back to equilibrium. The time evolution of the signal is therefore dependent on the chemical shifts, couplings and relaxation time constants involved. A spectrum is obtained by Fourier transformation

of the F.I.D.; since all of the resonances are detected simultaneously a pulse F.T. experiment can be carried out much more rapidly than a continuous wave experiment, and the obtainable sensitivity per unit time is therefore greatly increased.

The use of pulsed techniques also makes available a wide range of experiments in which use is made of the non-linear effects observed when more than one pulse is applied to the nuclei in a sample (4). Experiments of this type can provide information which could not be obtained directly in a continuous wave experiment. This thesis is concerned with the development of pulse sequences for the enhancement of sensitivity in N.M.R.

Sensitivity

It will be shown in section 2.4 that the value of γ has a large effect on the signal-to-noise ratio of the N.M.R. spectrum. It not only determines the value of $\underline{\mu}$ and the size of ΔN but also influences the magnitude of the E.M.F. induced in the detection coil, due to the Lenz's law dependence on the detection frequency. For nuclei such as ^{15}N, ^{199}Hg, and ^{113}Cd, which have low values of $|\gamma|$, the N.M.R. sensitivity is therefore poor. This situation may be improved either by increasing the magnitude of the initial polarization or by detecting the nuclear magnetism indirectly via a more sensitive nucleus.

Initial polarization may be increased by making use of the relaxation properties of the nucleus. For a two spin heteronuclear system AX saturation of X spin transitions results in an increase in S_A, the steady state polarization across A spin transitions. The enhancement factor, the nuclear Overhauser enhancement (N.O.E.) is

$$\frac{S_A'}{S_A^\circ} = 1 + \eta \qquad \text{.....[1.8]}$$

where $\eta = (\gamma_X/2\gamma_A) \times (T_1/T_{1dd})$

T_1 is the spin lattice relaxation time of the A nucleus, T_{1dd} is the corresponding value if dipolar interactions were to provide the only relaxation mechanism. The same result holds true for larger spin systems.

The maximum value η may take is therefore $(\gamma_X/2\gamma_A)$, about 3 in the case of ^{13}C detection with proton saturation. This maximum enhancement of sensitivity is obtained when dipolar interactions dominate the relaxation mechanism. In using N.O.E. for nuclei of negative γ such as ^{15}N, care must be taken that the condition $(T_{1dd}/T_1 \sim \gamma_X/2\gamma_A)$ is avoided since this would result in a serious reduction in the intensity of the signal, and in the worst case signal nulling may occur. The range of possible values of η for ^{15}N is 0 to -4.93; under favourable conditions the N.M.R. signal can be enhanced by a factor of ~-4, so that an inverted signal with enhanced sensitivity is produced. Under unfavourable conditions ($0>\eta>-2$) a reduction in the signal intensity is observed. This possibility of the signal intensity being reduced due to negative N.O.E. effects imposes restrictions on the N.M.R. experiment; in proton decoupled ^{15}N detection the duration of proton irradiation may need adjustment to avoid these effects.

An alternative method for the enhancement of the initial polarization is to carry out an experiment in which polarization transfer is achieved by R.F. pulses (5,6,7). The mechanism of this type of

polarization transfer experiment is discussed in section 2.5. The important feature of these experiments is that for a system AX_n, polarization across X spin transitions can be transferred to A spin transitions. This transfer is brought about by applying a series of pulses to both nuclear species; the pulse sequence achieves the polarization transfer by making use of the scalar coupling between the A and X nuclei. The maximum enhancement obtainable by this method is γ_X/γ_A and, being independent of the relaxation mechanism, is not prone to signal nulling as is the N.O.E. method. The enhancement obtained by this type of polarization transfer experiment is independent of the chemical shifts of the nuclei involved.

Polarization transfer may be used to enhance the sensitivity with which a nucleus can be detected in a simple N.M.R. experiment, or it can be used as an initial step to improve sensitivity of more complex experiments (8,9). An example of the use of the polarization transfer sequence INEPT as the initial step of a more complex N.M.R. experiment will be given in Chapter 3. In this experiment additional modification of the original pulse sequence is required in order to make best use of the enhanced signal.

In order to improve sensitivity further over that obtainable using a single polarization transfer step it is necessary to detect the nuclear magnetism via a more sensitive nucleus. For the AX_n spin system discussed above optimum sensitivity should be obtained if both the initial polarization and the final detection were to involve X spin transitions. The sensitivity of the resulting spectrum would then be determined by X spin parameters alone; however the experiment must be able to give A spin spectra, so that a method of obtaining

A spin spectra indirectly from X spin spectra is required. This may be achieved using a two-dimensional experiment.

Two-dimensional N.M.R.

Two-dimensional N.M.R. spectroscopy was first suggested by Jeener (10) in 1971; pulse sequences for this type of experiment contain two time variables, the time t_2 during which the F.I.D. is sampled, and a parameter time t_1. The signal modulation during t_1 is sampled by recording a series of F.I.D's for successively incremented values of t_1; Fourier transformation of the resulting data set with respect to both t_1 and t_2 results in a spectrum which is a function of the two corresponding frequency variables f_1 and f_2. A wide range of two-dimensional experiments now exists (11), the information available from each experiment being dependent on the form of the modulation experienced during t_1. A more detailed description of two-dimensional N.M.R. experiments will be given in Chapter 2.

Indirect detection experiments

By arranging that the detected X spin signals experience a modulation during t_1 which is dependent on the chemical shifts of A spins with which they share a scalar coupling, a spectrum correlating the two sets of chemical shifts can be obtained. This experiment has the desired property of indirectly measuring A spin chemical shifts by the detection of X spin signals.

There are two general approaches by which the desired form of two-dimensional spectrum may be obtained. In one approach (12) two successive polarization transfer steps are used; the initial step

transfers polarization from the more sensitive nucleus X to the A nucleus, and after the delay t_1 a second polarization transfer step regenerates X spin magnetization. The intensity of the detected X spin magnetization is modulated in t_1 by the A spin chemical shifts.

In the second approach (13) use is made of the properties of multiple quantum coherence (M.Q.C.); M.Q.C. will be discussed in Chapter 2 and so only a brief description of its properties will be given here. M.Q.C. corresponds to a transition in which two or more nuclei participate; thus a two spin system AX can give rise to double quantum coherence (D.Q.C.) or zero quantum coherence (Z.Q.C.). Although M.Q.C. cannot be detected directly in an N.M.R. experiment, its effects can be observed in a two-dimensional experiment if M.Q.C. is generated at the start of t_1 and reconverted into observable magnetization of one of the participating nuclei at the end of t_1 (14). The signal is modulated during t_1 by a linear combination of the chemical shifts of the nuclei involved; Z.Q.C. is modulated by the difference between the chemical shifts, D.Q.C. by the sum of the chemical shifts. The signal is not modulated in t_1 by scalar coupling between the nuclei involved in the transition which gives rise to the coherence, but will be modulated by couplings to 'passive' nuclei. The two approaches to indirect detection therefore give rise to different forms of spectra. The sequence based on polarization transfer correlates chemical shifts of X nuclei in f_2 with the chemical shifts of A nuclei in f_1; the multiple quantum sequence correlates the X nuclei chemical shifts in f_2 with a linear combination of A and X chemical shifts in f_1.

Both indirect detection methods have been used to enhance the sensitivity of nuclei of low $|\gamma|$ by making use of proton detection. Methods based on polarization transfer have been used to record spectra of ^{15}N (12,15) and ^{199}Hg (16,17); however at present multiple quantum techniques have received more attention, and have been used for ^{13}C (13,18,19,20), ^{57}Fe (21) and ^{113}Cd (22,23,24,25) in addition to ^{15}N (18,26,27,28,29,30).

The factor by which the signal-to-noise ratio may be improved using indirect detection is often quoted in terms of the ratio of the magnetogyric ratios of the nuclei involved; this leads to the enhancement factor $(\gamma_X/\gamma_A)^3$ for an X detected indirect spectrum of nucleus A over an unenhanced direct detection experiment (21,22). Unfortunately this expression takes no account of the other physical constraints involved (31) and leads to misleading claims concerning the sensitivity advantage of this type of experiment. The factors affecting sensitivity in N.M.R. experiments will be discussed in section 2.4; an experimental evaluation of the sensitivity enhancement available using indirect detection will be presented in Chapter 5.

When applied to nuclei of low natural abundance, indirect detection methods present problems due to the need to suppress signals from protons in the abundant isotope spin systems. For example, observation of ^{15}N by indirect methods requires that signals from protons in ^{14}N spin systems are suppressed by a factor of ~6000. This situation is made considerably worse if the spectra are run in protonated solvents; the high concentration of solvent protons present in the sample can also result in dynamic range problems. This will be discussed in Chapter 4, along with other instrumental aspects of this type of

experiment. Various modifications of the basic M.Q.C. technique have been suggested (18,32,33,34,35) in order to aid suppression and to decrease the dynamic range of the detected signal; however at present the literature does not contain any method which can achieve a high level of suppression across a wide range of frequencies.

This thesis is concerned with the development of pulse sequences which enhance sensitivity in N.M.R. Chapter 2 contains theoretical treatments of N.M.R. phenomena, along with a discussion of the factors which affect sensitivity in N.M.R. experiments. In Chapter 3 modifications of the carbon-relayed hydrogen-carbon pulse sequence of Kessler et al. (36) will be presented. These experiments illustrate the fact that the addition of a polarization transfer step to a pulse sequence may require changes to the way in which the sequence is applied if best use is to be made of the sensitivity gained. Chapter 4 outlines the demands made of a spectrometer if indirect detection experiments are to be carried out. The details of a new pulse sequence for indirect detection, which overcomes some of the suppression and dynamic range problems associated with indirect detection, are given in Chapter 5.

CHAPTER 2

THEORY

2.1 (A) Classical Treatment (1)

Bloch used classical arguments to predict the motion of a net magnetic moment for an ensemble of N spins, each of magnetic moment $\underline{\mu}$. The validity of this treatment rests on the equivalence between the classical equations of motion and the time dependence of the expectation value of the magnetization. In the absence of any applied magnetic field the incomplete cancellation of the moments $\underline{\mu}$ leads to an immeasurably small resultant moment of magnitude $N^{\frac{1}{2}}\underline{\mu}$; the application of a magnetic field of magnitude Bo causes an increase in the difference (Δn_o) between the populations ($n\alpha, n\beta$) of the levels α and β of a spin-$\frac{1}{2}$. For a nucleus of positive γ the α state is lower in energy than the β state; for a nucleus of negative γ the opposite is the case.

From Boltzmann statistics, using the high temperature approximation $\Delta E << KT$, Δn_o can be expressed as

$$\Delta n_o = n\alpha - n\beta = \frac{\hbar\gamma B_o n\alpha}{KT} = \frac{\hbar\gamma B_o N}{2KT} \qquad .....[2.1]$$

The net magnetic moment $\underline{M}$ of the ensemble is the resultant of the individual magnetic moments $\underline{\mu}_\alpha$ and $\underline{\mu}_\beta$ associated with the spins in each of the spin states. At equilibrium $\underline{M}$ lies along the field direction (usually taken to define the z axis of a Cartezian system) and has a magnitude:

$$|\underline{M}| = n\alpha\mu_{z\alpha} + n\beta\mu_{z\beta} = \Delta n_o \mu_{z\alpha} = \tfrac{1}{2}\gamma\hbar\Delta n_o \qquad .....[2.2]$$

Since $\mu_{z\beta} = -\mu_{z\alpha}$

Substitution for Δn_o leads to the expression for $\underline{M}$ in terms of the magnetogyric ratio γ and the total number of nuclei N,

$$\underline{M} = \tfrac{1}{4} N(\gamma\hbar)^2 \, |\underline{Bo}|/KT \qquad .....[2.3]$$

This is equivalent to the Curie Law for a sample containing spin-$\frac{1}{2}$ nuclei ($I = \frac{1}{2}$):

$$|\underline{M}| = N(\gamma\hbar)^2 \, I(I+1) \, |\underline{Bo}|/3 \, KT = \chi_o |\underline{Bo}| \qquad .....[2.4] \; (37)$$

where χ_o is the static bulk nuclear susceptibility.

If $\underline{M}$ and $\underline{Bo}$ are not colinear $\underline{M}$ is subject to a torque proportional to $\underline{M} \times \underline{Bo}$, so that the equation of motion of $\underline{M}$ is,

$$\frac{d\underline{M}}{dt} = \gamma[\underline{M} \times \underline{Bo}] \qquad .....[2.5]$$

Since $|\underline{M}|$ is proportional to γ^2 and $d\underline{M}/dt$ is dependent upon γ and $|\underline{M}|$, the rate of change of magnetic flux due to the motion of $\underline{M}$ is proportional to γ^3:

$$\frac{d\underline{M}}{dt} \propto \gamma^3 \qquad .....[2.6]$$

Since the signal-to-noise ratio of an N.M.R. experiment is dependent on the rate of change of magnetic flux it can be seen that γ will have an effect on sensitivity. This will be discussed more fully in section 2.4.

Consider the motion of $\underline{M}$ in a static magnetic field $Bo\hat{\underline{z}}$, subjected to a radio frequency field of amplitude B_1 rotating about the z direction with an angular frequency ω close to the Larmor frequency $\omega_o = -\gamma Bo$.

The motion of $\underline{M}$ will, in addition to precession, have a time dependence due to relaxation, the effect of which can be described by two time constants T_1 and T_2. T_1 is the spin-lattice relaxation time, a measure of the rate of transfer of energy between the nuclear spin system and its surroundings. T_2 is the spin-spin relaxation time; it accounts for the loss of phase coherence due to interactions between the nuclei of the system. Unlike T_1 processes, spin-spin relaxation does not involve a change of the total energy of the spin system. Combining the torque equation with the effects of relaxation leads to the Bloch equations in the laboratory frame of reference:

$$\frac{dM_z}{dt} = -\gamma[B_1 M_y \cos\omega t + B_1 M_x \sin\omega t] - (M_z - Mo)/T_1$$

$$\frac{dM_y}{dt} = -\gamma[BoM_x - B_1 M_z \cos\omega t] - M_y/T_2 \qquad .....[2.7]$$

$$\frac{dM_x}{dt} = \gamma[B_1 M_z \sin\omega t + BoM_y] - M_x/T_2$$

Where Mo is the z component of $\underline{M}$ at equilibrium.

Experimentally the signal is detected by means of the E.M.F.'s induced in the receiver coil in phase and in quadrature with B_1; these are proportional to M_x and M_y. Here x and y refer to a frame of reference rotating in synchrony with the applied radio frequency field, so that B_1 is stationary and along the x axis; from now on x and y will be with reference to this frame. During the application of a radio frequency pulse B_1 is the dominant component of the total effective field $\underline{B}_{eff}$. A 'hard' pulse is defined as one for which

γB_1 is much larger than the range of Larmor frequencies for the spin system; for such a pulse the difference in the Larmor frequencies can be ignored and all nuclei can be assumed to experience a field $\underline{B_1}$. Relaxation can also be ignored during the pulse as the duration of the pulse is short compared with T_1 and T_2. A pulse of length τ_p applied along the x axis rotates $\underline{M}$ by α radians about this axis, where $\alpha = \gamma B_1 \tau_p$. The value of τ_p may be used to adjust the value of α to, for example, a "90°" or a '180°' pulse (see Figure 2.1).

FIGURE 2.1

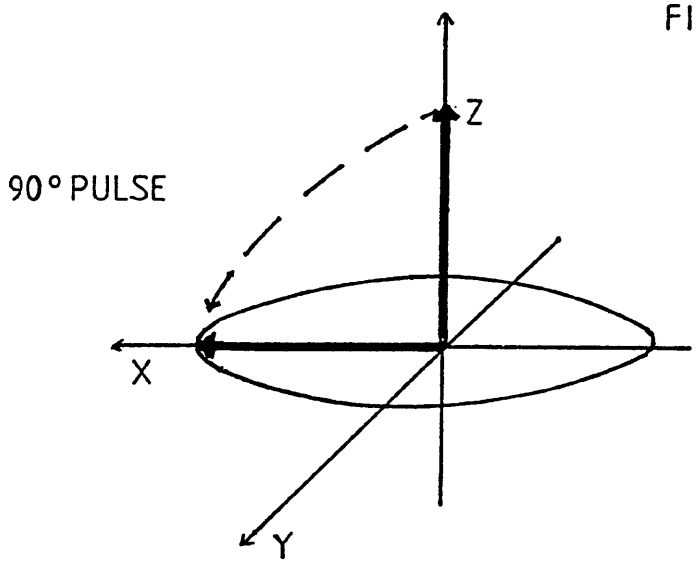

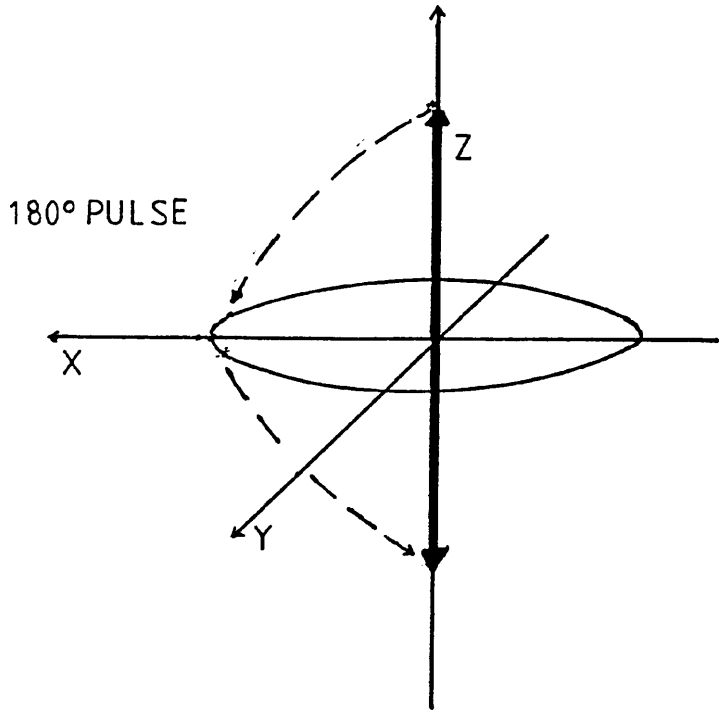

After the application of a pulse the component of $\underline{M}$ in the xy plane will precess about $B_{o\underline{z}}$; as transverse relaxation occurs the transverse magnetization will decrease in magnitude. Such pulses and periods of free precession are used to form the sequences used in pulse Fourier transform experiments.

The Bloch treatment neglects coherent interactions between spins and hence is only strictly applicable to ensembles of identical nuclei. When coherent interactions need to be considered it is necessary to pay attention to the quantized angular momentum of the nuclear spin and a full quantum mechanical description may become necessary. Such a description is that of density matrices, which suffices to describe all observables but avoids the necessity of specifying the state of every spin.

2.1 (B) Density Matrix Theory

If the wavefunction ψ of a state of a spin system is formed by a linear combination of eigenvectors ϕ_i of a complete basis set:

$$\psi = \sum_i C_i \phi_i \qquad \text{.....[2.8]}$$

Then the expectation value of an observable A is given by:

$$\langle A \rangle = \sum_{ij} C_i^* C_j \int \phi_i^* \hat{A} \phi_j \, d\tau \qquad \text{.....[2.9]}$$

$$= \sum_{ij} \sigma_{ij} A_{ij}$$

where σ is the matrix $\sigma_{ij} = C_i C_j^*$ and A is the matrix representation of the operator $\hat{A}$ ($A_{ij} = \int \phi_i^* \hat{A} \phi_j \, d\tau$).

Applying the requirement that A be Hermitian,

$$\langle A \rangle = \sum_i \sum_j \sigma_{ij} A_{ji} = \mathrm{Tr}(\sigma A) \qquad .....[2.10]$$

(Tr being the trace operation, $\mathrm{Tr}(AB) = \sum_j (AB)_{jj}$)

As an N.M.R. measurement yields an ensemble average it is sufficient for the matrix σ to contain the average values of $C_i C_j^*$; the matrix σ of values $\overline{C_i C_j^*}$ is known as the density matrix.

The basis in which the density matrix is most conveniently used is that in which the matrix representation of the time independent terms in the Hamiltonian ($\hat{H}$) for the system is diagonal (the use of a basis in which $\hat{H}$ is not diagonal would result in a mixing of the basis functions as a function of time). The usual starting point in constructing a basis set of states for a system containing a large number of identical sub-systems is the product basis set for the sub-system. For a sub-system of n spin-$\frac{1}{2}$ nuclei the product basis set consists of 2^n different combinations of α and β states, for example, for a two spin system the basis set is $\alpha\alpha$, $\alpha\beta$, $\beta\alpha$, $\beta\beta$. As will be seen later, when the scalar interactions between spins are small compared to the differences between the Larmor frequencies the product basis is an eigenbasis. The states corresponding to a given-off diagonal element of the density matrix may differ in phase but not in energy; thus according to the principle of equal <u>a priori</u> probabilities all phases are equally probable. Thus the ensemble average at equilibrium of the off diagonal elements must be zero. The diagonal elements, σ_{KK}, of the matrix represent the equilibrium populations of the states ϕ_K, where K = 1,2...n. Normalization requires that such elements sum to one; the magnitude of each element can be found from Boltzmann statistics.

$$\sigma_{KK} = \frac{\exp(-E_K/kT)}{Q} \qquad .....[2.11]$$

where $Q = \sum_{K=1}^{m} \exp(-E_K/kT)$, the partition function

Evolution of the Density Matrix

The time dependence of the density matrix is described by the Liouville-von Neumann equation,

$$\dot{\sigma}(t) = -i[\hat{H}(t), \sigma(t)] \qquad .....[2.12]$$

For a system evolving under a time-independent Hamiltonian, $\hat{H}$, the solution of equation [2.12] is,

$$\sigma(t) = \exp(-i\hat{H}t/\hbar)\sigma(0)\exp(i\hat{H}t/\hbar) \qquad .....[2.13]$$

For nuclear spins in an isotropic fluid in a static field $Bo\hat{z}$, the Hamiltonian $\hat{H}$ expressed in units of angular frequency (in the absence of relaxation) contains only terms in Ω and J,

$$\hat{H} = -\sum_j \Omega_j \hat{I}_{jz} + \sum_{j<k} 2\pi J_{jk} \underline{\hat{I}}_j \cdot \underline{\hat{I}}_k \qquad .....[2.14]$$

$$\Omega_j = \gamma Bo(1-\sigma_j)$$

σ_j = Shielding constant

All energy terms are in angular frequency units; $\underline{\hat{I}}$ and $\hat{I}_z$ are the operators for angular momentum and the z component of angular momentum respectively.

For a system consisting of two spin-$\frac{1}{2}$ nuclei A and B,

$$\hat{H} = -\Omega_A \hat{I}_{Az} \cdot -\Omega_B \hat{I}_{Bz} + 2\pi J \underline{\hat{I}}_A \cdot \underline{\hat{I}}_B \qquad \text{.....[2.15]}$$

$$= -\Omega_A \hat{I}_{Az} \cdot -\Omega_B \hat{I}_{Bz} + 2\pi J \hat{I}_{Az} \cdot \hat{I}_{Bz} + \pi J(\hat{I}_A^+ \cdot \hat{I}_B^- + \hat{I}_A^- \cdot \hat{I}_B^+)$$

where $\hat{I}^+$ and $\hat{I}^-$ are the raising and lowering operators respectively (see Appendix A).

Because of the action of the product terms $\hat{I}^+\hat{I}^-$ and $\hat{I}^-\hat{I}^+$ they are referred to as 'flip-flop' terms; they give non-zero matrix elements of $\hat{H}$ for the situation where the two basis functions involved have the same total z component of angular momentum M_I but have two spins which differ in their individual z angular momentum components. As the I_z operator also leaves M_I unchanged it can be seen that for any number of nuclei the matrix representation of the Hamiltonian will factorize into submatrices for each value of M_I.

To deduce the frequencies and intensities of the resonances for a given spin system, this block diagonal matrix H must first be diagonalized. The frequencies of the transitions are then the differences between the eigenvalues of $\hat{H}$ (recalling that $\hat{H}$ is in angular frequency rather than energy units), while the intensities are proportional to the square modulus of the corresponding matrix elements of the raising operator, $|I_{ij}^+|^2$. For systems of more than two spins, these calculations are normally performed numerically. Off-diagonal elements of $\hat{H}$ depend on the scalar couplings, J, while the differences between diagonal elements depend on the differences between chemical shifts. When $|J| << |\Omega_X - \Omega_A|$, the off-diagonal elements are negligible and the product basis is an eigenbasis; this condition is known as weak coupling. When weak coupling applies a useful simplification can be used, the so-called 'X approximation'.

In the X approximation the contribution to the expansion of $J\hat{I}_A\hat{I}_X$ from the flip-flop terms can be ignored. For a two spin system the Hamiltonian becomes,

$$\hat{H}_{AX} = -\Omega_A\hat{I}_{Az} - \Omega_B\hat{I}_{Bz} + J\hat{I}_{Az}\hat{I}_{Bz} \qquad .....[2.16]$$

Similar approximations can be made for a system containing any number of spins. The full expansion of the coupling term is included for non-X-approximated nuclei but only terms in $J\hat{I}_{iz}\hat{I}_{jz}$ for couplings between heteronuclei (or other nuclei of large $\Delta\Omega$). The approximated Hamiltonian commutes with the operators for M_I for each group of nuclei involved, thus each stationary state of the system has definite values of M_I for each group and so all transitions of the system can be associated with one group only. Thus the non-X region of the spectrum consists of sub-spectra in each of which the effective chemical shift of a nucleus i is $\Omega_i \pm \frac{1}{2} J_{iX}$.

Having diagonalized $\hat{H}$ and calculated the energy levels Ω_i for the spin system under study, the angular frequencies of the density matrix elements can be found. The time dependence of σ under the time independent Hamiltonian $\hat{H}$ is given by equation [2.13]. As the matrix representation of $\hat{H}$ is diagonal, the matrix representation of $e^{i\hat{H}t/\hbar}$ is also diagonal and contains the diagonal elements $e^{i\Omega_p t}$. Equation [2.13] may now be simplified as shown below,

$$\sigma_{pq}(t) = \exp(-i\hat{H}t/\hbar)\sigma_{pq}(0)\exp(i\hat{H}t/\hbar)$$

$$= \sigma_{pq}(0)\exp(i\Omega_{pq}t) \qquad .....[2.17]$$

where $\Omega_{pq} = \Omega_p - \Omega_q$

Radio Frequency Pulses

To calculate the effects of radio frequency irradiation on σ it is helpful first to transform $\hat{H}$ into a frame of reference rotating at an angular frequency ω in synchrony with the irradiating field, just as was done in the classical description. This reduces all of the Larmor frequencies Ω_i by an amount ω. The irradiation then adds a term $\hat{F}_\phi$ to $\hat{H}$,

$$\hat{F}_\phi = \sum_n \gamma B_1 I^n{}_\phi \qquad .....[2.18]$$

For a 'hard' pulse ($\gamma B_1 >> \Delta\Omega_i$, J_{ij}) $\hat{F}_\phi$ dominates $\hat{H}$: the effect of a pulse of duration τ about an axis ϕ is to generate a rotation of $\alpha = \gamma B_1 \tau$ radians about ϕ.

$$\sigma_\tau = e^{(-i\alpha I_\phi)} \sigma_o e^{(i\alpha I_\phi)} \qquad .....[2.19]$$

If the pulse is not hard, then the other terms in $\hat{H}$ become important and the effect of the pulse must be calculated explicitly. This is most simply done by diagonalizing the full $\hat{H}$ (which includes $\hat{F}_\phi$), transforming into the new basis to give σ' and then transforming σ' by $e^{i\hat{H}t}$. Transformation back to the radio frequency field free eigenbasis is then carried out.

2.1 (C) Product Operator Formalism (38)

Full density matrix analyses of pulse sequences are very cumbersome, but under weak coupling conditions great simplification may be obtained by expanding the density matrix in terms of the matrix representation of angular momentum operators for individual spins. Products of the angular momentum matrices form the un-normalized basis operators Bs.

$$\sigma(t) = \sum_s b_s(t) Bs \qquad \text{.....[2.20]}$$

$$Bs = 2^{(q-1)} \prod_{K=1}^{N} (I_{kx}, I_{ky}, I_{kz})^{a_s K} \qquad \text{.....[2.21]}$$

where N = number of nuclei in the spin system,

q = number of single spin operators in the product.

An outline of the nomenclature used for the spin operator products is shown below, an idea of the physical significance of these operators can be gained from Figure 2.2.

I_{kz} (or K_z)	Longitudinal (z) magnetization of spin K
I_{kx} (or K_x)	In phase x-magnetization of spin K
$2I_{kx}I_{lz}$ (or $2K_xL_z$)	x-magnetization of spin K antiphase with respect to spin L
$2I_{k\phi}I_{l\phi'}$ (or $K_\phi L_{\phi'}$) ϕ = x,y ϕ' = x,y	Two spin coherence of spins K and L
$2I_{kz}I_{lz}$ (or $2K_zL_z$)	Longitudinal two-spin order of spins K and L (the z-ordered state)

The processes taking place during any pulse sequence element are followed by examining the evolution of the product operators under the appropriate Hamiltonian. This evolution can be determined explicitly by differentiating equation [2.12].

FIGURE 2.2

Schematic spectra obtained from Fourier transformation of F.I.D.s induced by typical product operators

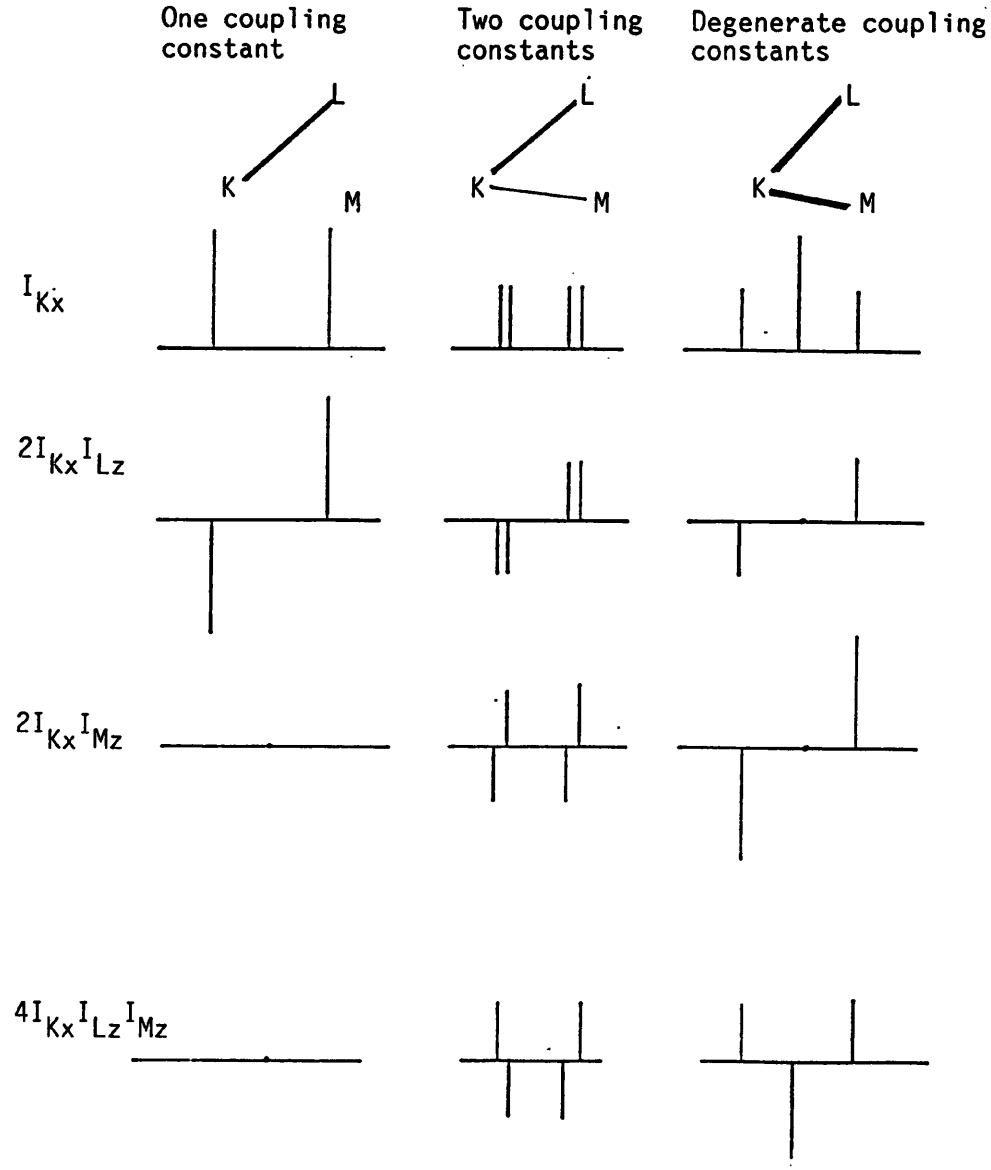

Single transition operators are produced by linear combination of the product operators; the schematic spectra for these single transition operators are formed by addition of the intensities in the above spectra.

$$\sigma(o) \xrightarrow{\hat{H}} \sigma(t)$$

$$\sigma(t) = \sigma(o)\cos\phi + [\sigma(o),\hat{H}]\sin\phi \qquad .....[2.22]$$

where $\phi = \beta$, the rotation angle of a pulse

$\phi = 2\pi\Omega\tau$ for precession due to chemical shift Ω

$\phi = \pi J\tau$ for precession due to spin-spin coupling

A summary of the effects of evolution is given in Table 2.1.

Table 2.1

Process	
Precession due to chemical shift Ω	$I_{kx} \xrightarrow{\Omega\tau I_{kz}} I_{kx}\cos(\Omega\tau) + I_{ky}\sin(\Omega\tau)$
	$I_{ky} \xrightarrow{\Omega\tau I_{kz}} I_{ky}\cos(\Omega\tau) - I_{kx}\sin(\Omega\tau)$
	$I_{kz} \longrightarrow I_{kz}$
	For terms such as $2I_{kx}I_{lx}$ the evolution is the product of the individual evolutions
Spin-spin coupling	$I_{kx} \xrightarrow{\pi J_{kl}\tau 2I_{kz}I_{lz}} I_{kx}\cos(\pi J_{kl}\tau) + 2I_{ky}I_{lz}\sin(\pi J_{kl}\tau)$
	$I_{ky} \xrightarrow{\pi J_{kl}\tau 2I_{kz}I_{lz}} I_{ky}\cos(\pi J_{kl}\tau) - 2I_{kx}I_{lz}\sin(\pi J_{kl}\tau)$
Radio frequency pulses	$I_{k\phi'} \xrightarrow{\beta I_{k\phi}} I_{k\phi'}\cos\beta + I_{k(\phi-1)}\sin\beta$
	ϕ' = axis along which the magnetization is originally orientated.
	ϕ = axis about which the pulse is applied.

In the convention of reference (4), $(\phi', \phi) = 0, 1, 2, 3$

phase = x, y, -x, -y

2.2 Principles of Pulse Fourier Transform N.M.R.

Immediately after a radio frequency pulse is applied, about the x axis of a rotating frame, to an ensemble of spins, the transverse component $\underline{M_{xy}}$ of the magnetization vector $\underline{M}$ is aligned along the -y axis. The magnitude of this component will decrease exponentially due to transverse relaxation and the vector $\underline{M_{xy}}$ will precess in the xy plane. For an ensemble containing groups of nuclei with different chemical shifts the different components of $\underline{M_{xy}}$ will precess at different rates according to their offset from the transmitter frequency. The amplitude of the y component of the transverse magnetization M_y as a function of time will be a decreasing exponential modulated by the precession rates of the components of the magnetization vector; this signal is referred to as a free induction decay (F.I.D.). For example, after a $90°_x$ pulse M_y is initially $M_y(+0) = M_0$ (the magnitude of $\underline{M}$); if the precession rate of a component M_i of $\underline{M_{xy}}$ is $\Delta\omega_i$ radians per second then the F.I.D., $M_y(t)$, is described by,

$$M_y(t) = -\sum_i M_i \cos(\Delta\omega_i t) e^{-t/T_2} \qquad \text{.....[2.23]}$$

where, $-\sum_i M_i = M_y(+0)$

The F.I.D. (a time domain function, s(t)) is related to the spectrum (a frequency domain function s'(ω)) by Fourier transformation (3).

$$s'(\omega) = FT(s(t)) = \int_{-\infty}^{\infty} s(t) e^{-i\omega t} dt \qquad \text{.....[2.24]}$$

Making use of the convolution theorem, which states that the Fourier transform of a product of two functions h(t) and f(t) is equal to the convolution of their individual Fourier transforms,

$$FT(h(t).f(t)) = FT(h(t)) \otimes FT(f(t))$$

$$= H(\omega) \otimes F(\omega) \qquad .....[2.25]$$

where $$H(\omega) \otimes F(\omega) = \int_{-\infty}^{\infty} H(\omega).F(\omega-\omega')d\omega' \qquad .....[2.26]$$

it can be seen that the spectrum ($FT(M_y(t))$) is described by,

$$(FT(M_y(t))) = \sum_i (FT(M_i \cos\Delta\omega_i t)) \otimes FT\ e^{-t/T_2(i)} \qquad .....[2.27]$$

Transformation of the exponential term gives rise to a Lorentzian curve; transformation of the cosine terms gives rise to a set of δ functions positioned at frequencies $\Delta\omega_i$. The effect of the convolution is to replace each of the δ functions by a Lorentzian curve thus producing the frequency domain spectrum. In this way the spectrum may be obtained by carrying out a Fourier transformation on the required F.I.D. Sensitivity may be improved by repeating the pulse (after a suitable relexation delay) and co-adding the F.I.D. to those previously acquired; after n such acquisitions (thousands if necessary) the resulting F.I.D. is Fourier transformed, giving a sensitivity improvement of $\sqrt{n}$

The application of more than one pulse to an ensemble of spins may be used in order to gain specific information about the spin system. The initial pulses will create a non-equilibrium state; this is then probed by the later pulses. For most pulse sequences the interval between the pulses is small compared to the relaxation times for the system so that the non-equilibrium state may be investigated before relaxation effects become significant. In order to study relaxation processes the interval between the pulses are of the order of T_1 or T_2; an example of this is the inversion recovery sequence for measuring T_1 values (39).

2.3 Two-Dimensional Spectroscopy

It has already been mentioned that pulse Fourier transform N.M.R. may be used to gain information about non-equilibrium states of spin systems; an extension of this technique is two-dimensional spectroscopy. If a delay t_1 is introduced between the formation of a non-equilibrium state and its observation then the F.I.D. is a function of t_1 as well as of the acquisition time t_2. By repeating the pulse sequence for a number of values of t_1 a signal matrix $s(t_1,t_2)$ may be built up. Fourier transformation of each of the F.I.D.s with respect to t_2 produces a data matrix $s(t_1,F_2)$; this may be Fourier transformed with respect to t_1 in order to produce a two-dimensional spectrum. The spectrum is a three-dimensional surface, the height of the surface above the plane described by the two frequency axes being proportional to signal intensity. The position of a peak in the spectrum is determined by the frequencies at which coherence precesses in the two intervals t_1 and t_2.

An experiment to produce a two-dimensional spectrum consists of four sections: preparation, evolution, mixing and detection.

Preparation Period

This consists of a delay to allow the system to relax back to equilibrium (or to a steady state situation) followed by one or more pulses leading to the formation of a non-equilibrium state.

Evolution Period

This is a period of duration t_1 during which the system evolves under some Hamiltonian $\hat{H}$. Pulses may be applied during t_1 in order to

suppress the effect of one or more of the terms in the Hamiltonian (for example a 180° pulse to remove heteronuclear coupling effects); in such cases the expression for precession may be simplified by considering the evolution under a Hamiltonian $\hat{H}'$ from which these terms have been removed.

Mixing Period

During this period coherence is exchanged between groups of levels in the system; this may be achieved by one or more non-selective pulses or by a series of selective pulses. Coherence which existed between levels m and n during t_1 may be converted to coherence between levels k and l, which will precess during t_2 and contribute to the F.I.D.

Figure 2.3 shows the pulse sequence for a simple homonuclear correlation experiment (40); this sequence will be used as an illustrative example of a two-dimensional experiment.

FIGURE 2.3

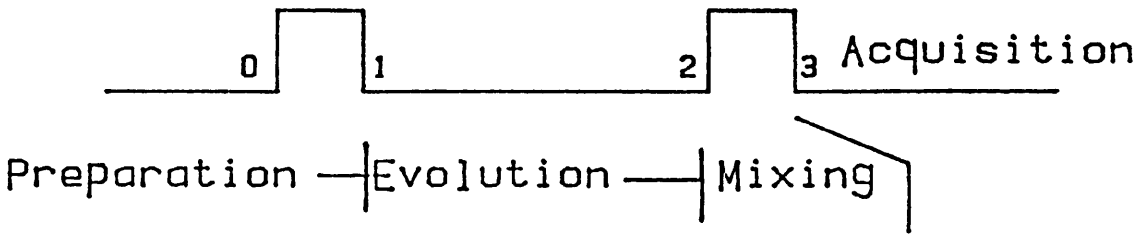

For a system of two nuclei L and K initially at equilibrium,

$$\sigma_o = K_z + L_z \xrightarrow{(\pi/2)(K_x + L_x)} \sigma_1 = -K_y - L_y$$

$$\underline{\Omega_K t_1 K_z + \Omega_1 t_1 L_z + \pi J_{KL} t_1 2K_z L_z} \quad \sigma_2 = [-K_y \cos\Omega_K t_1 + K_x \sin\Omega_L t_1$$

$$-L_y \cos\Omega_L t_1 + L_x \sin\Omega_L t_1] \cos\pi J_{KL} t_1$$

$$+[2K_x L_z \cos\Omega_K t_1 + 2K_y L_z \sin\Omega_K t_1$$

$$+2K_z L_x \cos\Omega_L t_1 + 2K_z L_y \sin\Omega_L t_1] \sin\pi J_{KL} t_1$$

$$\xrightarrow{(\pi/2)(K_x + L_x)} \sigma_3^{obs} = [K_x \sin\Omega_K t_1 + L_x \sin\Omega_L t_1] \cos\pi J t_1$$

(a) (b)

$$-[2K_y L_z \sin\Omega_L t_1 + 2K_z L_y \sin\Omega_K t_1] \sin\pi J t_1$$

(c) (d)

.....[2.28]

The most important observable terms at (3) are (c) and (d). (c) precessed with frequency Ω_L during t_1 and Ω_K during t_2, its position in the spectrum is $\omega_1 = \Omega_L$, $\omega_2 = \Omega_K$; (d) is at $\omega_1 = \Omega_K$, $\omega_2 = \Omega_L$. These are known as cross peaks; their existence is due to the transfer of coherence from one multiplet to another. Because this transfer is caused by scalar coupling between the nuclei K and L the presence of cross peaks indicates connectivities. Terms (a) and (b) precess at Ω_K and Ω_L respectively during both t_1 and t_2;

they therefore lie on the diagonal $\omega_1 = \omega_2$. A third group of peaks, not included in the expression for σ_3^{obs}, originate from magnetization which is longitudinal immediately prior to the second pulse. These axial peaks lie along the $\omega_1 = 0$ axis. By expanding the expressions for (a), (b), (c) and (d) in terms of $\Omega \pm J$ it can be seen that the cross peak doublets are in antiphase whereas the diagonal peak doublets are in phase (11).

The homonuclear correlation experiment described above is just one example of two-dimensional N.M.R. spectroscopy, a number of other two-dimensional experiments exist. The most important two-dimensional technique as far as this thesis is concerned is heteronuclear correlation spectroscopy which is described below.

For a system of two groups of nuclei I and S, magnetization which evolved as coherence of the I spins during t_1 may be transferred to the S spins during the mixing period. The S spin coherence then evolves during the acquisition, t_2. The two-dimensional spectrum produced by this experiment contains peaks which indicate connectivities between I and S nuclei. For a spin system consisting of protons and carbon-13, correlation information may be obtained by acquisition of carbon-13, transverse magnetization during t_2, the proton peaks are observed indirectly by Fourier transformation with respect to t_1.

Representation of Two-Dimensional Spectra

Before discussing the ways in which a graph of a two-dimensional spectrum may be formed, the form of the lines in the spectrum must be considered. If the signal $s(t_1,t_2)$ is amplitude modulated as a as a function of t_1:

$$s(t_1,t_2) = C\cos(\Omega_1 t_1)\exp(i\Omega_2 t_2) \qquad .....[2.29]$$

(ignoring the effects of relaxation)

Where C is a constant.

After carrying out two COMPLEX Fourier transforms on the signal matrix the form of the spectrum is,

$$s(\omega_1,\omega_2) = CA_2(\omega_2)\{A_1(\omega_1) + A_1(-\omega_1) + iD_1(\omega_1) + iD_1(-\omega_1)\} \qquad .....[2.30]$$

Where $A_n(\omega_n)$ denotes an absorption mode function in time dimension n,

$$A_n(\omega_n) = \frac{T_2^{(n)}}{1 + T_2^{(n)2}(\Omega_n-\omega_n)^2} \qquad .....[2.31]$$

the real part of a complex Lorentzian, and $D_n(\omega_n)$ denotes a dispersion mode function in time dimension n,

$$D_n(\omega_n) = \frac{T_2^{(n)2}(\Omega_n-\omega_n)}{1 + T_2^{(n)2}(\Omega_n-\omega_n)^2} \qquad .....[2.32]$$

corresponding to the imaginary part.

$T_2^{(1)}$ is the relaxation time constant during evolution.

$T_2^{(2)}$ is the relaxation time constant during detection.

It can be seen that the real part of $s(\omega_1,\omega_2)$ may be adjusted to contain only absorption mode contributions; however in such a spectrum lines would appear at $\pm\omega_1$ making it impossible to determine the sign of ω_1.

If the signal is phase modulated as a function of t_1,

$$s(t_1,t_2) = C \exp(i\Omega_1 t_1)\exp(i\Omega_2 t_2) \qquad .....[2.33]$$

then the spectrum will contain absorption and dispersion terms in both its real and imaginary parts. Thus the dispersion mode cannot be removed simply by taking linear combinations of real and imaginary components.

$$s(\omega_1,\omega_2) = C\{A_1(\omega_1)A_2(\omega_2) - D_1(\omega_1)D_2(\omega_2) + iA_1(\omega_1)D_2(\omega_2) + iD_1(\omega_1)\,A_2(\omega_2)\} \qquad .....[2.34]$$

The real part of the spectrum has the 'phase-twisted' lineshape produced by superposition of a two-dimensional absorption and two-dimensional dispersion lineshapes. Because of the dispersion component, the interpretation of overlapping lines can be very difficult. In order to remove the dispersion terms a second experiment may sometimes be performed in which the t_1 phase modulation is of the opposite sign. The subtraction of the two spectra from these experiments results in an absorption mode spectrum. The advantage of the phase modulated spectrum is that the sign of ω may be determined.

An alternative method of removing the complications due to the phase-twisted lineshape is to plot the signal in the absolute value mode. In this mode the quantity plotted is $|s|(\omega_1,\omega_2)$

$$|s|(\omega_1,\omega_2) = \{R^2(\omega_1,\omega_2) + I^2(\omega_1,\omega_2)\}^{\frac{1}{2}} \qquad .....[2.35[$$

where $R(\omega_1,\omega_2)$ and $I(\omega_1,\omega_2)$ are the real and imaginary parts of the spectrum respectively. The disadvantage of this mode of presentation is that the dispersion component causes severe line broadening,

particularly along sections parallel to the frequency axes, and intensity distortions where peaks overlap.

To obtain frequency discriminated spectra which are free from the effects of phase-twist and absolute value tailing the following method may be used (41). Two spectra are acquired with amplitude modulation in t_1. The first, s_c, has a cosine modulation in t_1, the second, s_s, is obtained from a pulse sequence in which the preparation pulses are shifted by 90°; this spectrum has a sine modulation in t_1. Assuming perfect phase adjustment of the spectrometer, s_c and s_s are given by

$$s_c(t_1,t_2) = \cos(\Omega_1 t_1)\exp(i\Omega_2 t_2)E_1E_2E_1'E_2' \qquad .....[2.36]$$

$$s_s(t_1,t_2) = \sin(\Omega_1 t_1)\exp(i\Omega_2 t_2)E_1E_2E_1'E_2' \qquad .....[2.37]$$

where $E_1 = \exp(-t_1/T_1)$, $E_2 = \exp(-t_1/T_2)$

$E_1' = \exp(-t_2/T_1)$, $E_2' = \exp(-t_2/T_2)$

Complex Fourier transformation of s_c with respect to t_2 gives,

$$s_c(t_1,\omega_2) = \frac{1}{2}[\exp(i\Omega_1 t_1) + \exp(-i\Omega_1 t_1)][A_2 + iD_2] \qquad .....[2.38]$$

Setting the imaginary part of this expression to zero we have,

$$s_c(t_1,\omega_2) = \frac{1}{2}[\exp(i\Omega_1 t_1) + \exp(-i\Omega_1 t_1)]A_2 \qquad .....[2.39]$$

Fourier transformation with respect to t_1 gives the following for the real part of $s_c'(\omega_1,\omega_2)$

$$\mathrm{Re}[s_c'(\omega_1,\omega_2)] = \frac{1}{2}[A_1^+ A_2 + A_1^- A_2] , \qquad .....[2.40]$$

where the superscripts indicate the sign of Ω_1

Applying a similar procedure to $s_s(t_1,t_2)$ leads to the following expression for the imaginary part of $s_s'(\omega_1,\omega_2)$

$$Im[s_s'(\omega_1,\omega_2)] = -\tfrac{1}{2}\,[A_1^+ A_2 - A_1^- A_2] \qquad .....[2.41]$$

The double absorption, frequency discriminated spectrum $s_r(\omega_1,\omega_2)$ is obtained from the following combination

$$Re[s_r(\omega_1,\omega_2)] = Re[s_c'(\omega_1,\omega_2)]-Im[s_s'(\omega_1,\omega_2)]$$

$$= A_1^+ A_2 \qquad .....[2.42]$$

Due to the linearity of the Fourier transform the linear combination may be carried out before the second transformation. The appropriate combination in this case is

$$s_r(t_1,\omega_2) = Re[s_c(t_1,\omega_2)] + iRe[s_s(t_1,\omega_2)]$$

$$= \cos(\Omega_1 t_1)A_2 + i\sin(\Omega_1 t_1)A_2 \qquad .....[2.43]$$

Graphical Representation

All two-dimensional spectra in this thesis will be presented in the form of contour plots; these are plots of signal intensity contours projected on to the plane defined by the frequency axes. The lowest amplitude for which a contour is recorded may be adjusted according to the noise level in the spectrum; the amplitude corresponding to the n^{th} contour is usually chosen to be equal to 2^n times this chosen amplitude. In order to obtain frequency or signal-to-noise ratio information cross sections through the spectrum, and projections onto one of the frequency axes will also be used.

2.4 Sensitivity in N.M.R.

The signal-to-noise (S/N) ratio of an N.M.R. experiment is a measure of its ability to distinguish between a weak signal from a sample and the background noise. For practical purposes the signal-to-noise ratio for a given signal is usually defined as

$$S/N = \frac{2.5\,S}{h_{p-t-p}} = \frac{S}{2\sigma_N} \qquad .....[2.44]$$

where h_{p-t-p} is the peak-to-peak noise amplitude found for a section of baseline, σ_N the r.m.s. noise amplitude, and S is the height of the signal. In discussing the factors which affect sensitivity the following processes must be considered.

(a) Detection

The signal in an N.M.R. experiment is detected by measuring the E.M.F. induced in a coil close to the sample. The systematic component of this E.M.F. is proportional to the net magnetic moment of the sample; in addition to this there is a random noise voltage arising from thermal motion of electrons in the coil. Thus, when first detected the signal has a certain amount of noise associated with it; this noise is dependent upon the effective resistance of the coil and on its temperature.

(b) Amplification

The signal is initially of low power and so must be amplified before being digitized. Amplification increases the power of both the signal and the noise, but contributions from thermal noise in the amplifier circuits act to reduce the S/N ratio.

(c) Processing

The ratio of signal to noise is further modified by the way in which the signal is processed.

These three factors are discussed in more detail below.

(a) The detection of the signal by the receiver coil

The traditional formula (37) for the signal-to-noise ratio available after a 90° pulse is arrived at by considering the amplitudes of the radio frequency voltage V available at the terminals of a solenoidal coil containing a number density N of nuclei of spin I on resonance with the transmitter. For a coil of inductance L, V is given by

$$V = \eta Q |\omega_0 \chi_0 B| (L\pi V_c)^{\frac{1}{2}} \qquad .....[2.45]$$

where B is the magnetic field strength, V_c is the coil volume, η is the filling factor, a measure of the proportion of the coil volume which is occupied by the sample. A discrepancy of a factor of two in the value of η may occur due to ambiguity in its definition. Reference (37) gives η in terms of the ratio of the sample volume to the coil volume, the maximum possible value of η is therefore one. Reference (42) uses the ratio of the integral of radio frequency field over the sample to that over all space, so that the maximum value of η in this case is 0.5. Here the definition of reference (42) will be used. Q is the quality factor of the coil used, this is a measure of the R.F. losses in the coil; Q is frequency dependent, $Q = L\omega/R$. The quantity χ_0 is the static nuclear susceptibility of the sample, given by the Curie law.

$$\chi_0 = \frac{N\gamma^2\hbar^2 I(I+1)}{3kT} \qquad .....[2.46]$$

The noise voltage across the terminals of the coil in the frequency interval Δf is

$$V_N = [4kTcR\Delta f]^{\frac{1}{2}}$$

where R is the effective resistance of the coil at the frequency used, and Tc the temperature of the coil. The expression for sensitivity therefore becomes,

$$(S/N) = \frac{\eta Q|\omega_0\chi_0 B|}{[4kTcR\Delta f]^{\frac{1}{2}}} (L\pi V_c)^{\frac{1}{2}} \qquad .....[2.47]$$

Since this formula was derived to give order of magnitude values for the special case of a solenoid, its application to other coil geometries (such as the saddle shaped coil generally used with superconducting magnets) is open to doubt.

An alternative approach (43) makes use of the reciprocity between the field experienced by a magnetic dipole placed at a point inside a coil carrying a current and E, the E.M.F. which would be induced in the same coil by the dipole rotating about the z axis with angular velocity ω_0.

$$E = -(d/dt)\{\underline{B}_1.\underline{m}\} \qquad .....[2.48]$$

B_1 is the field produced at the dipole of magnitude m by unit current flowing through the receiver coil.

Following a 90° pulse applied to a sample of volume V_c and net magnetic moment of magnitude M_0, E is given by,

$$E = -\int_{sample} d/dt\{\underline{B_1}.\underline{M_0}\}\, dV_s \qquad .....[2.49]$$

For a reasonably homogenous sample

$$E = K|\omega_0|(B_1)_{xy}M_0V_s\cos(\omega_0 t) \qquad .....[2.50]$$

where, in the terminology of reference (43), K is the inhomogeneity factor (K~1) and $K(B_1)_{xy}$ is the average over the sample of the component of B_1 in the xy plane.

Introducing the expression for noise used previously produces a new expression for the S/N ratio:

$$(S/N)_{r.m.s.} = \frac{K|\omega_0|(B_1)_{xy}M_0V_s}{(8kTcR\Delta f)^{\frac{1}{2}}} \qquad .....[2.51]$$

By introducing equation [2.3] an expanded form of equation [2.51] is obtained,

$$(S/N)_{r.m.s.} = \frac{\hbar^2}{4kT}.(V_sN)\,\frac{(K/B_1)_{xy}}{(8kTcR\Delta f)^{\frac{1}{2}}}.|\underline{Bo}|^2\gamma^3 \qquad .....[2.52]$$

The term R in the denominator of equation [2.52] introduces a further frequency dependence into the equation due to the so called 'skin effect'. An alternating current flowing through a conductor is confined, due to eddy currents, to a region near the surface of the conductor. Increasing the frequency of the current decreases the depth to which it may penetrate the conductor. As the frequency increases the cross-sectional area available for conduction decreases, and the effective resistance of the conductor therefore increases.

The dependence of R on ω is given, for an isolated conductor, by equation [2.53].

$$R = (1/p)(\mu\mu_0\omega_0\rho(Tc)/2)^{\frac{1}{2}} \qquad .....[2.53] \ (43)$$

1 is the length of the conductor, p its circumference and μ its permeability. $\rho(Tc)$ is the resistivity of the conductor at temperature Tc. However, it is not generally possible to calculate R for a coil of arbitrary geometry because of the proximity of one turn to another.

In order to use equation [2.52] it is necessary to know the value of $(B_1)_{xy}$, the temperature of the coil Tc, and its resistance, R, at the operating frequency. By making use of the following considerations it is possible to relate sensitivity to terms which are more easily measured.

When a coil is supplied with a power P from a matched transmitter this power is dissipated entirely in the resistance, R, of the coil. The current I in the coil is therefore equal to $(P/R)^{\frac{1}{2}}$, so that for K~1 the actual radio frequency field experienced by the sample is $(B_1)_{xy}\sqrt{P/R}$, allowing $(B_1)_{xy}$ to be related to the 90° pulse width t_{90} for an R.F. power P:

$$(B_1)_{xy} = (R/P)^{\frac{1}{2}}.\frac{1}{4t_{90}\gamma} \qquad .....[2.54]$$

Substituting this expression for $(B_1)_{xy}$ into equation [2.52] leads to a more convenient form:

$$S/N = \frac{\hbar^2}{4kT}.(V_sN).\frac{1}{4t_{90}}.\frac{|\underline{Bo}|^2\gamma^2}{(8kTcP\Delta f)^{\frac{1}{2}}} \qquad .....[2.55]$$

Equation [2.55] describes the maximum signal-to-noise ratio available at the terminals of a coil used to detect an N.M.R. signal, although at high frequencies it may break down where the phase of the induced E.M.F. is not constant throughout the coil (43). Equation [2.55] has the advantage that, for K~1, it requires only two experimental parameters, t_{90} and P (both easily measured), in addition to the active volume of the sample V_s.

The term in t_{90} and $P^{\frac{1}{2}}$ is a measure of the coupling between the coil and the nuclei in the sample, and of the quality factor Q of the tuned circuit. The important factors here are the geometry of the coil, its resistance and its inductance; in terms of equation [2.45], $(B_1)_{xy}$ is dependent upon Q and η. For best results with a fixed sample volume, the coil volume should be minimized (i.e. η maximized); thus N.M.R. probes containing more than one coil (for example to observe ^{13}C while decoupling ^{1}H) usually have the detection coil closest to the sample.

(b) Amplification of the signal

The sensitivity available at the terminals of the coil will undergo further degradation on amplification. One measure of the additional noise introduced is the noise figure of the amplification stage. The noise figure is defined in terms of the power ratio of equation [2.56] provided that the amplifier input is matched to the coil.

$$F = \frac{\text{Input signal power/Input noise power}}{\text{Output signal power/Output noise power}} \quad \text{.....[2.56]}$$

For a chain of amplifiers of gain G_0, G_1, G_2..... and noise figures F_0, F_1, F_2..... the overall noise figure, F, is given by equation [2.57].

$$F^2 = F^{02} + \frac{F_1^2}{G_0^2} + \frac{F_2^2}{G_0^2 G_1^2} + \ldots\ldots \qquad \ldots\ldots[2.57]$$

Thus the noise figure for the whole of the amplification stage can be kept low by arranging that F_o^2 is low and that the gains are all high.

(c) Processing of the signal

The effects of processing on the S/N ratio are discussed in detail in references (3) and (44).

The amplified signal sampled as a function of time t, describes the time domain function S(t). In most N.M.R. experiments use is made of time averaging in order to improve sensitivity. A pulse sequence is repeated n times with an interval T between successive transients, giving the experiment a total duration T_{total}. Each F.I.D. is sampled as a function of time for $0<t<t^{max}$, the n F.I.D.'s are then co-added, and the time averaged F.I.D. is Fourier transformed to give the spectrum S'(W).

For a F.I.D. containing a single signal of offset Ω recorded using quadrature detection, S(t) is given by,

$$S(t) = S^e(t)\exp(-i\Omega t) \qquad \ldots\ldots[2.58]$$

where $S^e(t)$ is the envelope function of the F.I.D., typically exponential. This would normally be weighted with a function h(t) before Fourier transformation in order to optimize the signal-to-noise ratio.

If the F.I.D's are sampled at M equidistant points, Δt apart then, if M is large, the peak height S in the frequency spectrum may be expressed as:

$$S = nM\overline{sh} \qquad .....[2.59]$$

where $$\overline{sh} = \frac{1}{t_{max}} \int_{o}^{t_{max}} S^{e}(t)h(t)dt$$

For optimum S/N ratio matched weighting should be used:

$$h(t) = S^{e}(t) \qquad .....[2.60]$$

The noise in the time domain depends on the bandwidth, F, of the spectrometer, usually determined by the analogue filters. Assuming white random noise the r.m.s. noise amplitude ρ_n in the time domain is,

$$\sigma_n = F^{\frac{1}{2}}\rho_n \qquad .....[2.61]$$

where ρ_n is the square root of the frequency-independent power spectral density. Because of the use of quadrature detection F is twice the cut-off frequency f_c of the analogue audio filters; to avoid folding of noise into the spectrum f_c is normally set equal to the Nyquist frequency f_N ($f_N = 0.5 \times \Delta t)^{-1}$.

The corresponding frequency domain function is obtained by summing the noise in all nM time-domain samples:

$$\sigma_N = (nMF)^{\frac{1}{2}}\overline{[h^2]}^{\frac{1}{2}}\rho_n \qquad .....[2.62]$$

where $F = M/t^{max}$,

and $$\left[\frac{1}{t^{max}} \int_{o}^{t_{max}} h^2(t)dt\right]^{\frac{1}{2}} = \overline{[h^2]}^{\frac{1}{2}} =$$ r.m.s. amplitude of the weighting function.

Substituting for F and applying the condition of matched signal weighting leads to equations [2.63] and [2.64].

$$\sigma_N = M(n/t^{max})^{\frac{1}{2}}[S^2]^{\frac{1}{2}}\rho_n \qquad .....[2.63]$$

$$(S/N)_u = \frac{S}{2\sigma_n T_{total}^{\frac{1}{2}}}$$

$$= \frac{1}{2}\overline{[S^2]}^{\frac{1}{2}}\left(\frac{t^{max}}{T}\right)^{\frac{1}{2}}\frac{1}{\rho_n} \qquad .....[2.64]$$

where $(S/N)_u$ is the signal-to-noise ratio obtained in unit time.

For a F.I.D. envelope $S^e(t)$ defined by

$$S^e(t) = S_i\exp(-t/T_2)$$

$$\overline{S^2} = S_i\frac{T_2}{2t^{max}}[1-E_2^2] \qquad .....[2.65]$$

where $E_2 = \exp(-t^{max}/T_2)$

$$(S/N)_u = \frac{1}{2}S_i\left(\frac{T_2}{2T}\right)^{\frac{1}{2}}\frac{1}{\rho_n}[1-E_2^2] \qquad .....[2.66]$$

The signal strength S_i during time averaging will depend on the recycle time T and the spin lattice relaxation time T_1 of the nuclear resonance. If pulses of flip angle β are used, then optimum S/N ratio is obtained when equation [2.67] (3) is satisfied.

$$\cos\beta_{opt} = E_1 = \exp(-T/T_1) \qquad .....[2.67]$$

The corresponding value of S_i is,

$$S_i = S_i^0 \left[\frac{1-E^1}{1+E_1}\right]^{\frac{1}{2}} \qquad .....[2.68]$$

where S_i^0 is the signal obtained when a 90° pulse is applied to a sample at equilibrium.

Assuming that there is no feed through of transverse magnetization from one transient to the next,

$$(S/N)_u = \frac{1}{2} S_i^0 \left(\frac{T_2}{2T}\right) \frac{1}{\rho_n} [1-E_2^2]^{\frac{1}{2}} \left[\frac{1-E_1}{1+E_1}\right]^{\frac{1}{2}} \qquad .....[2.69]$$

This may be written in the form,

$$(S/N)_u = \frac{1}{4} S_i^0 \left(\frac{T_2}{T_1}\right)^{\frac{1}{2}} [1-E_2^2]^{\frac{1}{2}} G(T/T_1)\ 1/\rho_n \qquad .....[2.70]$$

where

$$G(x) = 2\left[\frac{1-\exp(-x)}{x(1+\exp(-x))}\right]^{\frac{1}{2}} \qquad .....[2.71]$$

$G(T/T_1)$ is a slowly changing function of T; for T of the order of T_1 $G(T/T_1)$ is close to unity. Provided that the flip angle β is optimized according to the values of T and T_1 used then, for $0<T<3T_1$, sensitivity is not greatly affected by repetition rate (G(3) = 0.77, G(0) = 1.0). The value of E_2 is determined by the resolution desired in the resulting spectrum. Provided that the spectrum is well resolved, E_2 is small and does not affect sensitivity.

The relevant terms determining sensitivity here are therefore contained in the expression,

$$(S/N)_u \propto S_i^0 \left(\frac{T_2}{T}\right)^{\frac{1}{2}} \qquad .....[2.72]$$

The dependence on $(T_2)^{\frac{1}{2}}$ means that sensitivity decreases as linewidth increases; the $T^{\frac{1}{2}}$ dependence takes into account the effect of repetition rate.

It will be shown in the following section that for polarization transfer experiments the value of γ in equations [1.4] and [2.54] is different to that of equation [2.1]. The value of γ in equation [2.1] refers to the magnetogyric ratio (γ_p) of the species from which the polarization is transferred; in equations [1.4] and [2.54], γ is the corresponding value (γ_{obs}) for the detected species. Taking into account these two different γs, equations [2.55] and [2.72] can be combined to give the following expression for $(S/N)_u$.

$$(S/N)_u \propto (V_s N) \frac{1}{4t_{90°obs}} \left(\frac{1}{p}\right)^{\frac{1}{2}} \gamma_{obs}\gamma_p \frac{1}{(Lw)^{\frac{1}{2}}} \qquad .....[2.73]$$

It should be noted that the dependence on $(T_2)^{\frac{1}{2}}$ here is due to the use of matched filtration; if fixed filtration is used then $(S/N)_u \propto T_2$.

The use of two-dimensional spectroscopy introduces extra sensitivity considerations; it is shown in reference (45) that if matched filtration is used, the ratio of the sensitivity of an ideal two-dimensional spectrum to that of a one-dimensional spectrum of the same duration is

$$\frac{(S/N)_{2D}}{(S/N)_{1D}} = \left[\frac{E_{2D}}{E_{1D}}\right]^{\frac{1}{2}} = \left\{\frac{1}{2}\cdot\frac{T_2^{(1)}}{t_1^{max}}\left[1-\exp\left(\frac{-2t_1^{max}}{T_2^{(1)}}\right)\right]\right\}^{\frac{1}{2}} \qquad .....[2.74]$$

where $T_2^{(1)}$ is the spin-spin relaxation time constant during t_1. If $T_2^{(1)} >> t_1^{max}$ then sensitivity in the two-dimensional spectrum should be the same as that in the corresponding one-dimensional spectrum.

2.5 Polarization Transfer

In order to enhance sensitivity in N.M.R. experiments it may be arranged that γ_p is different from γ_{obs} (equation [2.73]). For example the sensitivity of a ^{13}C spectrum may be improved by carrying out an initial polarization transfer step from protons. γ_p is therefore the magnetogyric ratio of protons while γ_{obs} is the magnetogyric ratio of carbon. Polarization transfer is achieved by applying an appropriate sequence of pulses to both nuclear species; of the pulse sequences suitable for this application, the first to achieve non-selective polarization transfer was the INEPT sequence (Insensitive Nucleus Enhancement by Polarization Transfer) (5).

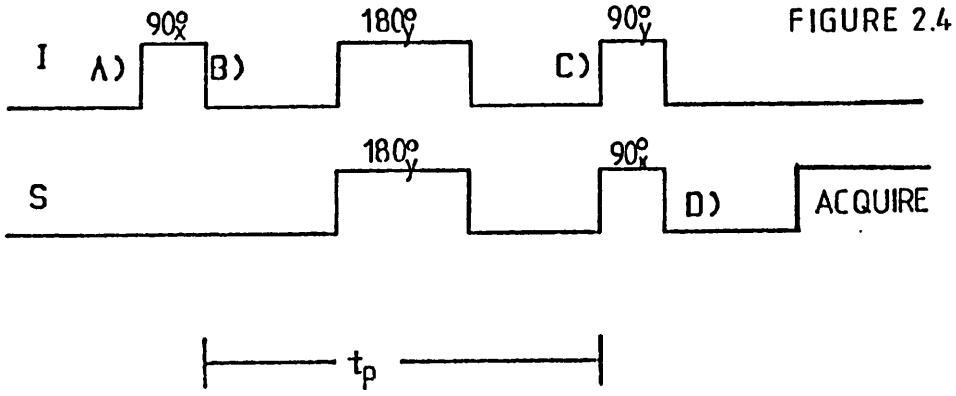

FIGURE 2.4

Pulse sequence for INEPT

Since the effects of any initial S spin magnetization can be removed, in the following product operator analysis only initial I spin magnetization will be considered.

$$(A)\ I_z \xrightarrow{(\pi/2)_x^{\,I}} (B)\ -I_y$$

From (B) to (C) precession due to chemical shifts is refocussed by the 180° pulses; the average evolution is under scalar coupling only.

$$(C)\ -I_y\cos(\pi Jt_p)+2I_xS_z\sin(\pi Jt_p)$$

$$2I_xS_z \xrightarrow{(\pi/2)_y^{\,I}(\pi/2)_x^{\,S}} 2I_zS_y$$

$$-Iy \xrightarrow{(\pi/2)_y^{\,I}(\pi/2)_x^{\,S}} -I_y$$

$\therefore$ at $(D)\ -I_y\cos(\pi Jt_p)+2I_zS_y\sin(\pi Jt_p)$

If an optimized value of t_p is used then the situation at (D) is described by I_zS_y. Having started from I spin polarization the INEPT experiment has produced S spin magnetization.

Since the signal originates from I spin polarization, the relevant factor b_s of equation [2.20] is related to the population difference across I spin transitions ($\Delta n(I)$). The intensity of the detected S spin signal is therefore proportional $\Delta n(I)$ rather than to the polarization across S spin transitions ($\Delta n(S)$); the I spin polarization has been transferred to the S spins. The value of γ_p in equation [2.73] is therefore γ_I, while the value of γ_{obs} is γ_s.

This enhancement of sensitivity is achieved independent of the chemical shifts of the nuclei involved.

S spin magnetization at (D) is in antiphase with respect to the heteronuclear scalar coupling; for an I_2S group the triplet intensities become -1:0:1 and for an I_3S group the quartet becomes -1:-1:1:1. The phases of these signals can be modified by the insertion of a refocussing delay before acquisition (46,47,48). The full pulse sequence for refocussed INEPT now becomes

FIGURE 2.5

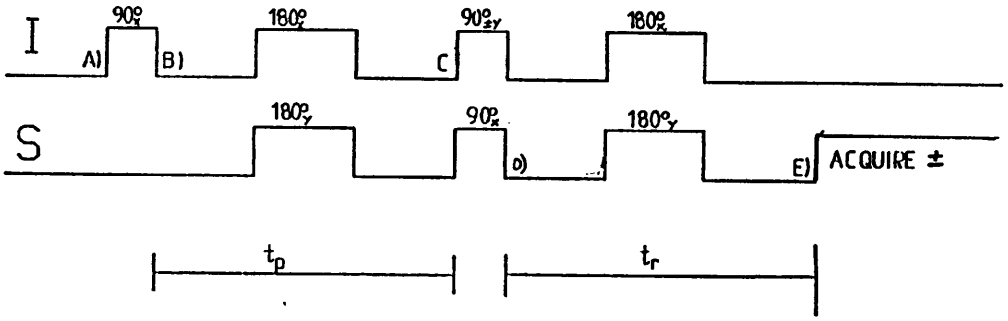

The average Hamiltonian between (D) and (E) contains only terms for scalar coupling,

$$-I_y \xrightarrow{\pi J t_r S_z I_z} -I_y\cos(\pi J t_r)+2I_x S_z \sin(\pi J t_r)$$

$$2I_z S_y \xrightarrow{\pi J t_r S_z I_z} 2I_z S_y \cos(\pi J t_r)-S_x \sin(\pi J t_r)$$

At (E) the terms giving rise to observable magnetization are:

$$\sin(\pi Jt_p)(2I_zS_y\cos(\pi Jt_r)-S_x\sin(\pi Jt_r)) \qquad .....[2.75]$$

Optimization of INEPT

A product operator analysis of the INEPT pulse sequence for other spin systems is given in reference (49). For observation of the S_x component only, for a spin system I_NS, the generalized formula [2.76] can be derived.

$$\sigma_S = -NS_pS_rC_r^{N-1}S_x \qquad .....[2.76]$$

$$S_p = \sin\pi Jt_p$$

$$S_r = \sin\pi Jt_r$$

$$C_r = \cos\pi Jt_r$$

J is the heteronuclear coupling constant J_{IS}, assumed here to be the only scalar coupling. For a system IS^1, S^2, S^3....S^n, where the indices indicate nuclei which are not necessarily equivalent Schenker and Philipsborn (50) have arrived at the following equation for the enhancement factor E_{INEPT} for the I multiplet components of a coupled spectrum.

$$E_{INEPT}\ (t_pm_s) = 2\frac{\gamma_S}{\gamma_I}\sum_p^n m_{sp}\sin(\pi t_pJ(I,S^p))\ \prod_{\substack{q\\ q\neq p}}^n\cos(\pi t_pJ(S^p,S^q)) \qquad .....[2.77]$$

m_s denotes the z eigenstate of the S nuclei.

For a decoupled spectrum this becomes,

$$E_{INEPT,dec.}(t_p t_r) = 2^{-n} \sum (E_{INEPT}(t_p, m_s)\sin(2\pi t_r \sum_p m_{sp} J(I,S^p))) \quad .....[2.78]$$

For the refocussed INEPT sequence the dependence of the signal intensities on the delay t_r varies with the multiplicity of the site as shown by equations

$$SI \propto \sin(2\pi J(I,S)t_r)$$

$$SI_2 \propto \sin(4\pi J(I,S)t_r) \quad .....[2.79]$$

$$SI_3 \propto 0.75(\sin(2\pi J(I,S)t_r) + \sin(6\pi J(I,S)t_r)) \quad (6)$$

For enhancement of sites of all three types a t_r value of $\frac{1}{2\pi J}\cos^{-1}(1/\sqrt{3})$ should be used, however, experiments carried out with different delays are useful for spectral editing (48).

2.6 Indirect Detection

A sensitivity improvement over S observed polarization transfer should be possible by arranging that γ_{obs} is the larger of the γ values in the spin system. For the IS_n spin system considered above this would require the direct detection of I spin magnetization. In an indirect detection experiment, nuclear magnetization arising from polarization of the more sensitive nucleus is modulated during the t_1 delay of a two-dimensional experiment by the chemical shift of the S nucleus with which it shares a scalar coupling. The detected I spin signal is then processed to obtain a two-dimensional spectrum in which I spin chemical shifts in f_2 are correlated with S spin chemical shifts in f_1. Such experiments may involve two successive polarization transfer steps or may make use of heteronuclear multiple quantum coherence.

Multiple-Quantum Methods

Conventional N.M.R. experiments involve the detection of transverse magnetization; this magnetization is associated with transitions which satisfy the selection rule $\Delta M_I = \pm 1$ and corresponds to single quantum coherence. Under appropriate conditions it is possible to create coherence between levels for which $\Delta M_I = \pm 0, 2, 3....$ This is termed multiple quantum coherence; it does not give rise to transverse magnetization and so can not be observed directly. For a weakly coupled two-spin system IS the energy levels are as shown in Figure 2.6, single quantum coherence is associated with the transitions (1,2), (1,3), (2,4), and (3,4); double quantum coherence is associated with transition (1,4) and zero quantum coherence with transition (2,3).

FIGURE 2.6

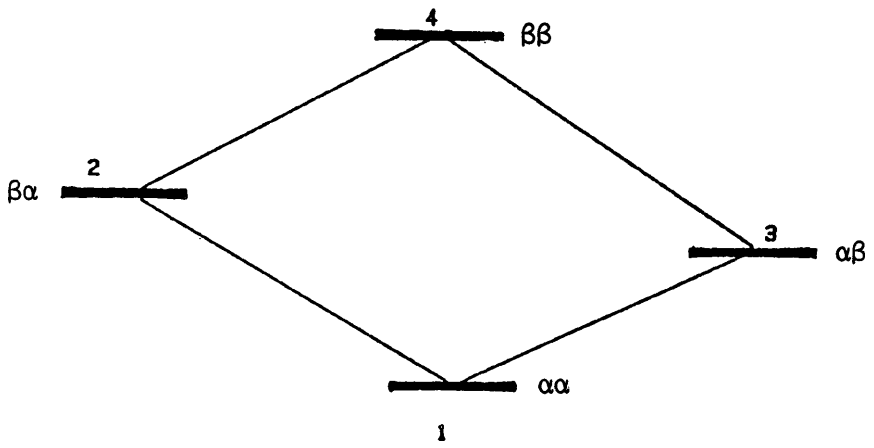

In order to study the behaviour of multiple quantum coherence a two-dimensional experiment must be performed. In such an experiment the multiple quantum coherence is allowed to evolve for a time t_1 before being converted to transverse magnetization by a suitable pulse or series of pulses. The f_1 dimension of the two-dimensional spectrum obtained in this way contains information about the evolution of the multiple quantum coherence.

From the expansions of the product operators given in Appendix A it follows that heteronuclear two spin coherence I_xS_y contains four components.

$$I_xS_y = \frac{1}{4i}(I^+ + I^-)(S^+ - S^-)$$

$$= \frac{1}{4i}(I^+S^+ - I^+S^- + I^-S^+ - I^-S^-) \quad .....[2.80]$$

(1) (2) (3) (4)

where I^+, I^-, I_x, I_y are the operators for I spin coherence

S^+, S^-, S_x, S_y are the operators for S spin coherence

Similarly for I_yS_y

$$I_yS_y = \frac{1}{4i}(I^+ - I^-)(S^+ - S^-)$$

$$= \frac{1}{4i}(I^+S^+ - I^+S^- - I^-S^+ + I^-S^-) \quad .....[2.81]$$

(1) (2) (3) (4)

Terms (1) and (4) represent heteronuclear double quantum coherence, terms (2) and (3) heteronuclear zero quantum coherence. Each of these terms represent a different coherence pathway. The use of phase cycling to distinguish these coherence pathways will be discussed in section 2.7.

In order to study the behaviour of multiple quantum coherence a two-dimensional experiment must be performed. In such an experiment, the multiple quantum coherence is allowed to evolve for a time t_1 before being converted into transverse magnetization by a suitable pulse or series of pulses. The f_1 dimension of the two-dimensional spectrum obtained in this way contains information about the evolution of the multiple quantum coherence. From the commutation expression

$$[2I_{K\lambda}I_{L\nu}, 2I_{K\mu}I_{L\xi}] = 0 \quad .....[2.82]$$

for $\lambda = \mu$ and $\nu = \xi$ or $\lambda \neq \mu$ and $\nu \neq \xi$ (38) it follows that

$$[I_xS_y, I_zS_z] = 0$$

From equation [2.82] it can be seen that there is no evolution under the Hamiltonian for scalar coupling between the nuclei involved in the multiple quantum coherence. MQC does evolve under couplings to passive nuclei, leading to multiplet structure in f_1.

In order to see the way in which MQC evolves under chemical shift operators it is necessary to consider the following linear combinations.

For pure double quantum coherence

$$\frac{1}{2}(2I_{Kx}I_{Lx} - 2I_{Ky}I_{Ly}) = \frac{1}{2}(I_K^+I_L^+ + I_K^-I_L^-) = \{DQT\}_x \quad .....[2.83]$$

$$\frac{1}{2}(2I_{Kx}I_{Ly} + 2I_{Ky}I_{Lx}) = \frac{1}{2i}(I_K^+I_L^+ - I_K^-I_L^-) = \{DQT\}_y \quad .....[2.84]$$

For pure zero quantum coherence

$$\frac{1}{2}(2I_{Kx}I_{Lx} + 2I_{Ky}I_{Ly}) = \frac{1}{2}(I_K^+I_L^- + I_K^-I_L^+) = \{ZQT\}_x \quad .....[2.85]$$

$$\frac{1}{2}(2I_{Ky}I_{Lx} - 2I_{Kx}I_{Ly}) = \frac{1}{2i}(I_K^+I_L^- - I_K^-I_L^+) = \{ZQT\}_y \quad .....[2.86]$$

The precession of these terms is described by

$$\{DQT\}_x \xrightarrow{(\Omega_K I_{Kz} + \Omega_L I_{Lz})\tau} \{DQT\}_x \cos(\Omega_K + \Omega_L)\tau + \{DQT\}_y \sin(\Omega_K + \Omega_L)\tau \quad .....[2.87]$$

$$\{ZQT\}_x \xrightarrow{(\Omega_K I_{Kz} + \Omega_L I_{Lz})\tau} \{ZQT\}_x \cos(\Omega_K - \Omega_L)\tau + \{ZQT\}_y \sin(\Omega_K - \Omega_L)\tau \quad .....[2.88]$$

Thus double quantum coherence evolves under the sum and zero quantum coherence under the difference of the chemical shift

frequencies of the nuclei involved in the transition. Of course the effect of either of these chemical shifts can be removed by applying the appropriate 180° pulse at the mid-point of t_1.

Detection of multiple quantum coherence requires that it be reconverted into transverse magnetization. This may be achieved in a number of ways (14). For the two spin system described above MQC may be converted into transverse magnetization of either species by the application of a 90° pulse,

$$I_x S_y \xrightarrow{90°_x(S)} I_x S_z \xrightarrow{\pi J I_z S_z} I_y$$

$$I_x S_y \xrightarrow{90°_y(I)} I_{-z} S_y \xrightarrow{\pi J I_z S_z} S_x \qquad \text{.....[2.89]}$$

2.7 Phase Cycling (51)

The signal detected at the end of an N.M.R. experiment arises from coherences, created by the first pulse, which have been modified by the action of subsequent pulses. In this way z magnetization associated with the system at equilibrium is converted into single quantum coherence (transverse magnetization) by the first pulse and then may be converted into a number of different orders of coherence (P_j) by subsequent pulses i; the effect of such a pulse may be described by equation [2.90], where U is the propagator representing the pulse.

$$U_i \sigma^P(t_i^-) U_i^{-1} = \sum_{P_j} \sigma^{P_j}(t_i^+) \qquad .....[2.90]$$

It will be seen that the observed signal is the result of coherence which has undergone changes in its order at various points during the pulse sequence being converted into single quantum coherence at the end of the sequence. The different pathways through the sequence are referred to as coherence transfer pathways and may be described by a vector $\Delta P = \{\Delta P_1, \Delta P_2 \ldots\ldots\ldots \Delta P_n\}$ where n is the total number of pulses and ΔP_i is the change in coherence order undergone at each pulse i for the pathway considered. As the signal arises initially from longitudinal magnetization (P=0) and is detected as transverse magnetization (P = -1), then $\sum_i^n \Delta P_i = -1$ is one of the necessary conditions for an observable signal.

The effect of increasing the phase of a pulse i by ψ_i can be seen from equation [2.91].

$$U_i(\psi_i)\sigma^P(t_i^-)U(\psi_i)^{-1} = \sum_P \sigma^P(t_i^+)\exp\{-i\Delta P_i \Delta\phi_i\} \quad .....[2.91]$$

For a phase shift ψ_i applied to each of the pulses, i, the total phase of the signal component from the pathway described by $\underline{\Delta P}$ is given by equation [2.92].

$$\sigma^{P=-1}(\psi_1,\psi_2....\psi_n,t) = \sigma^{P=-1}(\psi=0)\exp\{-i\underline{\Delta P}\,\underline{\psi}\} \quad .....[2.92]$$

where $\underline{\psi} = \{\psi_1,\psi_2....\psi_n\}$

During acquisition the phase ψ_{ref} of the detector may be cycled in order to eliminate the effects of instrumental imperfections. For the signal to build up coherently during this cycling there must be a constant relationship between ψ_{ref} and the signal phase i.e.,

$$\psi_{ref} = -\underline{\Delta P}\,\underline{\psi} = -\sum \Delta P_i \psi_i \quad .....[2.93]$$

The purpose of phase cycling is to remove the effects of signals arising from coherence transfer pathways other than those chosen. The phase cycling of a pulse acts, therefore, to remove orders of coherence other than those corresponding to the desired coherence transfer pathway(s). For a single pulse, if the highest order of coherence to be removed is r - 1 then the minimum required number of increments (N_i) of the pulse phase is equal to r. The phase ψ_i of the pulse during the L^{th} transient, relative to its phase in the first transient of the experiment, is ψ_L,

$$\psi_L = \frac{K_L 2\pi}{N_i} \quad , \quad K_L = 0,1,.....N_i-1 \quad .....[2.94]$$

Thus equation [2.93] can be re-written as,

$$\psi_{ref} = -\underline{\Delta P}\,\underline{\psi} = -\sum \Delta P_i \frac{K_i 2\pi}{N_i} \qquad .....[2.95]$$

It should be noted that phase cycling a single pulse does not achieve unambiguous selection of the desired coherence pathway. In general, for N_i experiments in which the phase of one pulse is cycled a series of coherence pathways will be selected corresponding to the series $\Delta P^{(selected)}$

$$\Delta P^{(selected)} = \Delta P^{(desired)} \pm nN \;, \quad n=0,1,2,...$$

Care must therefore be taken in the design of phase cycling schemes to ensure that only the desired coherence pathway can pass through the whole of the pulse sequence.

CHAPTER 3

QUATERNARY CARBON CORRELATION EXPERIMENTS

3.1 (A) INADEQUATE

Of the N.M.R. techniques used in structure determination some of the least ambiguous are those which provide direct evidence of scalar coupling between pairs of nuclei. The application of such techniques to pairs of ^{13}C nuclei is limited in natural abundance, due to the low probability of two ^{13}C nuclei occupying adjacent sites in the molecule; the probability of three adjacent ^{13}C nuclei is negligible. The low natural abundance of the desired spin systems (~1 in 10000) not only leads to poor sensitivity, but also gives rise to suppression problems. Signals from the monoisotopomer are 200 times more intense than the doublets from the two spin systems; thus these parent peaks must be suppressed if they are not to mask the satellite signals.

FIGURE 3.1

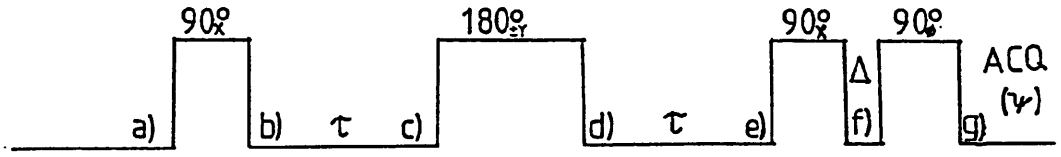

Figure 3.1 Pulse sequence for INADEQUATE

Suppression of signals from the monoisotopomer may be achieved using the INADEQUATE ('Incredible Natural Abundance Double Quantum Transfer Experiment') pulse sequence, which makes use of the fact that two spin coherence can be created in a system consisting of two scalar coupled nuclei. The INADEQUATE pulse sequence is shown in Figure 3.1.(52)

The effect of the sequence from (a) to (f) can easily be seen by employing a product operator analysis (38); due to the refocussing effect of the $180°_y$ pulse an effective Hamiltonian free from chemical shift effects will be assumed.

For a one spin system,

(a) C_{1z}

$\downarrow 90°_x$

(b) $-C_{1y}$

(c) $\downarrow J_{cc}$

(d)

(e) $-C_{1y}$

$\downarrow 90°_x$

(f) $-C_{1z} = S_0$

For a two spin system with scalar coupling J,

$$\text{(a)}\quad C_{1z}+C_{2z}$$

$$\Big|\ 90°_{x}$$

$$\downarrow$$

$$\text{(b)}\quad -C_{1y}-C_{2y}$$

$$\Big|\ J_{cc}$$

$$\downarrow$$

$$\text{(e)}\quad -C_{1y}\cos(2\pi J\tau)+2C_{1x}C_{2z}\sin(2\pi J\tau)$$

$$-C_{2y}\cos(2\pi J\tau)+2C_{2x}C_{1z}\sin(2\pi J\tau)$$

$$\Big|\ 90°_{x}$$

$$\downarrow$$

$$\text{(f)}\quad -C_{1z}\cos(2\pi J\tau)-2C_{1x}C_{2y}\sin(2\pi J\tau)$$

$$-C_{2z}\cos(2\pi J\tau)-2C_{2x}C_{1y}\sin(2\pi J\tau)$$

The effect of the three pulses is to invert longitudinal magnetization of nuclei in the one nucleus spin systems, giving rise to a signal component S_0 and to convert longitudinal magnetization of the two spin system into two spin coherence, S_2. The maximum yield of S_2 is achieved if τ is set equal to $(2n+1)/4J$, where n is an integer. From the expansions of the two spin order terms (section 2.6) it can be seen that S_2 is pure double quantum coherence.

It is the possibility of exciting two quantum coherence which is the key to discriminating between one spin and two spin systems. In order to achieve this discrimination, use is made of the different sensitivities of S_0 and S_2 to a change in the phase of the final 90° pulse; this read pulse re-converts the double quantum coherence into single quantum coherence which is then detected. The change in the order of coherence of S_2 brought about by the read pulse is minus

three; a 90° change in the phase of this pulse therefore results in a change of 270° in the phase of the detected signal. This results in the phase of the signal from two spin systems cycling in the opposite direction to that of the read pulse (Φ). For the signal S_0, the change in the order of coherence brought about by the read pulse is minus one; the phase of the signal from the one spin system therefore lags Φ by 90°. These phase relationships are summarized in Table 3.1. By making the receiver reference phase, ψ, follow the signal originating from S_2 this signal is added coherently while the S_0 signal is cancelled.

Table 3.1

Φ	S_0	S_2	ψ
+x	-y	+x	+x
+y	+x	-y	-y
-x	+y	-x	-x
-y	-x	+y	+y

Due to the low intensity of the satellite signals compared to the parent signals, care must be taken to remove any spurious signals arising from pulse imperfections. The effect of imperfections in the 180° pulse can be reduced by incrementing the phase of this pulse by 180° on successive blocks of four transients while leaving the rest of the phasecycle unchanged. This eight step phasecycle can be further expanded in order to correct for any inequalities in the two quadrature detection channels of the spectrometer. The eight step cycle is repeated four times with the phase of all of the pulses and of the receiver reference incremented by 90° between each increment. A thirty-two step phasecycle is therefore produced.

The spectrum obtained using this sequence contains a doublet for each nucleus of a J coupled pair; these doublets are in antiphase, the relative orientation of the peaks being dependent on the sign of the coupling constant. Connectivity information is obtained from such a spectrum by identifying sites which have the same coupling constant.

An extension of this technique (53) has been suggested in which τ is used as the time variable of a two-dimensional experiment ($2\tau = t_1$). This allows the measurement of connectivities over a wide range of J values in a single experiment, and removes the necessity of an initial knowledge of J for experimental optimization. It is therefore possible to observe one-bond and long-range couplings in the same spectrum (53). The two-dimensional spectrum contains four multiplets for each pair of coupled nuclei. Each multiplet exhibits doublet structure parallel to both frequency axes; the refocussing effect of the 180° pulse at the mid-point of t_1 has the effect of enhancing resolution in F_1, making the measurement of the coupling more accurate in this dimension.

Alternatively, the t_1 delay may be inserted immediately after the pulse which creates 2 quantum coherence and before the read pulse (point (f) in diagram 3.1)(54,55). The spectrum produced by this method correlates ^{13}C chemical shifts of each nucleus of a coupled pair with the double quantum frequency of the pair of nuclei, thus providing an unambiguous method of assigning coupled pairs of nuclei.

3.1 (B) INEPT-INADEQUATE

The sensitivity of the INADEQUATE technique may be improved if proton irradiation is used in order to establish a favourable N.O.E. Use may also be made of an INEPT or DEPT sequence as an initial step in the experiment. In addition to the gain in sensitivity due to polarization transfer, the INEPT-INADEQUATE (9) and DEPT-INADEQUATE (56) sequences allow a more rapid pulse rate. The rate of repetition of these sequences is limited by proton T_1's rather than the much longer ^{13}C T_1's; for small molecules, where there is a significant difference between the T_1's of the two species this increase in repetition rate can be the main advantage of the polarization transfer based sequences. The INEPT-INADEQUATE experiment is illustrated in Figure 3.2 for the case of a proton enhanced ^{13}C INADEQUATE experiment.

FIGURE 3.2

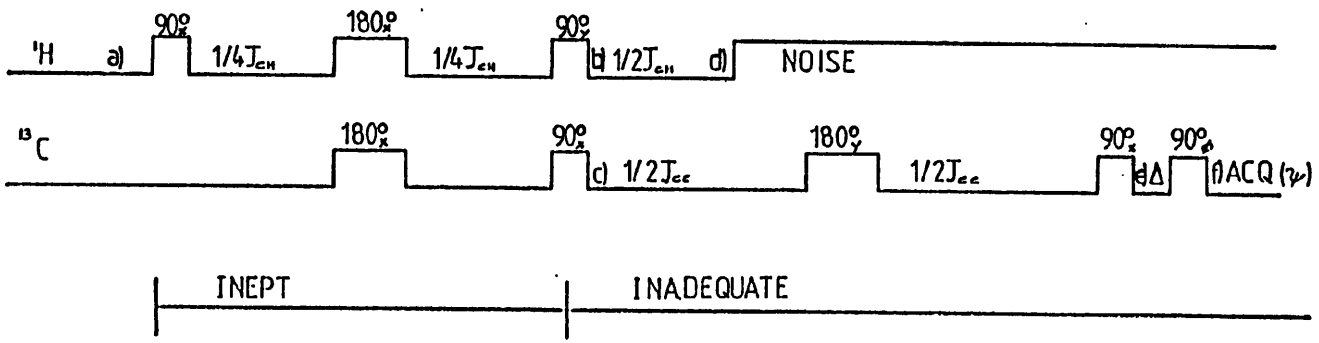

Pulse sequence for INEPT-INADEQUATE

Carbon transverse magnetization created at (c) is in antiphase with respect to the proton-carbon coupling; this is refocussed during the delay (c) to (d) after which proton noise decoupling is applied. As in an INEPT experiment, the refocussing delay has to be optimized according to the number of protons in the spin system. The refocussing introduces a 90° phase shift to the signal; for this reason the first 90° pulse at (c) is applied about the -y axis rather than the x axis as in the normal INADEQUATE experiment. The enhanced ^{13}C magnetization is converted into two-spin coherence and two quantum filtration carried out.

The filtration stage of the experiment shares the enhanced magnetization equally between both members or the coupled pair (36,56); the intensities of signals in the spectrum are therefore dependent on the INEPT enhancement for both spins in the system. In the case of a moiety containing a quaternary carbon, only the transverse magnetization of one member of the coupled pair can be efficiently enhanced by polarization transfer; the enhanced magnetization is then shared between both nuclei. Due to this sharing of magnetization the eventual sensitivity of the ^{13}C doublet for the unprotonated carbon is only half of that which would be available if all of the enhanced magnetization was transferred from the protonated carbon to the non-protonated carbon. In order to prevent this sharing of polarization, the multiple quantum filtration step may be replaced by a simple 'relay' sequence to give the C-relayed H-C INEPT sequence, Figure 3.3.

FIGURE 3.3

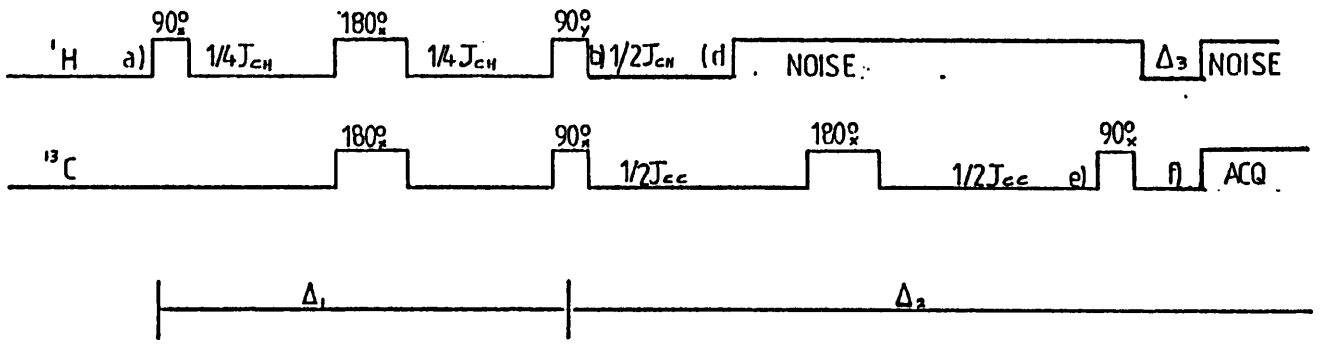

Pulse sequence for C-relayed H-C INEPT

From (a) to (e) this sequence is identical to the INEPT-INADEQUATE sequence except that all of the carbon pulses have the same phase and that at (e) a single $90°_x$ pulse is applied so that at (f) the final state of the system is $-C_{1x}C_{2y}$. All of the enhanced C_1 coherence has now been transferred to C_2 so that the peaks associated with this nucleus have maximum sensitivity. Experimental comparison (36) has confirmed that C-relayed H-C INEPT gives a ~2 fold enhancement of sensitivity over INEPT-INADEQUATE. The use of this sequence to provide unambiguous connectivity information has been demonstrated in ref. (57).

However, in addition to the relayed doublet peaks the spectrum also contains a strong central peak due to polarization transfer via long range H-C couplings (pathway b of Figure 3.4). Polarization transfer by this pathway is very inefficient, but typical efficiencies of a few percent for two- or three-bond couplings still give a signal considerably larger than the 0.5% of the parent unprotonated peak expected from the much less abundant spin system of pathway 3.4a (58,59), as illustrated by the spectra of ref. (36).

In one of the two-dimensional extensions of this technique, the C-relayed H-C-COSY, this transfer pathway leads to COLOC (60) like peaks in the spectrum. These COLOC peaks are particularly intense for ^{13}C nuclei coupled to methyl protons, use has been made of these peaks to identify tert-butyl groups in tert-Butylated 2-Naphthols (59). Despite their use in this two-dimensional variant, in one-dimensional spectra the long-range relayed peaks give no information and may obscure the antiphase doublet structure from the long-range carbon-carbon couplings, particularly since signals from pathway 3.4a are usually in quadrature with those of pathway 3.4b. The use of phase cycling to

FIGURE 3.4

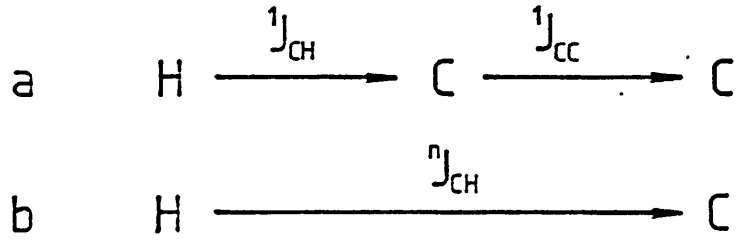

FIGURE 3.5

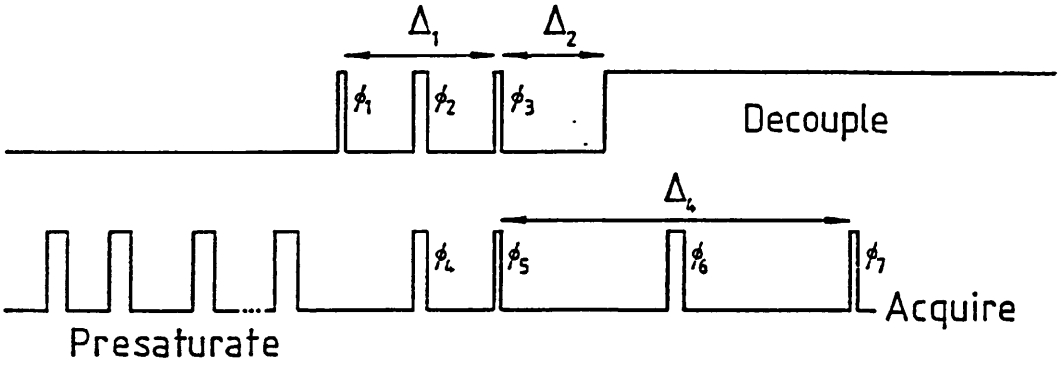

Pulse sequence for the HICCUP sequence
(Hydrogen-Intensified Carbon CoUPlings)

achieve discrimination between the two pathways can only be achieved by double-quantum filtration, which would simply represent reverting to the INEPT-INADEQUATE experiment.

3.2 Experimental

A simple extension (58) of the sequence of ref. (36) provides the desired discrimination by exploiting the very different magnitudes of one-bond and longer range coupling constants. If the pulse sequence of ref. (36), shown in a slightly modified form in Figure 3.5, is repeated with two different values of $1/(2^1J_{CH})$ and $3/(2^1J_{CH})$ for delay Δ_1 then the signals obtained for the unprotonated carbon-13 in the two possible spin systems will be very different. The signal from pathway 3.4a will be inverted in the second experiment relative to the first, due to the $\sin(\pi J\Delta_1)$ dependence of INEPT polarization transfer (6); the intensity of signals from pathway 3.4b will be an approximately linear function of Δ_1 since $^nJ_{CH} << {}^1J_{CH}$. Thus if pathway 3.4a gives a signal of intensity A with the shorter delay, then with the longer delay it will give an inverted signal -A. Pathway 3.4b gives a signal B with the shorter delay and 3B with the longer delay. Thus if the signal obtained with $\Delta_1 = 3/(2^1J_{CH})$ is subtracted from three times that obtained with $\Delta_1 = 1/(2^1J_{CH})$ the signal from pathway 3.4a will sum to 4A, whereas the signal from pathway 4b will be subtracted. The overall effect is to suppress the signals from the long range pathway 3.4b while retaining the antiphase doublet due to carbon-carbon coupling in the ^1H-^{13}C-^{13}C spin system. Very similar logic applies in the suppression of accoustic ringing (61); alternatively, this modification may be regarded as a crude but effective form of low-pass J filtration (62). The repetition rate advantage of this

experiment over an unenhanced INADEQUATE is of greatest advantage in applications involving small molecules which may have unprotonated carbons with particularly long T_1 values. Rapid pulsing of a conventional INADEQUATE sequence may result in the saturation of signals from such sites, whereas the rate of repetition of the polarization enhanced INADEQUATE is limited by the much shorter T_1 of the protons on adjacent carbons.

The action of this sequence is illustrated below for the methyl acetate spin system also used in ref. (36). Figure 3.6 shows that by subtracting spectrum 3.6b from three times 3.6a near perfect suppression of the parent peak is obtainable. This opens up the possibility of detecting longer range carbon-carbon couplings as illustrated in Figure 3.7. Using a much longer delay Δ_2 allows both the one-bond coupling (60 Hz) and the two-bond (2.7 Hz) to be seen, with no significant interference from $^1H-^{12}C-^{13}C$ spin systems.

In systems with short proton T_2's or extensive $^1H-^1H$ coupling it may be necessary to choose a weighting factor slightly less than three, but since the phase of the pathway 3.4b signal is fixed, it should always be possible to obtain good suppression if appropriate weighting is chosen. While an eight-step phase cycle gives good suppression, for best results the 32-step cycle of Table 3.2 is recommended. The level of exclusion of unwanted peaks in the spectra is an order of magnitude better than that expected from the basic INADEQUATE experiment. This high level of suppression is assisted by the combination of ^{13}C presaturation with phase alternated polarization transfer which rigorously excludes signals other than those of pathways 3.4a and 3.4b.

FIGURE 3.6

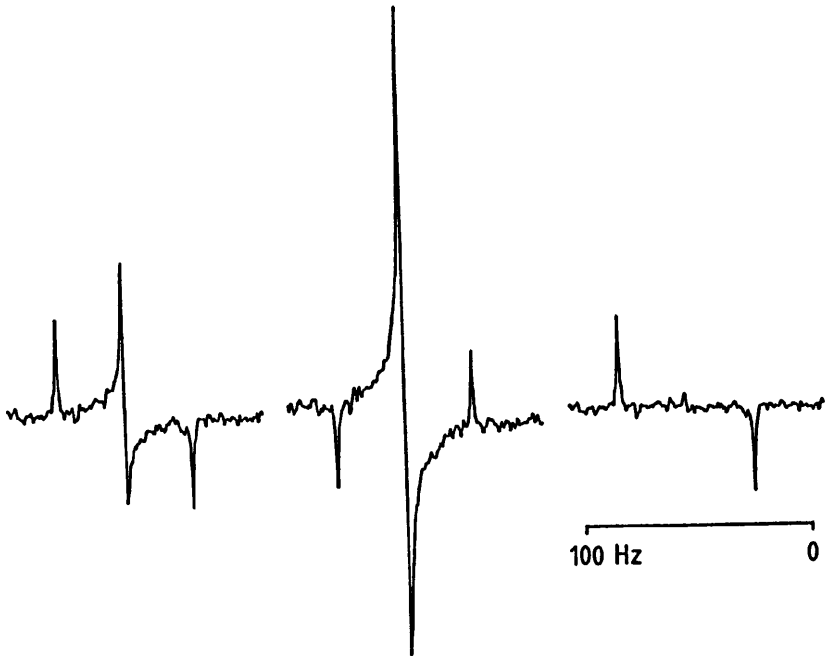

Ester carbonyl regions of ^{13}C spectra of a 50:50 mixture of methyl acetate and deuteriochloroform, measured using the sequence of figure 3.4 with the 10 mm probe of a Varian XL300 spectrometer, Δ_2 was 1.5 ms, and Δ_4 10 ms. 32 transients were recorded in 5 minutes for Δ_1 = 3.84 and Δ_1 = 11.52 ms Spectrum c shows the result of subtracting trace b from three times trace a.

FIGURE 3.7

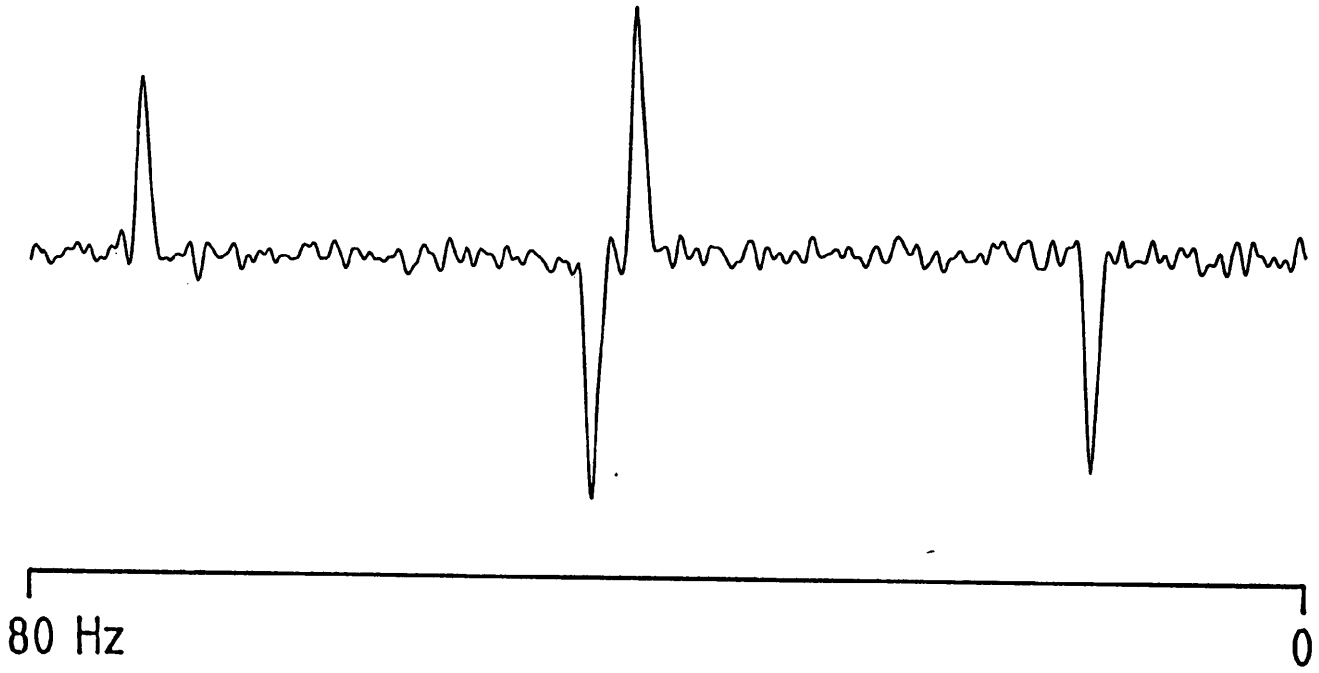

^{13}C spectrum of the ester carbonyl of methyl acetate using the same sample and experimental method as for figure 3.6, but with Δ_4 = 0.192 s. 800 transients were averaged in a total data acquisition time of 2.6 h for each value of Δ_1. Mild Lorentz-Gauss resolution enhancement was used to emphasize the doublet character of the central feature, which shows a splitting of 2.7 Hz due to long-range coupling.

Table 3.2

ϕ_1	$02 + 0_4 2_4$
ϕ_2	0123
ϕ_3	1
ϕ_4	$0_8 1_8 2_8 3_8$
ϕ_{5-7}	0123 2301
Receiver	0123

Phases are listed using the convention of ref. (4), representing phase shifts in units of 90°; e.g., $0_4 2_4$ represents the sequence of phases 0 0 0 0 180 180 180 180 0 0 .....

The C-relayed H-C COSY experiment mentioned above is carried out (36) by including a proton spin labelling delay t_1 after the first proton pulse of the C-relayed H-C INEPT sequence. Spectra obtained using this technique provide correlation (63) of the carbon chemical shifts of non-protonated carbons with the proton chemical shifts of sites with which they share a C-C coupling. A more convenient form of correlation spectrum is one in which both frequency axes indicate carbon chemical shifts; this technique would remove the possibility of ambiguity arising from protons having similar chemical shifts.

The pulse sequence for this experiment is obtained by including a delay t_1 in place of the delay Δ_2 in the sequence of ref. (36) (Figure 3.3); the sequence produced is an INEPT enhanced ^{13}C-^{13}C COSY (64). Due to the unidirectional transfer of coherence in this experiment the resulting spectrum is asymmetric about the diagonal;

this unusual feature of the spectrum (which means that there is only one cross peak for each pair of coupled nuclei) prevents the loss of sensitivity associated with sharing the signal intensity between two cross peaks in the analogous double quantum filtered experiment. Signals arising from long range polarization transfer are not a problem in this experiment as they only give rise to diagonal peaks.

A much greater problem is the presence of intense signals originating from the protonated carbons of mono- ^{13}C molecules; these would appear as extremely strong signals on the diagonal of the resulting spectrum. The effects of these signals can be seen in the spectrum of Figure 3.8. This spectrum was obtained from a 36% w/w sample of 3-methyl anisole (Figure 3.9) in a 10 mm sample tube; the INEPT-C-C-COSY sequence was used with $\Delta_1 = \Delta_2 = 3.1$ms. For each of 128 t_1 increments two free induction decays were acquired, 32 transients being accumulated for each FID. The phase of ϕ_5 (Figure 3.5) was increased by 90° for the second set of FIDs and the results were combined as in the hyper-complex method of phase-sensitive 2D data processing (65,41) to obtain frequency sign discrimination in f_1. The diagonal signals have to be reduced by one or two orders of magnitude in order to obtain a reasonably clean correlation spectrum. In order to achieve this suppression a delay $\Delta_3 = 1/2J$ is included just after the final ^{13}C pulse; this ensures that the signals from protonated sites are in antiphase with respect to the carbon-proton coupling at the start of acquisition. By applying modulated off resonance decoupling during acquisition the antiphase signals from protonated carbons are effectively nulled, any residual signals are reduced in intensity by being broadened. To reduce the 'tailing' of the residual CH_n peaks pseudo-echo weighting (66) is used in the t_2 domain. The full pulse sequence is shown in

FIGURE 3.8

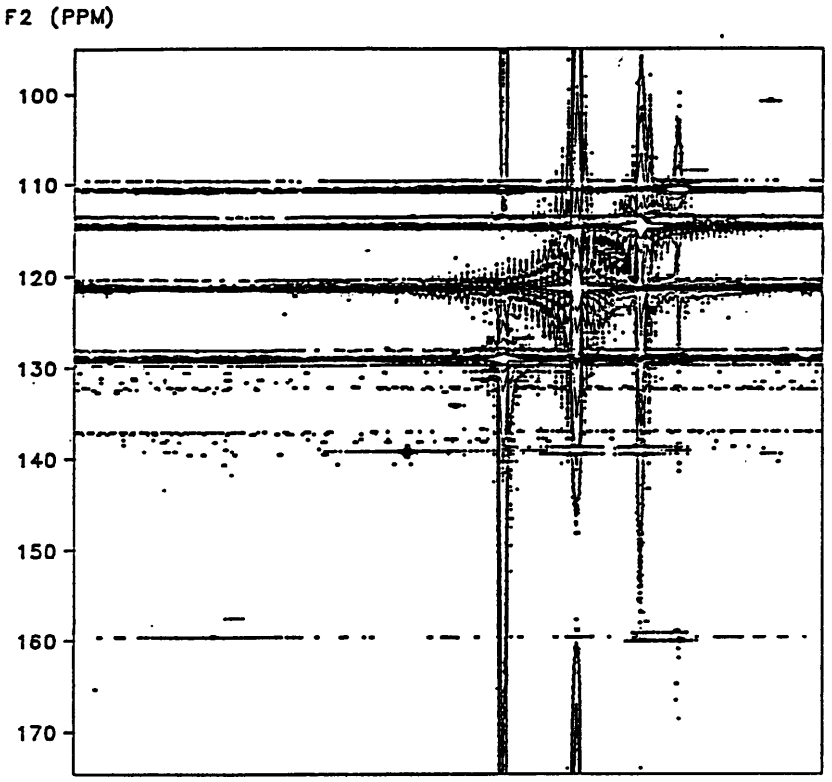

2D ^{13}C–^{13}C correlation spectrum of 3-methylanisole;
Δ_3 = 0, a 7 s delay was used between transients.
No decoupler offset was used during data acquisition and no weighting was used prior to double Fourier transformation.

FIGURE 3.9

3-methyl anisole

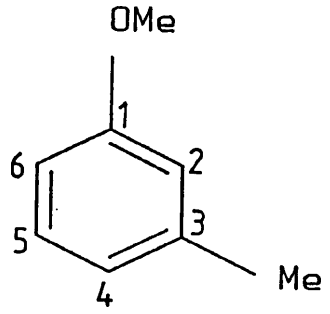

FIGURE 3.10

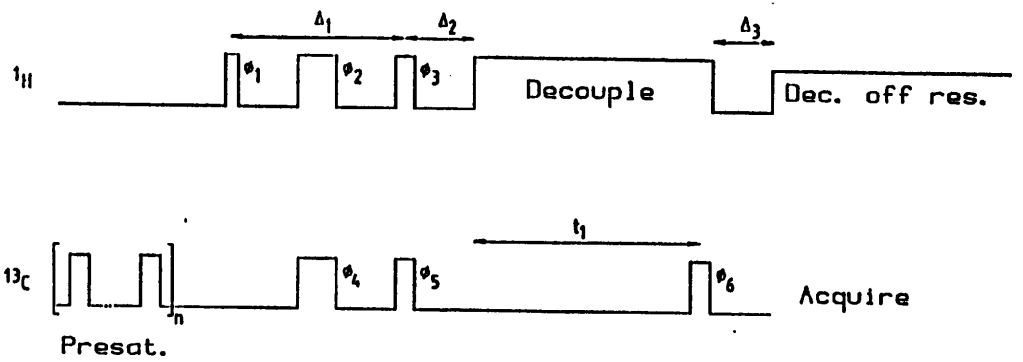

Pulse sequence for the measurement of ^{13}C–^{13}C correlations by hydrogen-carbon-carbon coherence relay. The value of Δ_2 is adjusted according to multiplicity, just as in the normal INEPT experiment. A delay to allow proton T_1 relaxation takes place between ^{13}C presaturation and the first proton pulse.

Figure 3.10. A spectrum acquired using this sequence is shown in Figure 3.11, acquired under the same conditions as the spectrum of Figure 3.8 but with Δ_3 = 3.1ms, pseudo-echo weighting in both t_1 and t_2 and an offset of 10 kHz for modulated off-resonance decoupling during acquisition of the FID. In this spectrum the intensity of the diagonal peaks is greatly reduced, the absence of intense tailing allowing easy identification of the cross peaks. Both one-bond and long range $^{13}C-^{13}C$ correlation peaks are present in this spectrum; the one-bond peaks are easily distinguished due to their greater width in the f_2 domain.

The development of these sequences shows how pulse sequences can be built up from existing units; polarization transfer schemes may be added to standard experiments in order to enhance sensitivity, but care must be taken if best use is to be made of the enhancement gained. The combination of existing sequences in this way can introduce new problems into the experiment; an example of this is the presence of long-range polarization signals in spectra obtained by the C-relayed H-C INEPT experiment. The sensitivity advantage of the two-dimensional relay experiment over the corresponding INADEQUATE based experiment must be weighed up against the much poorer suppression of the diagonal signals in the relay experiment.

FIGURE 3.11

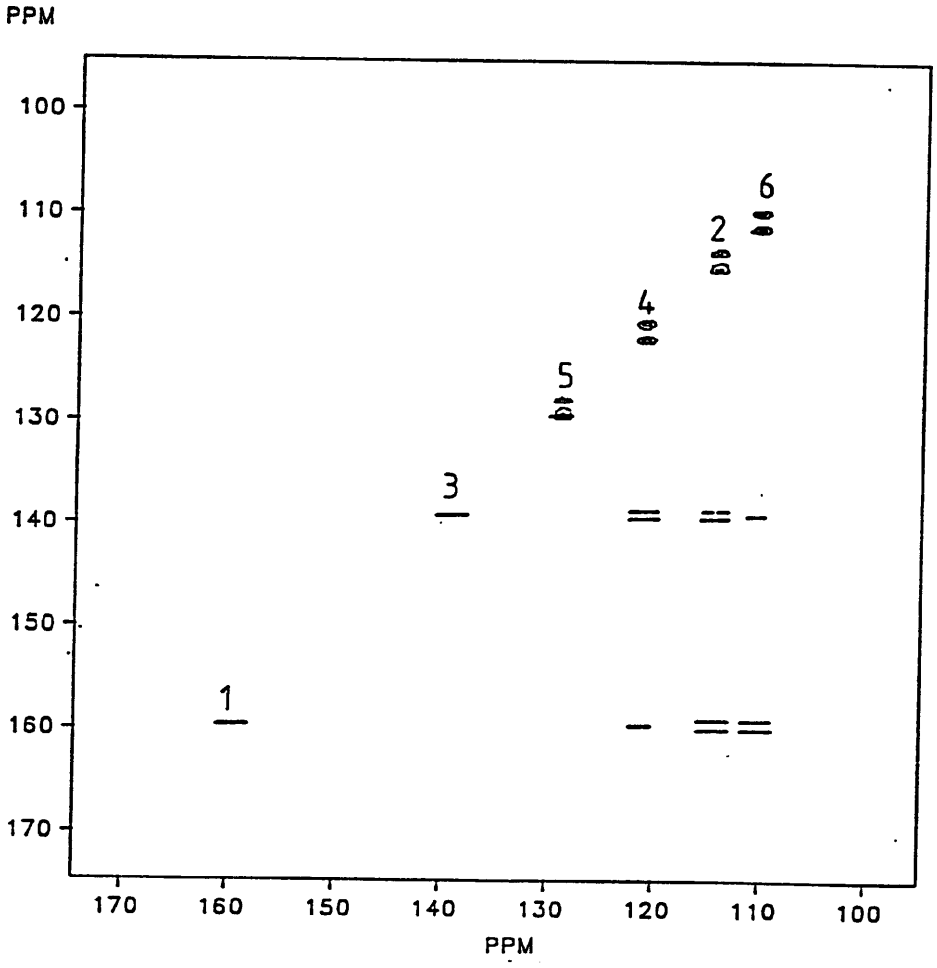

2D ^{13}C-^{13}C correlation spectrum of 3-methyl anisole obtained under identical conditions to figure 3.8 but with Δ_3 = 3.1 ms; pseudo-echo weighting was used in both t_1 and t_2. An offset of 10 kHz was used for modulated off-resonance decoupling during the acquisition of free induction decays. The one-bond correlation signals may easily be distinguished from longer range cross-peaks by virtue of their greater width in the f_2 domain. The assignments of the ^{13}C chemical shifts are marked by the respective diagonal peaks.

CHAPTER 4

INSTRUMENTAL REQUIREMENTS OF INDIRECT DETECTION EXPERIMENTS

There are three main problems associated with the indirect detection experiments reported in the literature: (1) the spectrometer must be able to detect protons while supplying X-spin pulses, which is the reverse of the usual method of observation; (2) for effective phase cycling a very high level of stability is required; and (3) a signal with a high dynamic range is produced. These problems will be discussed in detail below.

4.1 Reverse Observation

In a conventional N.M.R. experiment the signal is detected with respect to the transmitter (Tx) frequency; this is arranged by feeding a signal from the Tx local oscillator (L.O.) to the MIXER (Figure 4.1). In a spectrometer containing two transmitters for heteronuclear applications, one will be able to supply X spin pulses over a range of frequencies (this will be referred to as the transmitter, Tx) while the other may be used to irradiate protons in order to achieve heteronuclear decoupling (this will be referred to as the decoupler), or may be used to supply coherent proton pulses as part of a pulse sequence. The usual mode of operation of such a spectrometer involves the detection of X spin magnetization; it is therefore the Tx L.O. signal which is fed to the MIXER. In an indirect detection experiment the opposite is the case; proton signals are detected directly, requiring that the MIXER be supplied with an L.O. signal from the decoupler. The following modifications are made to the spectrometer in order to carry out indirect detection experiments, they are illustrated in Figure 4.2.

FIGURE 4.1a

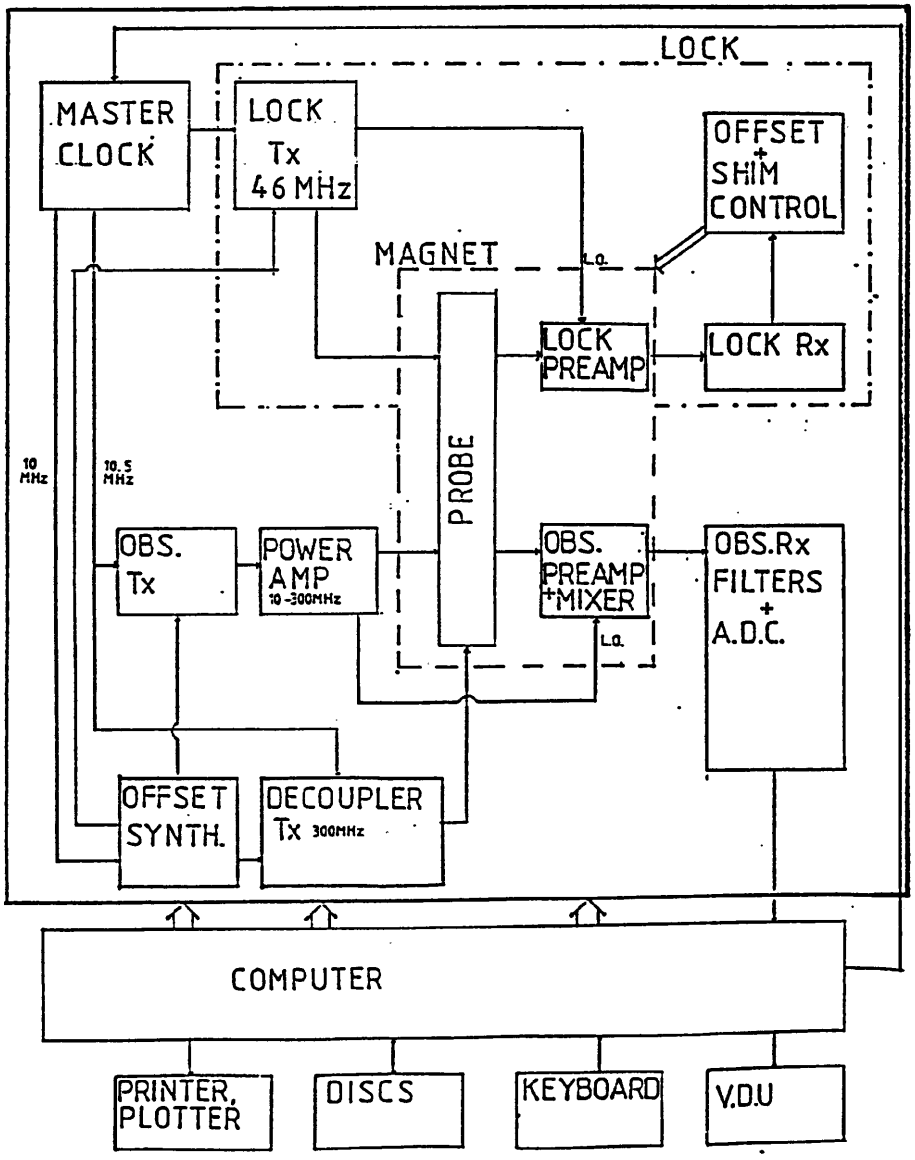

Schematic diagram of a Varian XL300 spectrometer in normal operation. The transmitter, decoupler and detection circuits are shown in more detail in figures 4.1b, 4.1c and 4.1d.

FIGURE 4.1b

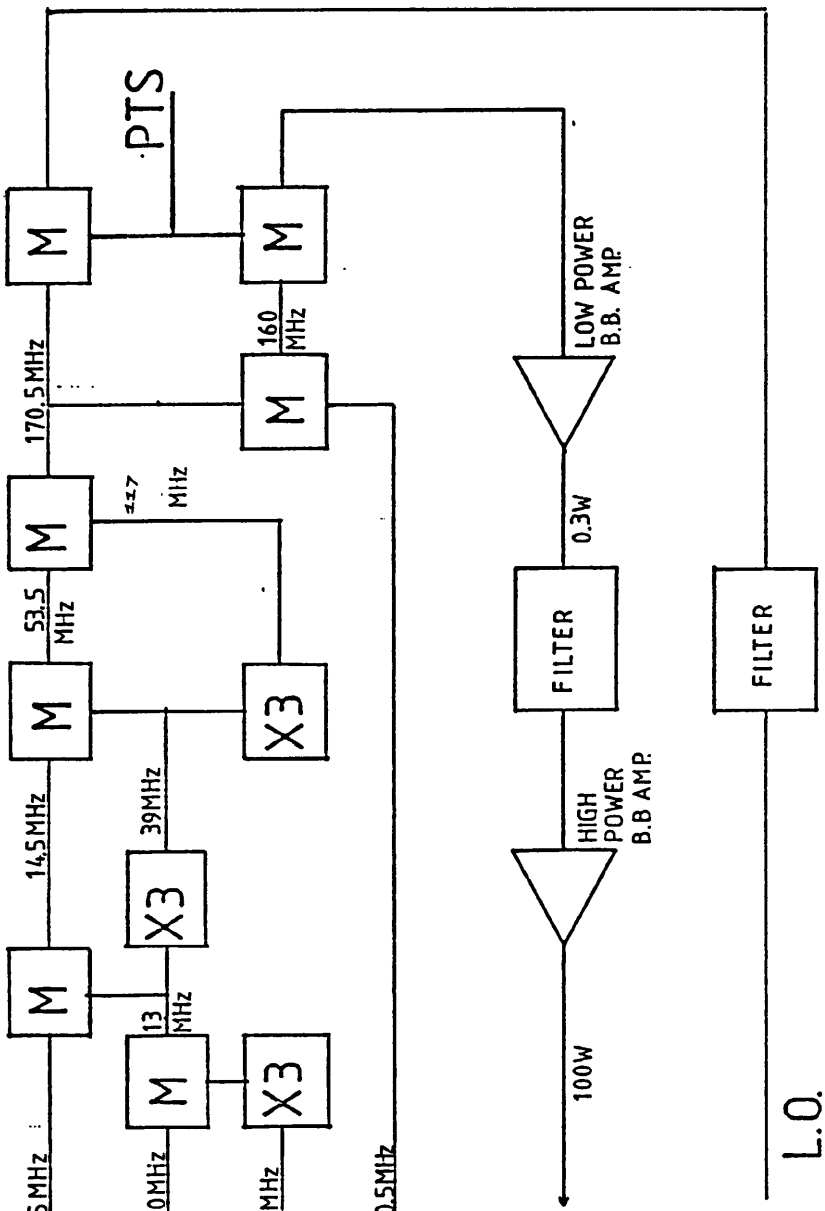

Transmitter frequency synthesis. For ^{15}N the PTS provides 190.4001 MHz, the high power output is therefore 30.4001 MHz and the L.O. frequency is 19.9001 MHz. The 10.5 MHz input of the transmitter is generated from a 2.5 MHz supply in the master clock.

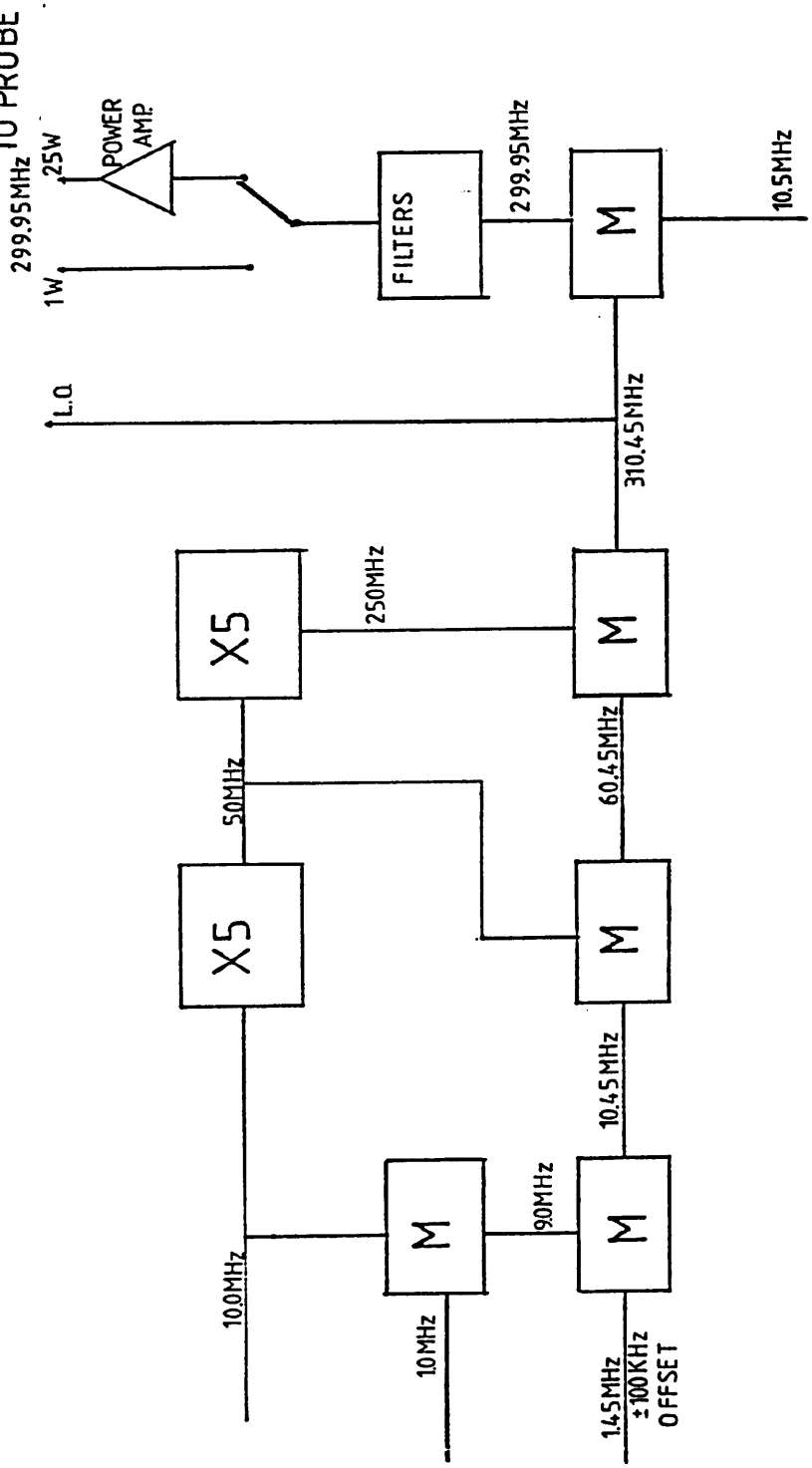

FIGURE 4.1c

Decoupler frequency synthesis and power amplification. For the heteronuclear work described in this thesis the high power (25 W) output is used.

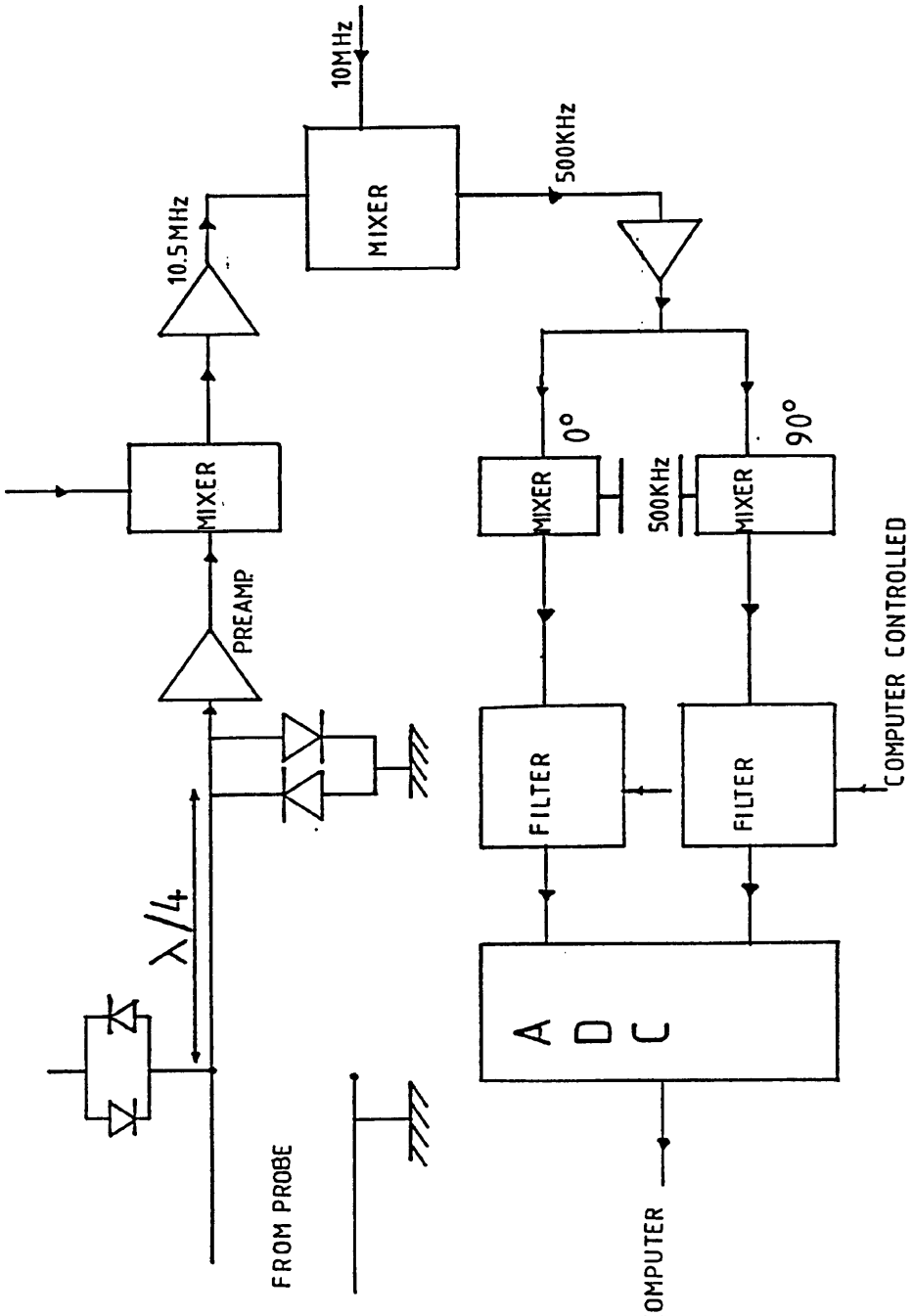

FIGURE 4.1d

Detection stage of Varian XL300 spectrometer.

FIGURE 4.2

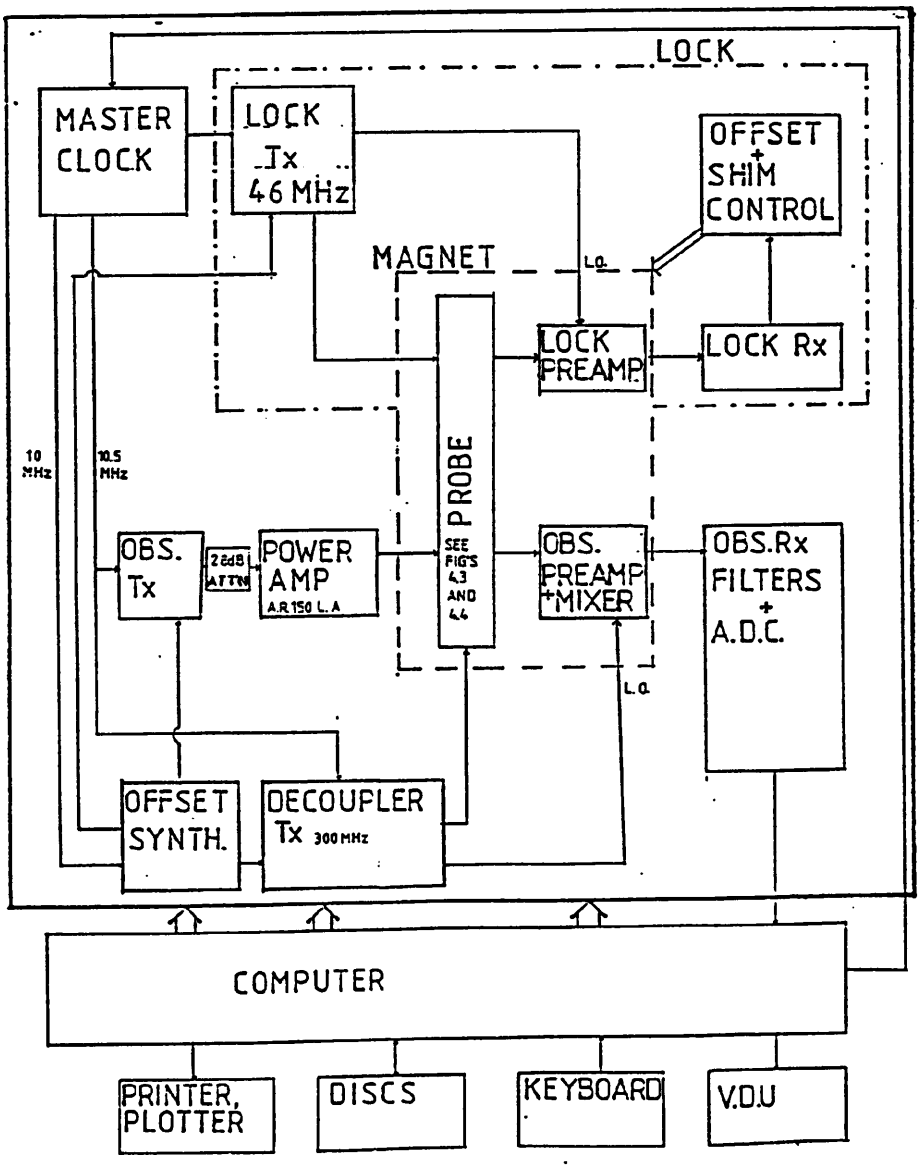

Schematic diagram of Varian XL300 spectrometer in indirect detection mode. Details of coil design and tuning are shown in figures 4.3 and 4.4.

(1) The decoupler output is fed to the proton coil of the probe; the transmitter is therefore free for X nucleus irradiation.

(2) For spectra run with no X nucleus irradiation during t_2, the transmitter output of the spectrometer is fed into the X nucleus tuning network via two 300 MHz notch filters. If X nucleus decoupling is to be applied then the low power output of the transmitter is fed via 28 dB of attenuation to the input of an Amplifier Research 150 L.A. broad band power amplifier; the output of this unit is fed to the X nucleus tuning network. To prevent any noise from the power amplifier interfering with the observe or lock channels, its output is fed via a set of crossed diodes and two 300 MHz notch low pass filters; as an added precaution a high pass filter is included between the detection coil and the observe preamplifier. To allow detection of protons during X nucleus irradiation, the receiver gating (which in a conventional experiment switches the receiver off during X spin pulses) is disconnected.

(3) For best signal-to-noise in this type of experiment, the proton detection coil must be as close as possible to the sample; the X spin coil is therefore the outer of the two coils, the opposite of the case in a conventional X detected experiment. To obtain a probe of the desired geometry for indirect detection, a 5 mm proton probe was modified by mounting a saddle-shaped X irradiation coil inside the Dewar vessel which surrounds the probe head; to minimize interaction between the two coils the X nucleus coil was mounted rotated through 90° relative to the proton coil, (see Figure 4.3). The tuning network for this coil is shown in Figure 4.4; the variable capacitors are mounted inside the probe body, and extra capacitance

FIGURE 4.3

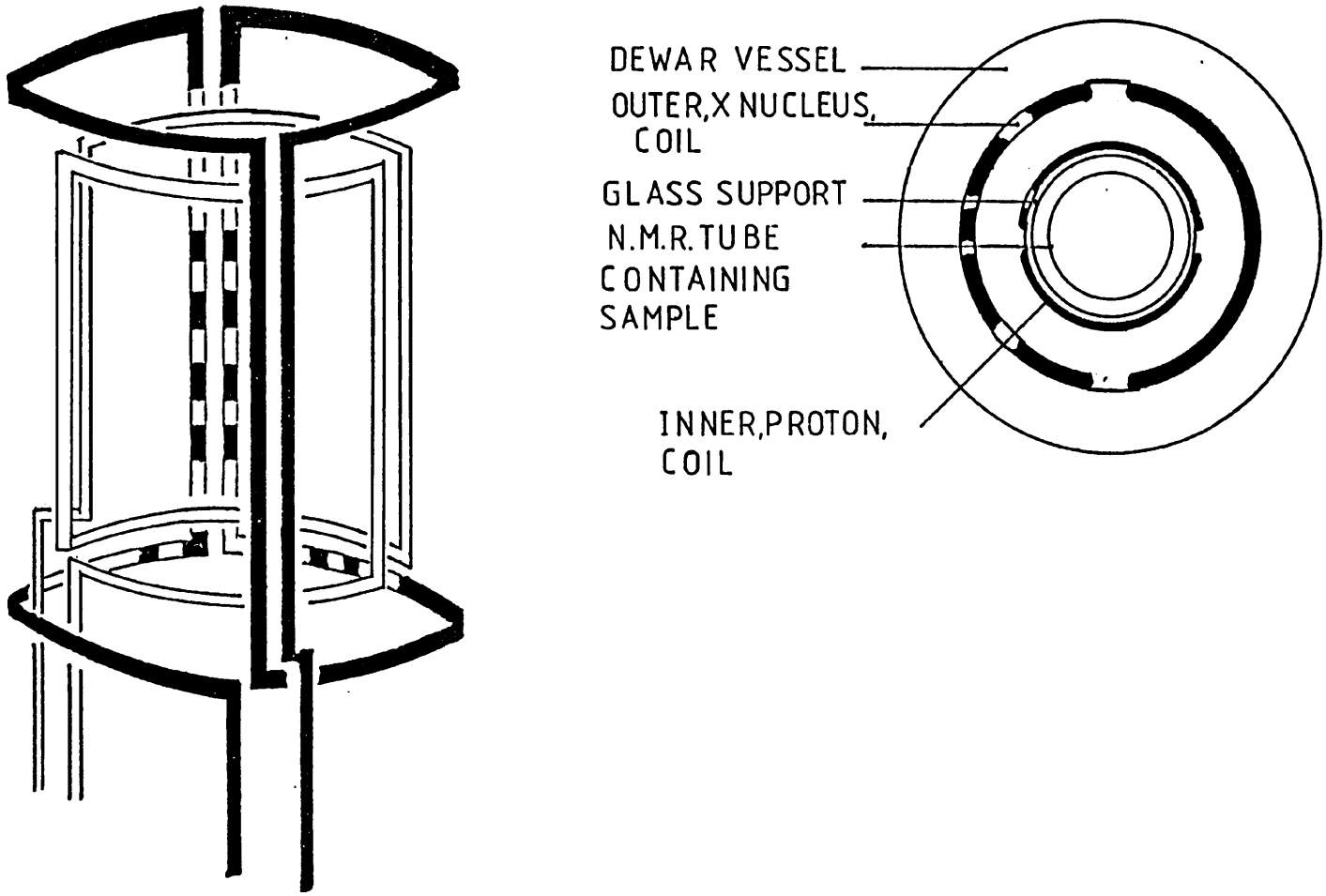

Diagram illustrating the positioning of an X nucleus coil in a standard Varian 5 mm proton probe. The outer coil is rotated through 90° with respect to the proton detection coil.

FIGURE 4.4

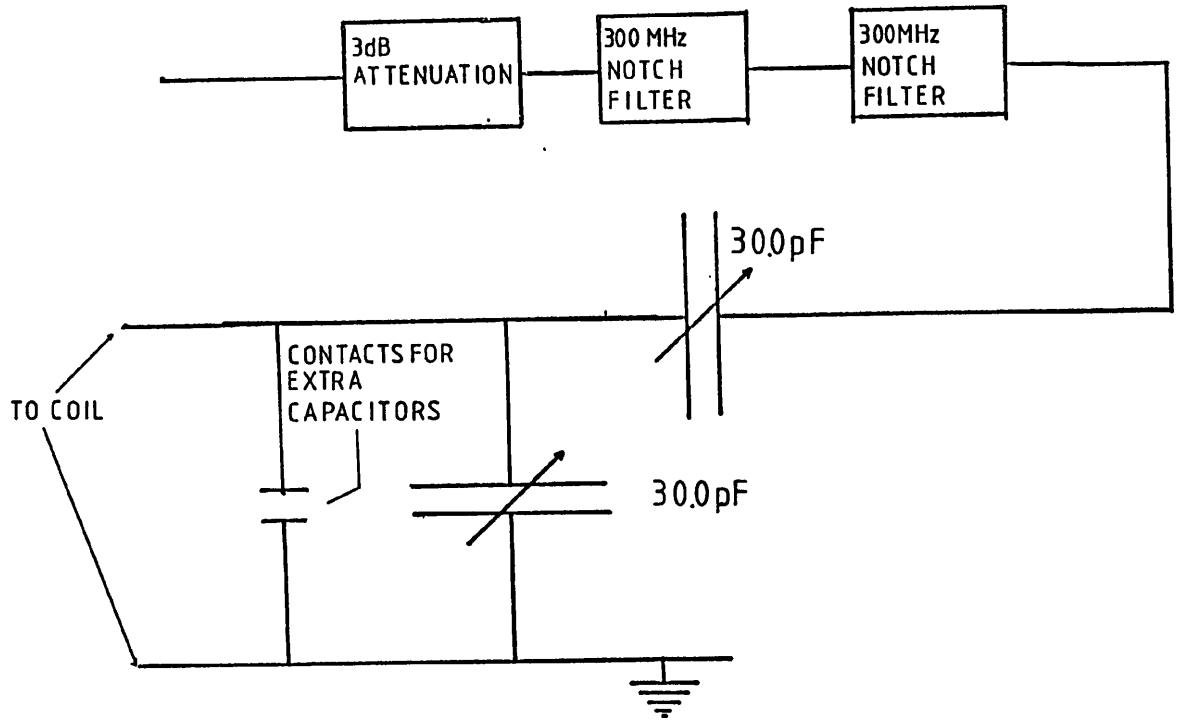

Tuning network for the inserted X nucleus coil. The tuning capacitors are mounted inside the probe. Additional capacitors can be introduced between the contacts, these are mounted close to the coil.

may be introduced by inserting chip capacitors into the contacts provided close to the coil. No additional capacitance is needed to tune the coil to ^{13}C, an additional 200 pf is required for ^{15}N. Using a transmitter with a nominal 100 W output the 90° pulse widths for these two nuclei are 40 and 50 μseconds respectively.

Calibration of the X Irradiation Coil

The inserted coil was calibrated using a modulated spin echo method based on the pulse sequence of ref. (67). The calibration pulse sequence is shown in Figure 4.5; the phases of the θ' pulse and of the detection reference frequency are incremented by 180° on successive blocks of four transients, so that non-satellite signals are subtracted. The behaviour of the satellite signals can be seen from the following product operator description of this sequence.

$$(A)\ H_z \xrightarrow{90°_x} (B)\ -H_y \xrightarrow{\pi H_z X_z} (C)\ H_x X_z$$

$$\xrightarrow{180°_x(H),\ \phi_x(X)} (D)\ H_x(X_z\cos(\phi)-X_y\sin(\phi))$$

$$\xrightarrow{\pi H_z X_z} (E)\ H_y\cos(\phi)\ \text{(only observable term)}$$

For the pulse pair $\theta_x\theta_{-x}$, $\phi=0$ and the detected signal is H_y; for the pulse pair $\theta_x\theta_x$, $\phi=2\theta$ and the detected signal is given as $H_y\cos(2\theta)$. The magnitude of the detected signal in an experiment consisting of a multiple of eight transients is $|H_y(1-\cos(2\theta))|$, the signal therefore has a null at $\theta=180°$. A number of experiments are performed with different values of θ, and the 180° pulse width is found from the signal null. The calibration curve obtained in this way is shown in Figure 4.6.

FIGURE 4.5

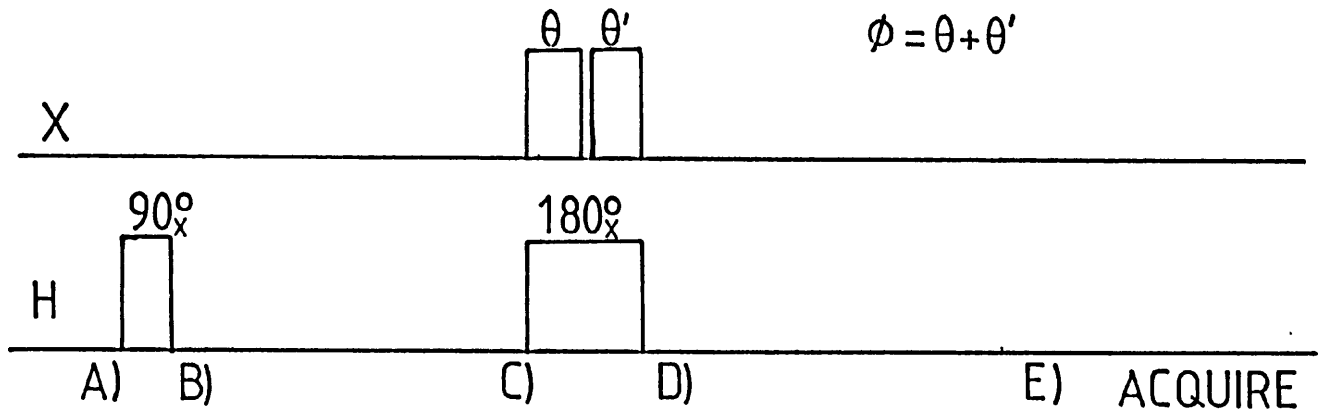

Pulse sequence for calibration of the X nucleus coil. $\theta' = \theta$ or 2θ depending on the form of calibration curve required. The phase of the second X pulse, and of the acquisition reference, is incremented by 180° on successive blocks of eight transients.

FIGURE 4.6

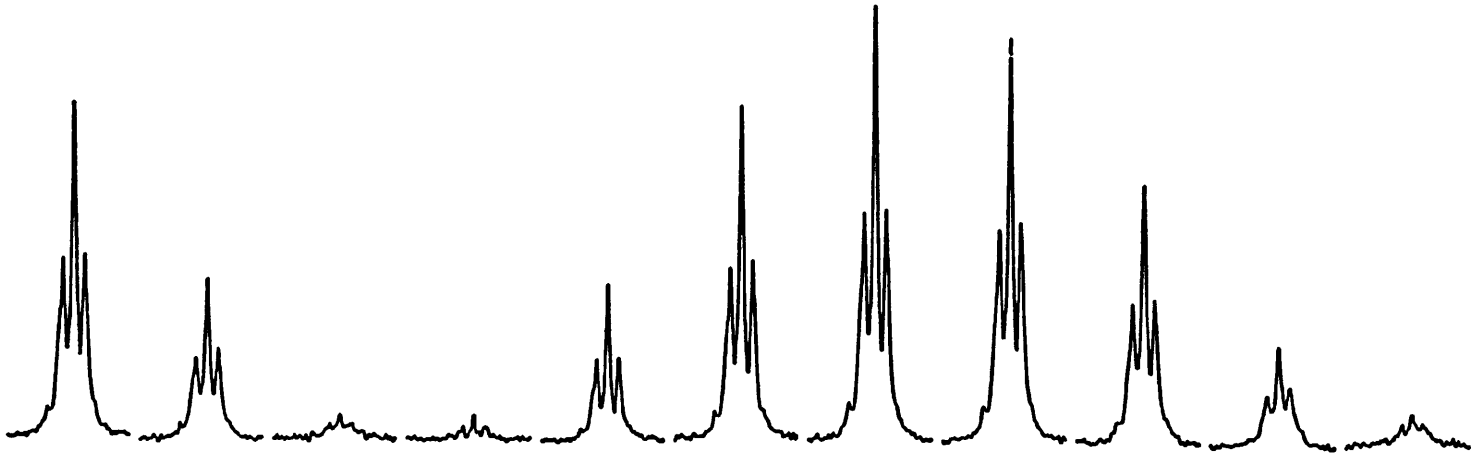

Calibration curve for ^{15}N pulses applied using the modified probe; the sample used was of ^{15}N enriched Boc-Gly-OMe in DMSO-d_6. For this calibration $\theta' = \theta$; the value of θ was incremented in 10 microsecond steps starting from 50 microseconds. A 90° pulse width is around 38 microseconds.

This form of calibration experiment has the disadvantage that the signal intensity never changes sign; application to natural abundance samples is particularly time consuming since considerable time averaging is required if the null is to be accurately located. A slightly modified version of the sequence (68) was found to be useful in this application. This sequence, which is obtained by changing the second X pulse (θ') to $\pm 2\theta$, gives a final signal which depends on θ as $|H_y(\cos\theta - \cos(3\theta))|$. The signal intensity changes sign at $\theta = 90°$, providing a much more easily located null; an example of the use of the modified sequence is shown in Figure 4.7.

The speed with which pulse calibration and pulse sequence optimization could be carried out was considerably increased by the use of ^{15}N enriched samples. Calibration experiments were carried out on a 0.97 M sample of $^{15}NH_4NO_3$ (98% enriched) in DMSO-d_6. A model AX spin system was provided by the nuclei of the BOC-*GLY-OMe amide group. This compound was prepared from enriched glycine (98% ^{15}N), BOC protection was carried out by the method of ref. (69), and methylation by the method of ref. (70).

4.2 Stability

While a number of different approaches have been used in order to reduce the intensity of non-satellite peaks in indirect detection experiments, in all previously reported experiments the removal of these peaks is heavily dependent on phase cycling (section 2.7). In a proton observed ^{13}C experiment the level of suppression required is of the order of 2000:1 for satellite peaks to be observed unhindered by residual parent signals; for ^{15}N the required suppression ratio

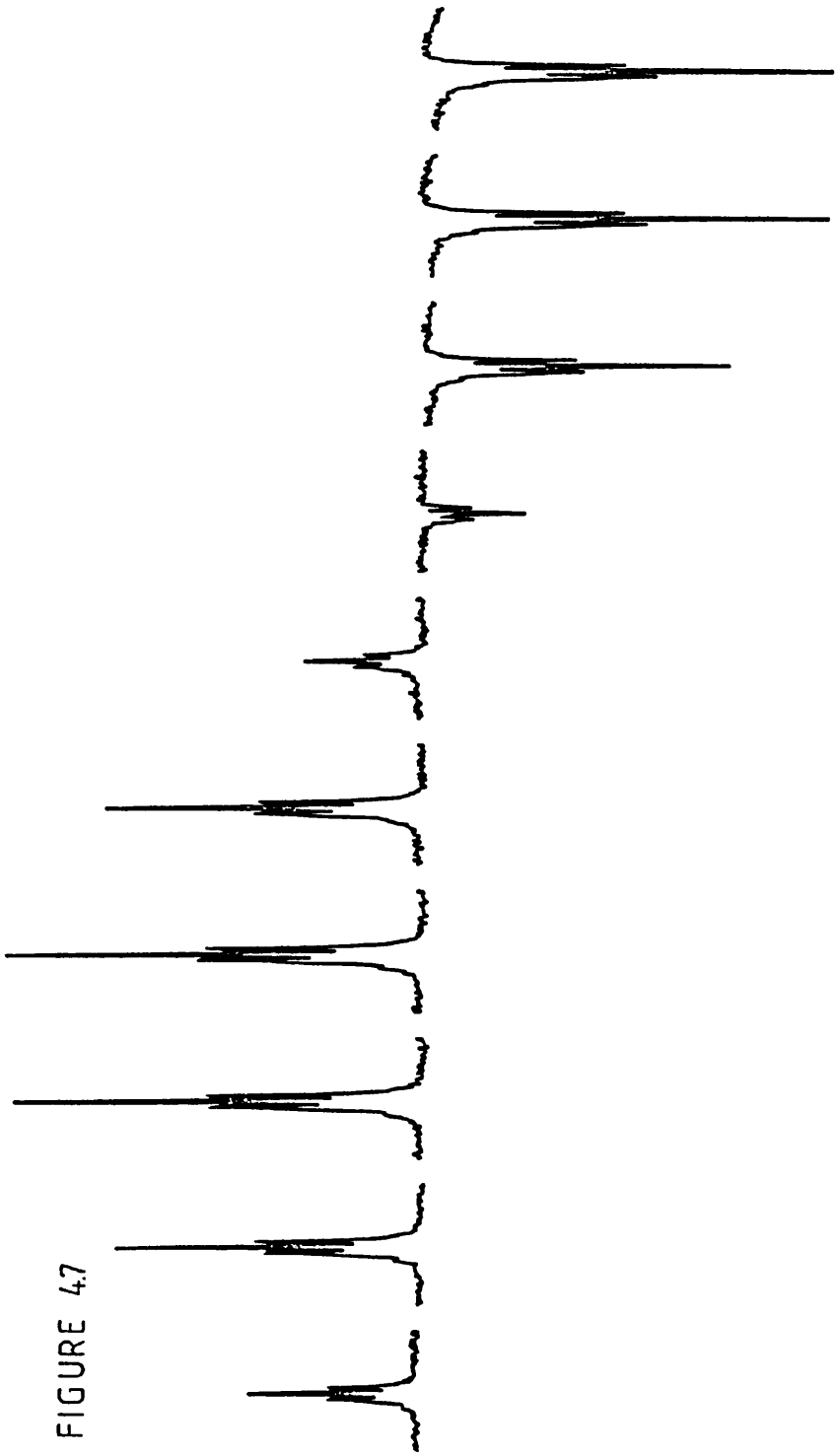

FIGURE 4.7

Calibration curve run on the same sample as used for figure 4.7. In this calibration $\theta' = 2\theta$; the value of θ is incremented in 5 microsecond steps starting at 10 microseconds.

is of the order of 6000:1. Effective removal of parent signals requires that the amplitude and phase of the proton magnetization behaves in a predictable and consistent way. This requires that the amplitudes of the pulses involved in the sequence are constant, and that their phases are set accurately on each transient. Errors in either the amplitudes or phases of the pulses will result in poor suppression. The spectrum of Figure 4.8 shows an early attempt at carrying out an indirect detection experiment using the Varian XL-300 spectrometer; the pulse sequence for this experiment is shown in Figure 4.9 and will be discussed in more detail in Chapter 5. A 50:50 $CHCl_3$:$CDCl_3$ sample was used; to prevent feed through of coherence from one transient to the next the proton T_1 was adjusted to 0.1 sec by addition of $Cr(acac)_3$; the time between transients was 0.9 sec and the total duration of the experiment was 20 hours. The delay between transients was long in relation to the proton T_1 in order to ensure that the signal acquired in each transient originated from an identical well-relaxed state. The poor suppression of the parent signal in this experiment suggested that attempts to apply this experiment to less favourable conditions, such as ^{15}N in the presence of intense signals from aromatic protons, would be unsuccessful.

Since non-equilibrium effects have been eliminated from this experiment the poor suppression must be due to pulse irreproducibilities. It was therefore necessary to carry out a series of experiments to find the cause of this instability.

Using a doped methanol sample a number of identical one-pulse experiments were carried out over a short time, typically 128 experiments over four minutes, each experiment consisting of one 30° pulse.

FIGURE 4.8

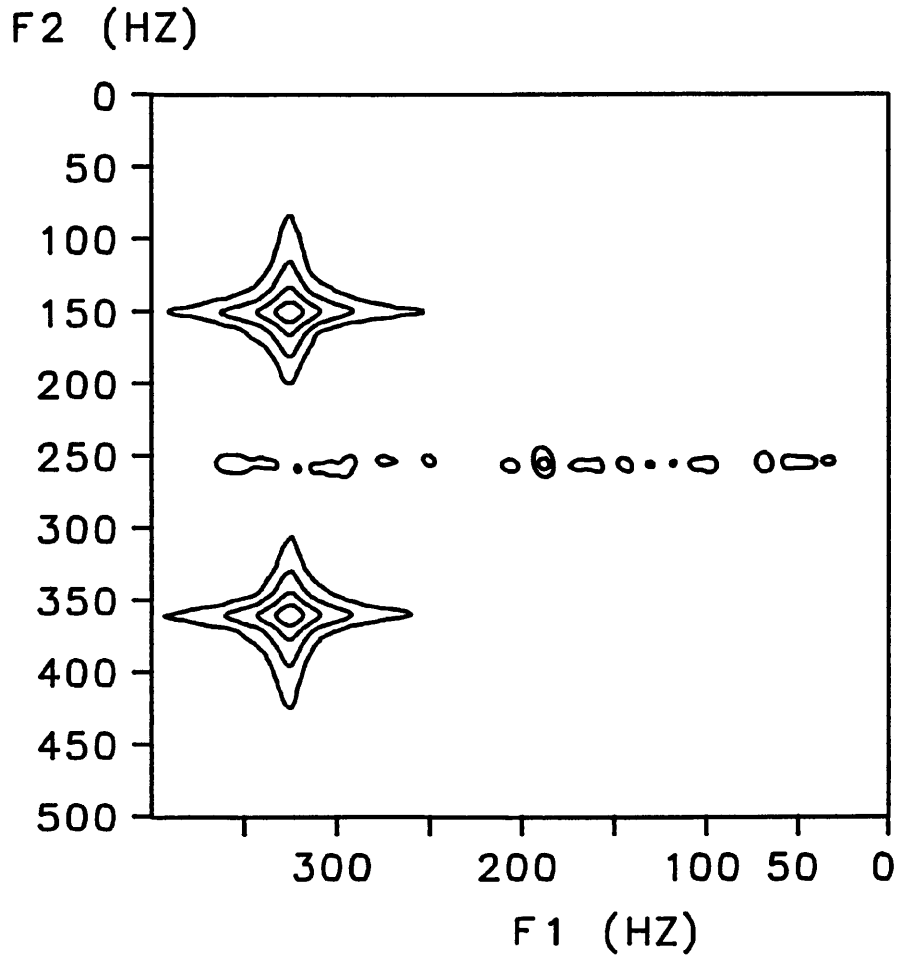

This indirect detection ^{13}C ^{1}H correlation spectrum was produced using the pulse sequence of figure 4.9. The unsuppressed parent signals at 250 Hz in F_2 (unreferenced) illustrate the suppression problems encountered when attempting this type of experiment of a spectrometer of poor pulse reproducibility.

FIGURE 4.9

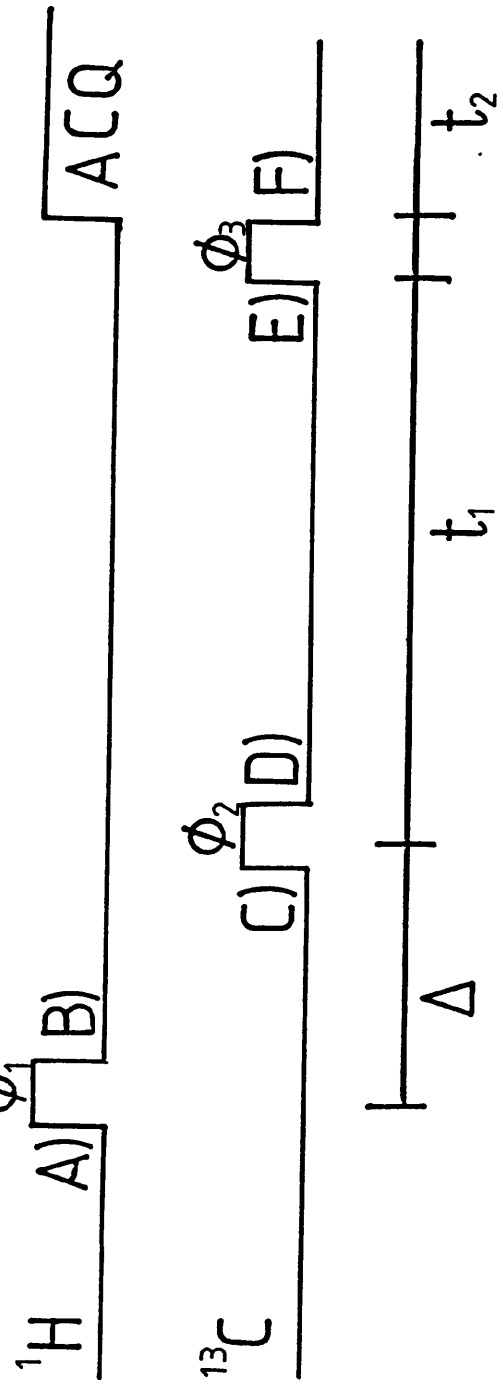

Pulse sequence used to generate figure 4.8. The phases of the pulses are:

$\phi_1 = 0_8 1_8 2_8 3_8$

$\phi_2 = 0_8 1_8 2_8 3_8 -1230$

$\phi_3 = 0$

Acq = -(1230)

$\Delta = 1/2J_{CH}$

The standard deviations, S_p and S_a, of the phase and amplitude of the signals obtained in this way were used as a measure of the stability of the instrument; by repeating this test for different experimental conditions and comparing the reproducibility obtained in each case, it was possible to locate the sources of the instability. For example, the test was carried out with and without the lock, in both cases the standard deviation of the phase error was 2.6° for proton observation and 0.8° for ^{13}C, and interference from the lock was therefore eliminated as a cause of the instability. Similarly it was found that by switching off the gating of the 2.5 MHz signal used in the transmitter frequency synthesis, stability could be improved. Evidently part of the irreproducibility arises from the possibility of gating the 2.5 MHz signal on or off at different points in its cycle.

Master Clock 2.5 MHz Gating	S_p	S_a
OFF	1.5°	20.0
ON	2.6°	117.0

(S_a is given on a scale where 5000 is the full signal height)

An idea of the timescale of the remaining instabilities was gained by carrying out a series of experiments in which different levels of attenuation were included between the transmitter and the coil; the pulse width was adjusted to give the same flip angle (30°) in each experiment. The values of S_p and S_a in these experiments reflect the time taken for the pulse r.f. amplitude and phase to stabilize. Using 20 dB of attenuation (PW30° ~ 30 μsec) S_p was reduced to 0.8°,

S_a was reduced to 10.2; there was therefore a component of the instability which acted on a time scale of less than 30 μseconds. Computer simulation indicated that the remaining instabilities did not arise solely from rounding errors in frequency synthesis.

By carrying out experiments similar to the above it was possible to locate the following faults in the transmitter. Firstly, cross-talk between the decoupler and transmitter frequency synthesisers gave rise to a large component of the amplitude instability. Secondly, it was found that there were 10–20% noise spikes on the transmitter L.O. output. These were traced to a fault in the construction of the transmitter circuit board which caused an intermitent shorting of one of the L.O. filter stages. For a 30° pulse applied with no attenuation, S_p was now 0.5° and S_a 7; these values did not reduce significantly on introduction of attenuation, indicating that the short time scale instabilities had largely been removed.

Initially the decoupler output had a considerable phase drift with respect to the decoupler L.O. (60° over the duration of a 4 minute experiment, see Figure 4.10). Replacement of one of the zener diodes across a power supply rail cured this problem. The low power and high power outputs of the decoupler board were now found to have the following values of S_p and S_a for unattenuated 30° pulses.

	S_p	S_a
Low power (PW 30° = 35 μsec)	0.7°	5
High power (PW 30° = 3.5 μsec)	3°	64
(High power with 20 dB attenuation) (PW 30° = 35 μsec)	1°	1

FIGURE 4.10

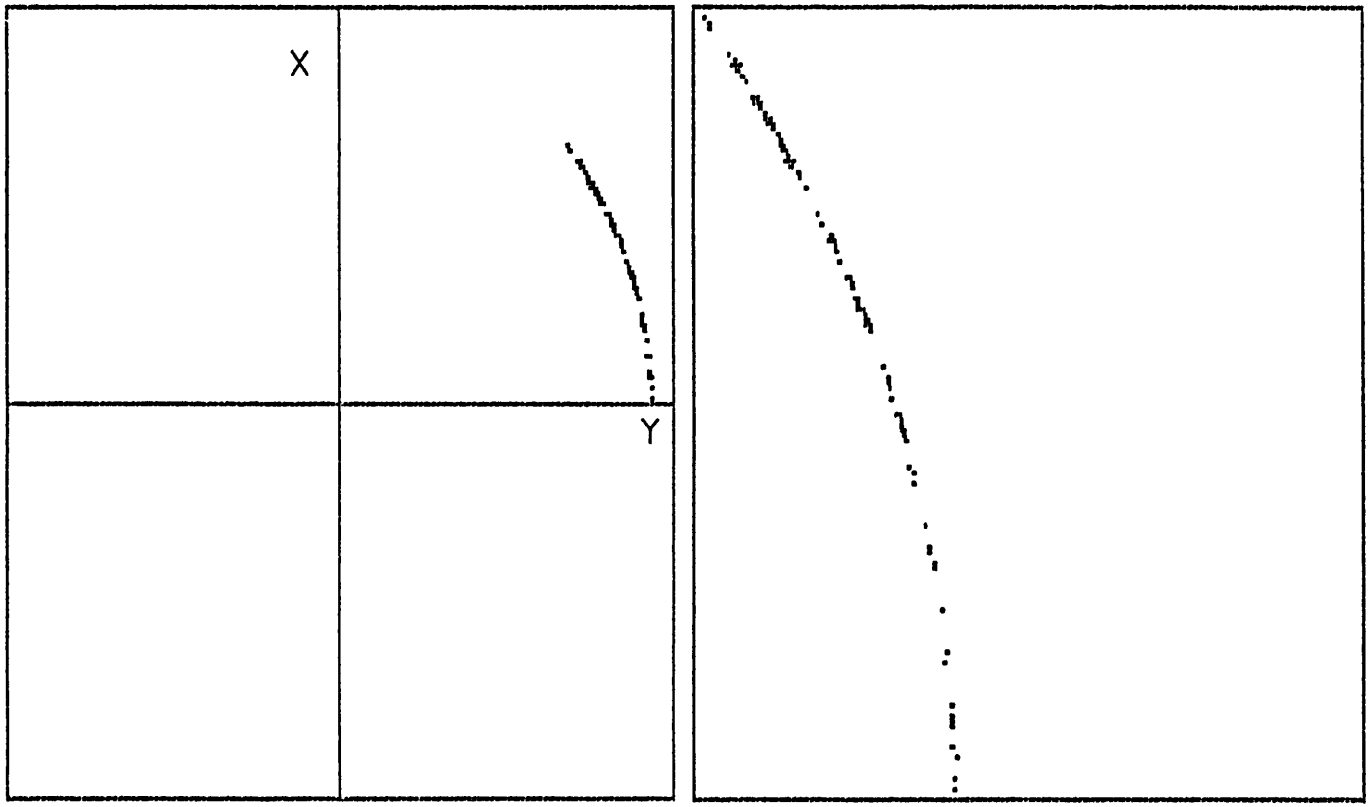

Graph showing the amplitude and phase of the signal observed following a 30° pulse applied by the decoupler to a doped methanol sample. The points on the graph correspond to the position of the tip of the magnetization vector in the xy plane. An expanded plot of the region of interest is shown on the right.

Due to the high reproducibility of the low power output of the decoupler, this output has been used to produce the best results from the three pulse indirect detection sequence.

4.3 Dynamic Range

In an N.M.R. experiment the signal and noise voltages from the detection coil are amplified by a low noise preamplifier (71) before being fed to the main amplification stage of the spectrometer. The amplified signal is then digitized by an analogue to digital converter (ADC); the second amplification stage is provided with variable gain so that degradation of the signal-to-noise can be minimized. For best signal-to-noise the output of the amplifier should reflect, as accurately as possible, the signal-to-noise of the output of the detection coil; this will not be the case if there is a large effect due to thermal noise in the amplifier (noise factor greater than one). The effect of noise originating in the amplifier can be minimized by providing the amplifier with a large gain so that the signal and noise from the detection coil are amplified to a level well above that of the amplifier noise.

Not only does a high gain prevent degradation of signal-to-noise, but it also allows best use to be made of the ADC. For an N bit ADC the maximum possible resolution is 2^{N+1}; this is only achieved if the signal has sufficient amplitude to turn on the most significant bit of the ADC. To achieve the best possible digitization of the signal, the amplifier gain should be set so that the signal amplitude is of the order of the maximum which can be represented by the N bits

of the ADC. Since a signal more intense than this cannot be dealt with by the ADC there is an upper limit on the possible amplifier gain.

In the case of a signal containing more than one component the maximum gain of the amplifier is limited by the amplitude of the sum of the components; for example, if a proton spectrum is acquired from a solution in H_2O the amplifier gain will have to be set low to prevent overload of the ADC. Low gain settings may lead to problems in the digitization of signals of low amplitude; the intensity of the weak components of the signal may fall below the level corresponding to the least significant bit (LSB) of the ADC. Since a change in intensity of less than this value cannot be detected (72) the weak signal will only be accurately digitized if one of the following conditions is fulfilled:

(1) The r.m.s. value of the thermal noise level is greater than the level corresponding to the least significant bit of the ADC. Accurate digitization will then be achieved provided that there is sufficient time averaging.

(2) In a situation where there is little thermal noise, the different time decays of the two components causes their relative contributions to the detected signal to vary as a function of the sampling time. Underestimations and overestimations of the intensity of the weak component will therefore take place at different points during the sampling time. The averaging of these estimations over the whole of the sampling time can lead to accurate intensities of the weak component after Fourier transformation.

(3) For long time averaging, differences between scans can introduce a variability which allows the weak component to be digitized.

In cases (2) and (3) the thermal noise falls below the level which can be digitized; the apparent noise in the spectrum is therefore dominated by quantization errors and Fourier transform noise. In these cases the apparent signal-to-noise ratio after digitization is less than the signal-to-thermal-noise ratio of the amplified signal. Only in case (1) is the best signal-to-noise ratio obtained with correct digitization. To obtain this condition the ADC must be able to digitize the strong signal component, while at the same time its least significant bit must correspond to the thermal noise level of the amplified signal.

The large dynamic range of signals obtained in indirect detection experiments carried out in protonated solvents can result in poor digitization of the correlation signals. This can be seen by considering the case of a 200 mM solution of an amide in H_2O; the concentration of water protons in this sample is 1.5×10^5 times that of the H-^{15}N protons. For the ^{15}N amide proton signals to turn on the LSB of the ADC, and for the water proton signals to be accurately digitized, the ADC would require 17 bits. Since the largest ADC's on commercial spectrometers have only 16 bits, the H-^{15}N signals cannot be accurately digitized in the absence of thermal noise twice as intense as the signals under study. For the spectrometer used in the experimental work of this thesis the signal-to-noise ratio expected for a single transient experiment on

a sample of water, assuming a 1 Hz line width, is 3.4×10^5. For the water proton signal to be digitized by an ADC in which the LSB is of the order of the noise level, a 19 bit ADC would be required. The only way in which the H-^{15}N proton signals can be accurately digitized, under conditions of optimum sensitivity is to reduce the intensity of the water proton signals before digitization.

CHAPTER 5

INDIRECT DETECTION EXPERIMENTS

5.1 (A) Multiple Quantum Methods

The presence of a scalar coupling between the two spins of a heteronuclear spin system, IS, can allow transverse magnetization of either nuclear species to be converted into heteronuclear two spin order. This contains equal amounts of two quantum coherence and zero quantum coherence, which may in turn be reconverted into transverse magnetization of either of the two coupled nuclei. The evolution of two-spin coherence is dependent upon the chemical shifts of both of the nuclei involved; double quantum coherence evolves as $\omega_I+\omega_S$, zero quantum coherence as $\omega_I-\omega_S$. These properties of multiple quantum coherence suggest the following strategy for the enhancement of sensitivity for nuclei of low γ. First the transverse magnetization of the more sensitive nucleus is converted into heteronuclear multiple quantum coherence (M.Q.C.). After the evolution period, t_1, of a two-dimensional experiment the M.Q.C. is reconverted into I spin transverse magnetization which is then detected. In the resulting two-dimensional spectrum proton chemical shifts in the f_2 dimension are correlated with multiple quantum evolution frequencies in the f_1 dimension. Since transverse magnetization is both created and detected through the I spin, the sensitivity of this technique is independent of the magnetogyric ratio of S.

The first experiment to use M.Q.C. in this way was carried out by Mueller (13) using the pulse sequence of Figure 5.1.

FIGURE 5.1

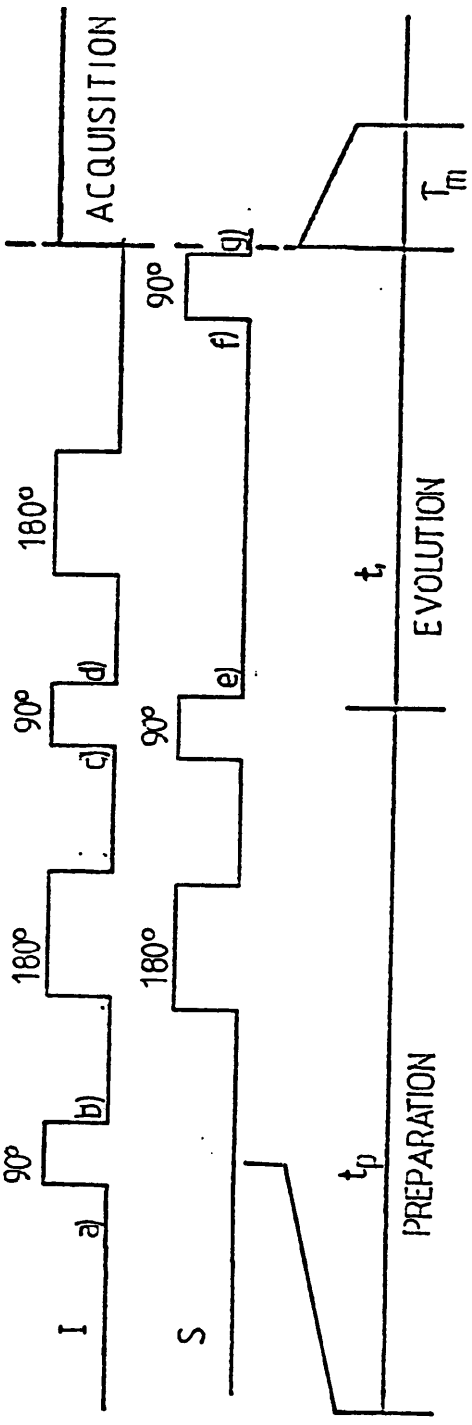

ALL PULSES OF A GIVEN FREQUENCY HAVE THE SAME PHASE

Pulse sequence for heteronuclear multiple quantum coherence spectroscopy.

The preparation period is a heteronuclear version of the simple two pulse scheme used for the generation of homonuclear double quantum coherence, (73) pulses being applied to both nuclear species. The second 90° I pulse has no effect on the generation of M.Q.C. but can help suppress magnetization arising from I nuclei not coupled to S nuclei, or from non-optimum choice of t_p. This sequence shows similarities with the INEPT sequence; in the preparation stage of both sequences initial I spin magnetization is allowed to evolve under heteronuclear scalar coupling while the effects of chemical shift are refocussed. The antiphase I spin magnetization produced is then converted either into antiphase S spin magnetization in the case of INEPT, or into M.Q.C. in the case of the experiment of Mueller. In both cases the antiphase I spin magnetization is converted into the desired coherence by the application of pulses to both nuclear species. The sequences differ in that the I pulses used in the multiple quantum experiment all have the same phase whereas the second I pulse of the INEPT sequence is phase shifted by 90° with respect to the first pulse of the sequence. The mechanism of the multiple quantum sequence can be seen in the following product operator description of the process; here all pulses are assumed to be about the x axis.

(a) I_z

$\downarrow$ 90°(I)

(b) $-I_y$

$\downarrow J_{IS}$

(c) $I_x S_z \sin(\pi J t_p) - I_y \cos(\pi J t_p)$

$\downarrow$ 90°(I)

(d) $I_x S_z \sin(\pi J t_p) - I_z \cos(\pi J t_p)$

$\downarrow$ 90°(S)

(e) $-I_x S_y \sin(\pi J t_p) - I_z \cos(\pi J t_p)$

(generation of two spin coherence)

$\downarrow t_1$

(f) $-I_x(S_y \cos(\Omega_S t_1) - S_x \sin(\Omega_S t_1))\sin(\pi J t_p) - I_z \cos(\pi J t_p)$

$\downarrow$ 90°(S)

(g) $-I_x(S_z \cos(\Omega_S t_1) - S_x \sin(\Omega_S t_1))\sin(\pi J t_p) - I_z \cos(\pi J t_p)$

(regeneration of I spin transverse magnetization)

The 90° pulse at (c) only affects residual I_y magnetization which results from missetting of t_p. Neglecting the effects of relaxation, the $-I_z$ term does not evolve during t_1 but is inverted by the 180° pulse; for perfect pulses this term gives rise to no transverse magnetization and will not be considered further. The term $I_x S_y$ contains equal amounts of double quantum coherence (D.Q.C.) and zero quantum coherence (Z.Q.C.) (section 2.6); these evolve

during t_1. At the mid-point of the evolution period the 180° pulse interconverts Z.Q.C. and D.Q.C. which removes the effects of proton chemical shifts during t_1 so that only the S chemical shift is considered above.

This description of the experiment can easily be extended to larger spin systems; in this case the nuclei involved in the multiple quantum coherence may experience homonuclear scalar couplings which act during t_1. Heteronuclear couplings are not seen in f_1; such couplings between the spins involved in the transition cause no evolution, while couplings to passive nuclei are refocussed by the 180° pulse.

The first term in the expression for the situation at (g) gives the intensity of I transverse magnetization, which is in antiphase with respect to S_z; if S decoupling is to be applied during t_2, a refocussing delay 1/2J must be inserted at (g) in order to allow rephasing of the doublet components. The second term at (g) represents unobservable two spin coherence I_xS_x. Since the only chemical shift modulation during t_1 is ω_S, the form of the spectrum produced by this sequence is a direct shift correlation, the frequency in both dimensions being dependent on just one chemical shift.

A more elegant sequence involving fewer pulses has been demonstrated (26) for the enhancement of ^{15}N. The basic sequence contains only three pulses as shown below.

FIGURE 5.2

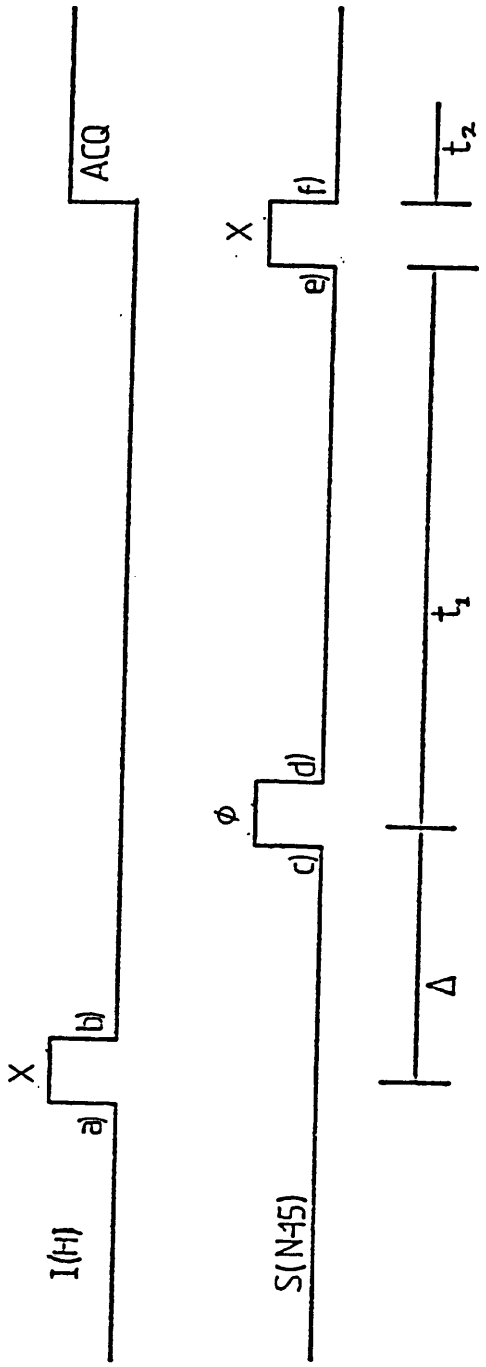

Three-pulse sequence for obtaining indirect detection correlation spectra by use of multiple quantum coherence. All pulses give 90° rotations.

The action of the preparation period is much the same as for the sequence of Figure 5.1; however, as only one 90° proton pulse is applied there is no need to refocus chemical shifts during the preparation period. As in sequence 5.1, the detected I magnetization is in antiphase at the start of the acquisition, so that a refocussing delay must be included if S decoupling is required. The detected signal contains components modulated in t_1 by both zero and double quantum frequencies. In order to determine the sign of the offset of the S resonance frequency relative to the transmitter it is necessary to distinguish between the two coherence pathways. For a signal to be detected the change in the order of coherence at the I pulse must be minus one (section 2.7); thus the change in the order of coherence at the S pulse (d) must be -1 and +1 for zero quantum and double quantum coherence respectively. It can be seen that changing the phase of the first S pulse by 90° changes the phase of the detected signal by -90° in the case of the zero quantum coherence pathway and by +90° in the case of the double quantum coherence pathway. A two step phase cycle is therefore capable of distinguishing between the two pathways. In practice a four step cycle is used, in order to achieve cancellation of signals from I spins not coupled to S spins. Table 5.1 shows how the phases D and Z of the signals from the double quantum pathway and zero quantum pathway respectively are dependent on the phase ϕ of the first S spin pulse.

Table 5.1

Step no.	ϕ	D	Z
1	X	X	X
2	Y	-Y	Y
3	-X	-X	-X
4	-Y	Y	-Y

To obtain both zero and double quantum correlations in one experiment the spectra from steps 1 and 3 are subtracted and stored separately from the difference of spectra 2 and 4. The resulting two data sets can be processed to give either of the correlation spectra. As noise in the Z.Q.C. spectrum is not correlated with that in the D.Q.C. spectrum it is possible to increase sensitivity by co-adding the two spectra. This procedure is not straightforward, as it requires that both spectra are first converted into the form of direct shift correlation spectra. This form of correlation spectrum may be obtained either by modification of the experiment or by manipulation of the spectrum obtained using the original pulse sequence (26). One way in which the experiment can be modified is to include a 180°(I) pulse at the mid-point of t_1 in order to refocus the effect of I spin chemical shifts during this delay; alternatively, the delay between the initial I pulse and the start of acquisition can be fixed so that the duration of evolution under proton chemical shifts is constant, independent of the value of t_1. The data manipulation method of obtaining a direct shift correlation spectrum requires that the spectrum obtained from the three pulse sequence be sheared

according to $(F_1', F_2') = (F_1 + F_2, F_2)$ where $(F_1, F_2) = (\Omega_S - \Omega_I, \Omega_I)$ for a zero quantum spectrum, or $(F_1', F_2') = (F_1 - F_2, F_2)$ where $(F_1, F_2) = (\Omega_S + \Omega_I, \Omega_I)$ for a double quantum spectrum.

The sequence of Figure 5.2 has been used together with ^{15}N labelling to generate a ^{1}H-^{15}N shift correlation spectrum of E.Coli tRNA (28,74,75). To obtain a spectrum of the slowly exchanging imino protons of E.Coli tRNA a six hour acquisition was used for a sample containing 0.5 mM ^{15}N, proton acquisition being at 360 MHz; 'WALTZ' decoupling of ^{15}N was used during acquisition to improve sensitivity, but the full factor of two improvement expected from decoupling was not achieved (74). A similar approach has been used (29) to study the coat proteins of the filamentous bacteriophages fd and pfl. This combination of ^{15}N labelling with M.Q.C. spectroscopy can be particularly powerful when applied to large proteins (33) where the proton spectra are crowded with broad resonances, making assignments difficult in conventional 1-D spectra. Selective ^{15}N labelling results in only a few resonances being observed thereby reducing the overlap problem, while at the same time the ^{15}N chemical shift dispersion greatly increases resolution.

Natural abundance ^{15}N-proton shift correlation spectra of gramicidin-S have been obtained (27) in a 3 hour acquisition on a sample of effective concentration of 36 mM of the sites of interest. The experiment was run at 360 MHz in a 5 mm tube.

In natural abundance studies of rare nuclei a major problem is the elimination of artifacts from protons not coupled to the species of interest. For each molecule containing the spin system of interest there will be a large number of molecules containing the corresponding

abundant isotope spin system. The protons in the more abundant spin systems will have the same chemical shift as the protons under study, but will not have the same heteronuclear coupling; these protons give rise to 'parent' peaks in the proton spectrum. Residual signals from these 'parent' peaks can give rise to artifacts which overlap the region of interest in the proton spectrum. Protons from other spin systems may also overlap this region of the spectrum; an example of this problem is the presence in the spectrum of gramicidin in ref. (27) of signals originating from the protons of the aromatic groups. These signals, which overlap the resonance of the valine amide proton, are particularly difficult to remove by phase cycling alone as their long relaxation times lead to feed through of magnetization from one transient to the next; in addition, their sharp lines make high instrumental stability essential for accurate subtraction. N-H shift correlation spectra run in aqueous solution present particular problems of suppression and dynamic range. Due to the possibility of chemical exchange of the amide protons with the solvent, such spectra often have to be run in H_2O rather than D_2O, and in order to see the correlation peaks it is necessary to suppress the water peaks. This suppression is difficult to achieve by phase cycling alone due to the high instrumental stability which this would require (Chapter 4). Even when H_2O excitation is minimized by the use of selective excitation schemes, the residual solvent signal can still give rise to artifacts which may be folded into the region of interest (30).

If a direct shift correlation spectrum is required, a 180°(I) pulse may be included at the mid-point of t_1 as in the pulse sequence of Figure 5.1. Imperfections in this pulse may cause extra suppression problems and so extra phase cycling may be required in order to remove

the artifacts produced. The effects of an imperfect proton refocussing pulse can be reduced by using a modified form of the 'Jump-return' sequence (76), $90°_x-2\tau-90°_x$ (33,34) in place of the usual 180° pulse. The transmitter is placed on resonance with the signals to be observed and the value of τ is adjusted to $\frac{1}{4}(\nu_{Tx}-\nu_{water})$. Signals on resonance experience a 180° pulse while the water resonance, having changed their phase by 180° during the delay τ, experience a net flip angle of zero. Similarly the initial proton pulse may be replaced by the sequence $90°_x-\tau-90°_y$ (33,34); transverse magnetization is created on resonance while the water proton magnetization is returned to the z axis. In order to prevent the problem of imperfect pulses exciting solvent resonances, the simple three pulse version of the sequence should be used (18) and the proton pulse replaced by a 45° pulse adjusted to minimize excitation of H_2O; for example (28) a Redfield 2-1-4 pulse may be used. This sequence was used to obtain a shift correlation spectrum from 50 mg of bovine pancreatic trypsin inhibitor (MW 65000) in 0.4 ml 90% H_2O 10% D_2O in 11 hours at 500 MHz (18). The zero quantum and double quantum spectra obtained were processed to give direct shift correlations and the resulting spectra co-added to improve sensitivity.

In order to decrease the requirement for high instrumental stability to remove the unwanted parent signals an alternative approach (35) may be used. This technique is restricted to the special case where the electric field gradient at the nucleus is such that there is a significant quadrupole broadening effect for protons bound to ^{14}N. The T_2 of these protons is therefore shorter than the corresponding ^{15}N bound protons. The pulse sequence for this technique is shown as follows.

FIGURE 5.3

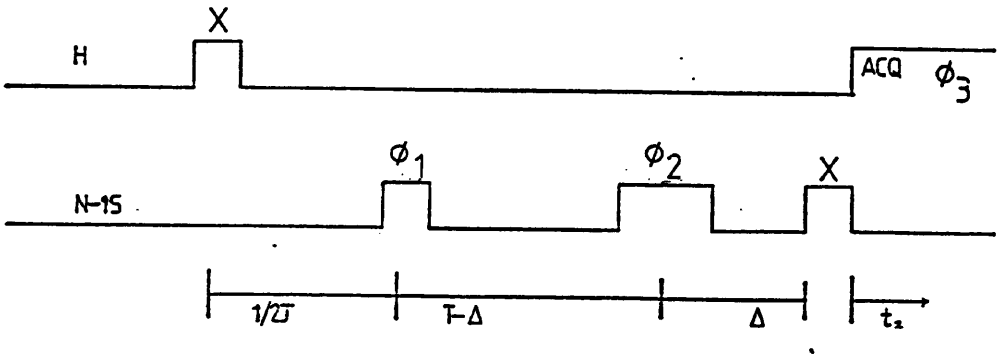

$$\phi_1 = 0,1,2,3$$
$$\phi_2 = 0,1,2,3$$
$$\phi_3 = 0,1,2,3 + 0,2$$

Indirect correlation experiment of reference 35. Narrow pulses give a 90° rotation, wide pulses a 180° rotation.

The first time domain of the experiment is defined by the variable delay Δ between the 180°(^{15}N) refocussing pulse and the 90°(^{15}N) read pulse; $z\Delta_i = t_1$. Incrementation of Δ between successive blocks of transients causes the F.I.D.'s to be modulated in t_1 by the ^{15}N chemical shifts, but retains a constant delay T between creation of M.Q.C. and the detection of transverse magnetization. The delay T is fixed at a value which allows significant relaxation of ^{14}N bound protons. The sensitivity of this technique (the so-called POWER SPIN experiment) S_{ps} compared to that of the H.M.Q. experiment, S_{reg} is given by:

$$\frac{S_{ps}}{S_{reg}} = \frac{2T.\exp(-t/T_2)}{T_2[1-\exp(-2T/T_2)]}$$

It is claimed that a four-fold improvement in parent peak suppression can be achieved with minimal loss of sensitivity by use of the correct T value, but such optimization requires a knowledge of the T_2 values involved. In addition the significant difference between the T_2 values of protons in the two spin systems, which is necessary for this technique to work, is not common. The constant time delay used in this experiment has the added effect of suppressing proton chemical shifts and proton-proton couplings in f_1; the resulting spectrum is therefore a direct shift correlation. For large molecules, where the range of T_2 values is small, it may be that the only advantage of this experiment over H.M.Q. is the form of spectrum produced.

For ^{13}C shift correlation experiments on small molecules, problems due to the detection of unwanted signals can be reduced by use of a modified pulse sequence (32) in which all protons not directly attached to the low γ nucleus are saturated at the start of the experiment. Protons coupled to the low γ nucleus are unaffected (or for molecules in the fast motion limit can be slightly intensified by the homonuclear N.O.E. effect). To achieve this effect a 'BIRD' sequence is applied at a time τ before the first proton pulse of the sequence, Figure 5.4.

The total time between the start of detection in one transient and the excitation pulse of the next transient is T; by suitable optimization of this delay and of Δ it can be arranged that longitudinal magnetization of all the inverted transitions is close to zero just before the first proton pulse of the H.M.Q. sequence. Not only does this facilitate the removal of unwanted peaks, but it also helps avoid dynamic range problems (19). Application of this technique is limited due to negative N.O.E. effects in larger molecules, which will tend to decrease the intensity of protons coupled to ^{13}C. However it has been pointed out (18) that for macromolecules the suppression of signals from protons not attached to ^{13}C is not such a problem. First, their broad lines make suppression less susceptible to magnetic field fluctuations. Second, the relatively low concentrations used mean that to obtain acceptable sensitivity considerable time averaging is needed, which helps to reduce the intensity of the unwanted peaks.

An extension of the H.M.Q. experiment provides correlation spectra for determination of long-range $^{1}H-^{13}C$ connectivities (20) in the

FIGURE 5.4

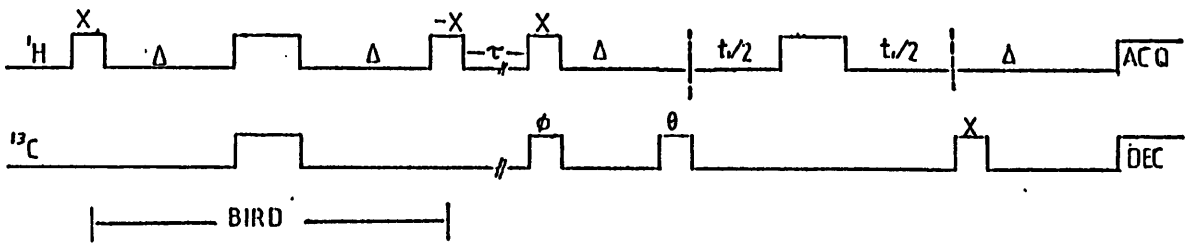

BIRD-HMQ pulse sequence. Narrow pulses give a 90° rotation, wide pulses a 180° rotation. $\Delta = 1/2J$

$90°_{\phi}$ = presaturation pulse

$90°_{\theta}$ is cycled as ϕ in Table 5.1

$T = \tau + 2\Delta$ + acquisition time.

presence of one bond couplings as a more sensitive alternative to the H,C-COLOC experiment. The pulse sequence for this experiment is shown below.

FIGURE 5.5

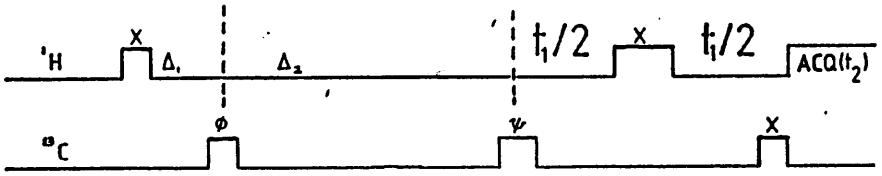

Δ_1 is optimized for the generation of multiple quantum coherence between directly connected nuclei (Δ_1=1/2 $^1J_{CH}$); by alternating the phase ϕ along the $\pm x$ axis but leaving the acquisition phase constant, peaks arising from one-bond connectivities can be removed. The delay Δ_2 allows proton transverse magnetization to evolve under the two-bond or three-bond heteronuclear coupling $^nJ_{CH}$, and the pulse 90°ψ then generates multiple quantum coherence between the two coupled spins. After the evolution period t_1 the 90°$_x$ ^{13}C pulse regenerates proton transverse magnetization, which is then detected. The signal is modulated in t_1 by ^{13}C chemical shifts and by homonuclear proton couplings. As with the conventional H.M.Q. experiment, signals from

protons which do not participate in the desired multiple quantum transitions are removed by phase cycling the ^{13}C pulses and adjusting the receiver phase accordingly. The full phase cycling for this sequence is shown in Table 5.2.

Table 5.2

Step	1	2	3	4	5	6	7	8
ϕ	X	X	-X	-X	X	X	-X	-X
ψ	X	-X	X	-X	Y	-Y	Y	-Y
Rx	X	-X	X	-X	Y	-Y	Y	-Y

Absorption mode 2D spectra cannot be produced by this sequence as the signal is phase-modulated by homonuclear scalar couplings during the long delay Δ_2. The data collection procedure used in the four-pulse H.M.Q. experiment cannot therefore be used in this experiment. Instead, the receiver is cycled through all four phases, together with the second ^{13}C pulse, in order to introduce artificial phase modulation and the spectrum is then displayed in the absolute value mode. Multiple-bond correlation spectra for the high-field proton and high field carbon resonances of coenzyme B_{12} have been obtained using this sequence (19,20). As with the one-bond connectivity experiments, peaks correlated with the protons of a methyl group show the highest intensities, but they also suffer from the highest level of t_1 ridges originating from protons not coupled to ^{13}C. If a proton has more than one long-range coupling then the intensity of each cross peak can be related to the relative magnitude of the coupling constant; use may be made of this dependence in conformational studies.

The detection of a nucleus by a method in which sensitivity is independent of γ is particularly attractive for use with $^{57}Fe(\gamma=\gamma_H/31)$; the first application of indirect 2-D N.M.R. to this nucleus was reported by Benn and Brevard (21) in their study of (η^5-cyclopentadienyl).1,2-ethanedylbis(diphenylphosphane).hydridoiron. This compound has an unusually high $^1J(Fe,P)$ (61.6 Hz, all previous reported values being less than 35 Hz) which was made use of in a ^{31}P observed ^{57}Fe indirect experiment. This allowed an accurate value of $\delta^{57}Fe$ to be measured; using this information, a ^1H observed ^{57}Fe indirect experiment was obtained yielding information on J(P,Fe) and $^2J(P,H)$. The proton observed experiment used an 8%(w/w) solution of the compound in toluene d_8 in a 5 mm N.M.R. tube inserted in a 10 mm probe; the total acquisition time was 2 hours at 300 MHz.

^{113}Cd is another nucleus of low γ ($\gamma=\gamma_H/4.5$) for which indirect observation would seem to be of advantage. For ^{113}Cd studies of metalloproteins, direct observation has several problems; the magnetogyric ratio of ^{113}Cd is negative and so its signals may be nulled under conditions of partial N.O.E., and the ^{113}Cd nuclei of interest have long T_1 values due to the absence of directly bonded protons. In such complexes correlation experiments must rely on long-range (two or three bond) couplings; the presence of several such couplings makes the system very susceptible to the generation of higher orders of coherence thereby lowering the yield of the experiment. It is claimed (22) that the benefits of detecting the nucleus of higher γ more than compensate for such losses, and that even in the presence of extra couplings the H.M.Q. method gives good sensitivity. Such an experiment has been carried out (22) on $^{113}Cd_6$-metallothionein (MW~6000) using 0.4 mL of a 3 mM sample, with a total acquisition time of 10 hours.

Use can be made of $^{1}H-^{113}Cd$ H.M.Q. spectroscopy in the characterization of metalloproteins such as spinach (Spinacia oleracea) plastocyanin (23). The only proton resonances to appear in the H-Cd shift correlation spectra are those from amino acid side chains which ligate the cadmium. This subspectrum identifies the resonances from the metal ligand residues. Another advantage of indirect observation over conventional shift correlation experiments is that the indirect experiment gives the higher digital resolution in the proton dimension where it is most needed (24). For metallothioneins containing few cadmium ions the two-dimensional technique may not be necessary, the appropriate information being obtained from a one-dimensional variant of the experiment in which t_1 is fixed at a small value (24).

There is no necessity for the $^{1}H-^{113}Cd$ coupling to be resolved for these techniques to work, but attention has to be paid to the coupling constants involved and to possible losses by T_2 relaxation. In practice, where a wide range of J values is present in the molecule a number of experiments with different Δ values may have to be performed (23,24,25). Some correlations may remain undetectable due to efficient transverse relaxation during Δ (24), or due to very small values of J. The latter situation may be an unavoidable result of the stereochemistry involved; for example the Karplus relationship predicts that for cysteine residues ligating Cd^{2+} one member of a β-CH_2 pair should have a small coupling when the other has a large coupling (24).

Phase modulation due to scalar coupling during the refocussing delay may prevent pure absorption spectra being recorded, thus hindering the measurement of $^{1}H-^{113}Cd$ J values. It has been suggested (25) that the effects of such modulation may be removed by the application of

'purge' procedures. A ^{113}Cd 90° pulse applied immediately before acquisition will convert proton magnetization out of phase with respect to the ^{1}H–^{113}Cd coupling into heteronuclear multiple quantum coherence, thus preventing its detection. The same result could be achieved by the use of ^{113}Cd decoupling during acquisition. In order to remove the effects of ^{1}H–^{1}H couplings it may be necessary to use a z filter $90°_{x}(H)\ \tau_z\ 90°_{\xi}(H)$ just before acquisition, τ_z being varied during time averaging. The use of extra pulses in this way to achieve absorption mode 2D spectra may lead to experimental problems; it has been reported (19) that when used in ^{13}C–^{1}H correlation experiments the extra pulse may lead to a reduction of sensitivity and cause problems with suppression of protons not bound to ^{13}C.

5.1 (B) Polarization Transfer Methods

An alternative to the multiple quantum experiment for indirect observation is the use of polarization transfer. Transverse magnetization of the insensitive nucleus, enhanced by polarization transfer from protons, is allowed to precess for a time t_1 before a second polarization transfer step. The second step regenerates proton magnetization, which is then detected. A two-dimensional spectrum obtained in this way correlates proton chemical shifts in f_2 with X nucleus chemical shifts in f_1. The first experiment to use this approach, carried out by Bodenhausen and Ruben (12), is illustrated below.

FIGURE 5.6

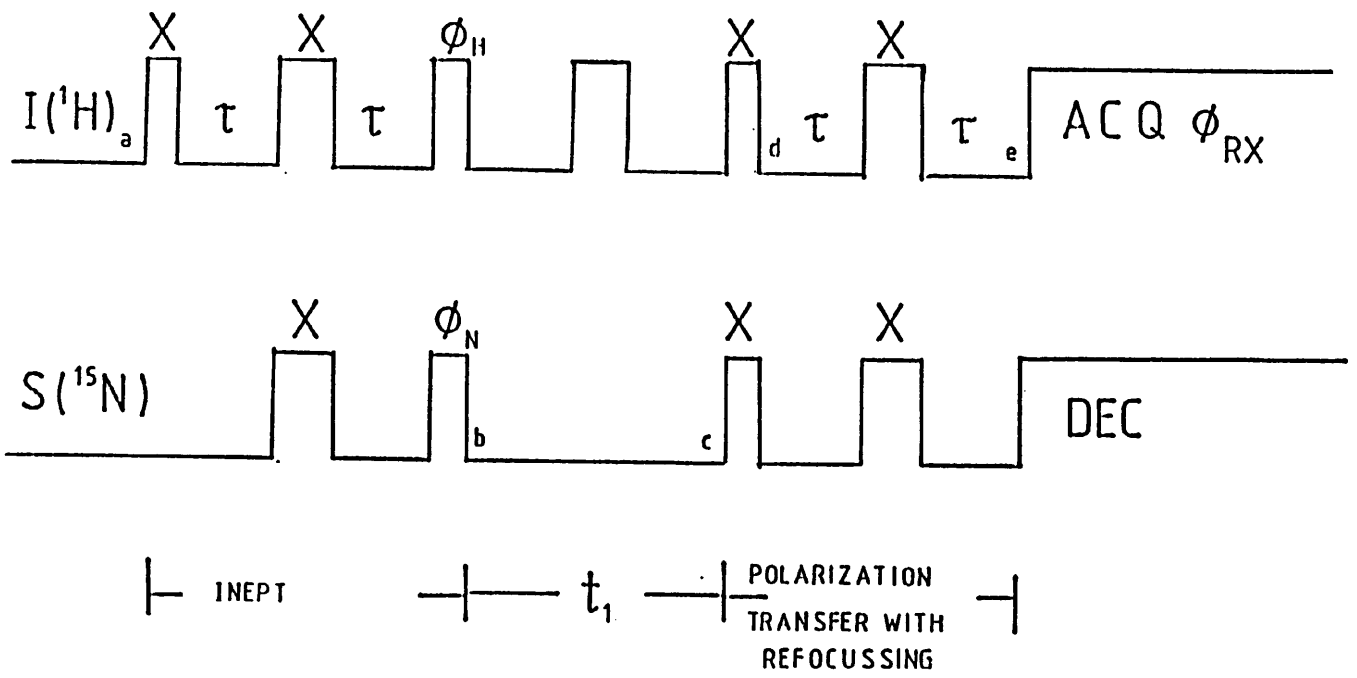

Indirect correlation experiment of reference 12. The phase cycling for this experiment is shown in Table 5.3.
Narrow pulses give a 90° rotation, wide pulses a 180° rotation.

From a to b this is an INEPT sequence, the transferred signal at b for a system IS and for an optimized value of τ is given by I_zS_y. The situation at b can be discussed in terms of the population differences (Chapter 2) which exist across the S spin transitions. The population differences associated with the two S transitions at b are $2\Delta+2P$ and $-2\Delta+2P$ where equilibrium population differences are 2Δ for spin I and 2P for spin S. If the phase of the second 90° I pulse is changed to -y the corresponding population differences are $-2\Delta+2P$ and $2\Delta+2P$. In the original experiment the phase of this pulse was alternated and alternate F.I.D.'s subtracted in order to remove the 2P dependence. It will be shown below that the 2P term has no effect (77) provided a 180° pulse is included at the mid-point of t_1.

During t_1 the system evolves under S spin chemical shifts only, heteronuclear scalar couplings being refocussed by the 180°(I) pulse. The situation at c is described by,

$$I_zS_y\cos(\Omega_S t_1)-I_zS_x\sin(\Omega_S t_1)$$

Polarization transfer back to I is now carried out by the two 90° pulses.

$$I_zS_y \xrightarrow{90_x(S)} I_zS_z \xrightarrow{90_x(I)} -I_yS_z$$

$$-I_zS_x \xrightarrow{90_x(S)} -I_zS_x \xrightarrow{90_x(I)} I_yS_x$$

(unobservable multiple quantum coherence)

The 2P term discussed above originates from the equilibrium population across S spin transitions; at b this gives rise to in-phase magnetization which, provided that a 180°(I) pulse is applied at the mid-point

of t_1, remains in phase at c. Since this magnetization cannot be transferred to the I spins it is not necessary to employ phase cycling to suppress it.

The out-of-phase magnetization $-I_y S_z$ is refocussed during the delay d to e. Acquisition of the free induction decay $S(t_2)$ at e for various values of t_1 followed by double Fourier transformation produces a two-dimensional shift correlation spectrum of I chemical shifts against S chemical shifts.

As in the case of the simplest H.M.Q. experiment, the elimination of signals from I spins not coupled to S spins relies on phase cycling of S pulses. Phase cycling of the first $90°_I$ pulse and the first $90°_S$ pulse as in Table 5.3a removes parent peaks and signals originating from imperfections in the $180°_I$ pulse. The reduced form of the phase cycle, for use where imperfections in this pulse are not expected to be a problem, is shown in Table 5.3b.

Table 5.3a	$90°_I$	$90°_S$	Acq
	+	+	+
	+	−	−
	−	−	+
		+	−

Table 5.3b			
	+	+	+
	−	−	+

The spectra produced by this sequence suffer from the presence of a large number of artifacts, the intensities of which are

proportional to the signal intensity. In addition the absence of any saturation mechanism or semiselective pulses in this sequence means that its application in H_2O (15) suffers from the problems mentioned in Chapter 4. In an attempt to reduce the complexity of this experiment, a modified sequence has been used (15) in which the 180° pulses are removed leaving a heteronuclear sequence for the observation of stimulated echoes. This sequence suffers from reduced resolution in the f_1 dimension and poor sensitivity, particularly if attempts are made to include solvent suppression.

The sequence of ref. (12) has been used to improve the sensitivity of ^{199}Hg in studies of adducts of ethyl mercury phosphate with amino acids and with ribonuclease (16,17). The enhancement of ^{199}Hg by indirect observation is important in this application not only because of the low magnetogyric ratio and low natural abundance (16.9%) of ^{199}Hg, but also because the directly observed Hg signal decays rapidly and so causes problems due to its requirement for a short receiver off delay.

Despite the growing use of indirect observation experiments, as yet no full analysis of the enhancement available by these techniques has been presented. The claimed dependences of sensitivity on γ^3 (31) or $\gamma^{5/2}$ (16) fail to take into account factors such as the difference in Q of the detection coils at different frequencies, the different line widths of the two species, and the different repetition rates of the experiments. Since the actual enhancement observed is also dependent on both the spectrometer and the sample, these claimed enhancement factors are misleading and should not be used to predict the signal-to-noise ratio expected from an indirect detection experiment.

Previously reported indirect detection techniques require a high level of instrumental stability for good suppression to be obtained; the level of suppression achieved, even for a pulse sequence using extensive phase cycling, is heavily dependent on the stability of the N.M.R. spectrometer's R.F. system. Methods aimed at reducing the dynamic range problem for samples run in protonated solvents require careful optimization for the solvent used; these sequences also increase the level of stability required in order to obtain artifact free spectra. There is at present in the literature no generally accepted technique which can achieve the required suppression over a wide spectral width for application in protonated solvents.

5.2 The NEMESIS Pulse Sequence for Indirect Detection

5.2 (A) Introduction

The suppression and dynamic range problems associated with indirect detection experiments arise from the fact that signals are acquired from all of the protons in the sample. In order to overcome these problems it is necessary to arrange that the only signals detected and digitized are those originating from protons in the desired spin system; transverse magnetization from all other protons must be suppressed before the start of acquisition. The presence of the heteronucleus in the desired spin system provides a mechanism by which this may be achieved. For example, initial proton saturation followed by polarization transfer from the heteronucleus ensures that the only proton transverse magnetization present during acquisition is that associated with protons of the heteronuclear spin systems.

This approach has been used in a proton observed C-13 correlation experiment based on an inverse-INEPT sequence (78). This experiment for ^{1}H observed ^{13}C detection was primarily designed to obtain shift correlation spectra in which the greater digital resolution is in the proton dimension, rather than to provide a means of sensitivity enhancement, but it illustrates a convenient approach to parent peak suppression and the reduction of the dynamic range of the signals. Saturation was achieved by irradiating the protons at the start of each transient; irradiation for 1 second was sufficient to achieve the desired level of suppression but a 4 second irradiation was used in order to build up a favourable N.O.E. This N.O.E. enhancement helped improve the sensitivity of the experiment. While this approach is of use for nuclei of positive magnetogyric ratio its use may be

undesirable for nuclei of negative γ since signal loss may occur due to incomplete N.O.E. enhancement. In addition, the repetition rate of the experiment is limited in this experiment by the T_1 of the hetero-nucleus rather than that of the protons, thus the sensitivity of the technique is reduced due to reduced time averaging.

A more widely applicable approach would have to incorporate proton signal suppression into a sequence in which the initial polarization as well as the detected magnetization is associated with proton transitions. Such a sequence would have its sensitivity determined by proton parameters alone, but would have none of the suppression and dynamic range problems associated with the H.M.Q. experiment. In an experiment of this type polarization transfer from protons to the X nucleus would be followed by attenuation of proton magnetization, and a second polarization transfer step, from the X nucleus to protons, would then be carried out before the start of data acquisition.

In order to prevent losses due to X nucleus relaxation the suppression scheme for such an experiment would have to be short compared to $T_1(X)$, this may limit the achievable level of suppression. Since complete saturation of protons can only be obtained on a time scale of $\sim 5T_1$, the attenuation of proton magnetization has to rely on spatial randomization, for example, by means of field gradients applied parallel to the z axis (section 5.2(D)); this introduces the further requirement that the X nucleus magnetization be aligned along the z axis during the proton suppression delay. A pulse sequence which fulfils these requirements is introduced below; in section 5.3 this experiment will be compared with existing indirect detection techniques. Extensions of the basic experiment will be discussed in

sections 5.5, 5.6, 5.7, while the observed sensitivity advantage of indirect detection will be discussed in section 5.4.

5.2 (B) Pulse Sequence Description

Figure 5.7 illustrates a pulse sequence which has the properties discussed above. From (A) to (F) this is a refocussed INEPT experiment carrying out polarization transfer from protons to the X nucleus. At (F) the enhanced X nucleus magnetization is in phase along the x axis, and the $90°_{y}(X)$ pulse aligns this magnetization along the z axis at (G). The delay (G) to (H) is included to achieve suppression of proton signals (section 5.2(D)); pulses are applied to the protons and field gradients are applied parallel to the z axis, randomizing proton magnetization while leaving X-spin z magnetization unaffected. X nucleus transverse magnetization is then regenerated and is allowed to precess during the evolution period t_1; proton decoupling is applied during this delay so that correlation peaks are singlets in f_1. A second polarization transfer step (J) to (N) transfers magnetization back to protons, and the resulting proton signal is acquired; X nucleus decoupling may be applied during acquisition.

This experiment may be regarded as a modified form of the experiment of Bodenhausen and Ruben (12) involving a delay during which the enhanced X nucleus magnetization is stored and proton magnetization is randomized. Due to the form of this experiment it has been given the acronym NEMESIS (N.M.R. Enhanced Measurement Entailing Successive INEPT Sequences). A product operator description of the sequence is given below for a two spin system; it is assumed that all delays have been optimized ($\Delta_1=\Delta_2=1/2J$).

FIGURE 5.7

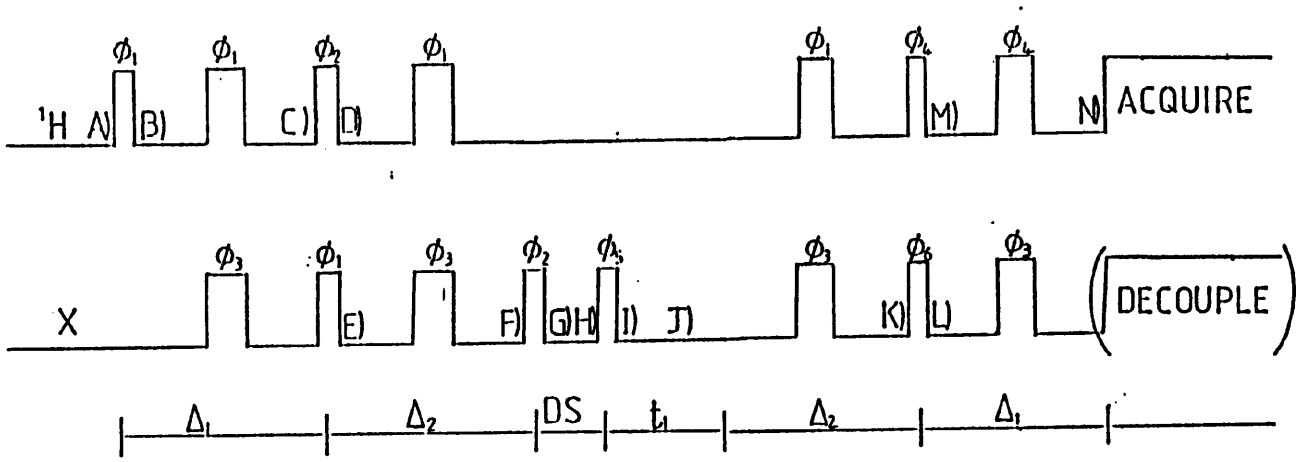

Pulse sequence for the NEMESIS experiment, the phases of the pulses are as shown in Table 5.5. Narrow pulses give a 90° rotation, wide pulses a 180° rotation. To achieve randomization of proton coherences field gradients and proton irradiation are applied during the saturation delay DS.

$$\text{(A) } H_z \xrightarrow{90°_x(H)} \text{(B) } -H_y \xrightarrow{\pi J\Delta_1 2H_zX_z} \text{(C) } H_xX_z$$

$$\xrightarrow{90°_y(H)} \text{(D) } -H_zX_z \xrightarrow{90°_x(X)} \text{(E) } H_zX_y$$

$$\xrightarrow{\pi J\Delta_2 2H_2X_z} \text{(F) } -X_x \xrightarrow{90°_y(X)} \text{(G) } X_z$$

(polarization storage)

$$\text{(H) } X_z \xrightarrow{90°_x(X)} \text{(I) } -X_y \xrightarrow{\Omega_x t_1 X_z}$$

$$\text{(J) } -X_y\cos(\Omega_x t_1)+X_x\sin(\Omega_x t_1)$$

$$\downarrow \pi J\Delta_2 2H_zX_z$$

$$\text{(K) } X_xH_z\cos(\Omega_x t_1)+X_yH_z\sin(\Omega_x t_1)$$

$$\downarrow 90°_y(H)$$

$$\text{(L) } X_xH_x\cos(\Omega_x t_1)+X_yH_x\sin(\Omega_x t_1)$$

$$\downarrow 90°_x(X)$$

$$\text{(M) } X_xH_x\sin(\Omega_x t_1)+X_zH_x\sin(\Omega_x t_1)$$

$$\downarrow \pi J\Delta_1 H_zX_z$$

$$\text{(N) } X_xH_x\cos(\Omega_x t_1)+H_y\sin(\Omega_x t_1)$$

The first term at (N) represents unobservable heteronuclear two spin coherence, the second represents in phase proton transverse magnetization modulated in t_1 by the X nucleus chemical shift as $\sin(\Omega_X t_1)$. Phase shifting of the X pulse at (H) by 90° allows a second F.I.D. to be obtained, in which the detected signal has a cosine modulation with respect to t_1; the two data sets obtained in this way can be processes by the hypercomplex method (41) to obtain phase sensitive spectra.

Figure 5.8 shows an example of a spectrum obtained using the NEMESIS pulse sequence for an 80 mM solution of the cyclic decapeptide antibiotic gramicidin S in DMSO-d_6; due to the symmetry of this molecule the effective concentration of the sites of interest is 160 mM. The sensitivity and suppression levels in this spectrum will be discussed in later sections; the assignments of the resonances in this spectrum are shown in Table 5.4.

FIGURE 5.8

Proton detected nitrogen-15 correlation spectrum of Gramicidin S (80 mM in DMSO-d_6) obtained using the NEMESIS pulse sequence. Assignments of the resonances in this spectrum are shown in Table 5.4.

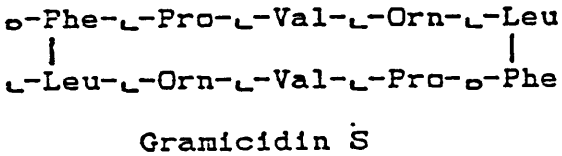

Gramicidin S

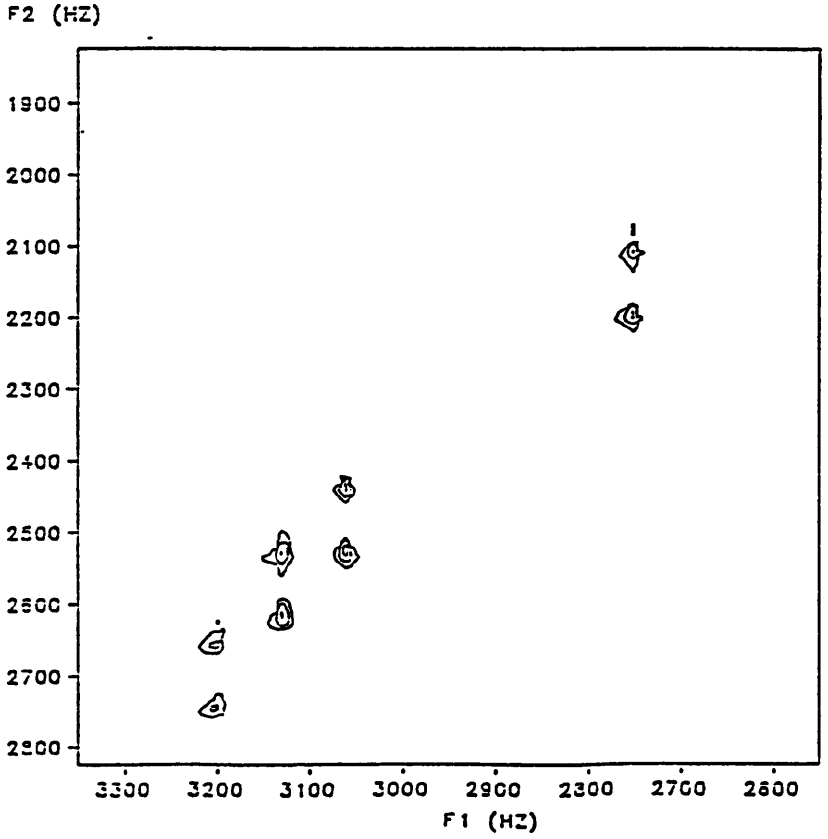

Table 5.4

^{1}H and ^{15}N chemical shifts for Gramicidin S in DMSO-d_6 at 30°C

Residue		Val	Leu	Orn	Phe
Amide ^{1}H	expt. (a)	7.1	8.2	8.5	8.9
	lit. (b)	7.22	8.31	8.62	9.11
Amide ^{15}N	expt. (c)	90.55	100.70	102.98	105.26
	lit. (d)	112.91	123.05	125.18	126.93
α protons	expt. (a,e)	4.32	4.47	4.65	---
	lit. (b)	4.42	4.58	4.77	4.36

(a) Referenced externally to Me_4Si at 30°C. See Figure 5.8.

(b) Reference 79, referenced to Me_4Si at 22°C, no temperature correction has been applied.

(c) Referenced externally to $^{1}NH_4NO_3$ in DMSO-d_6.

(d) Reference 80, referenced to NH_3 at 25°C and corrected to 30°C.

(e) See Figure 5.19.

5.2 (C) Optimization of the Sequence

The product operator description given above may easily be extended to larger spin systems, and to non-ideal cases, by remembering that it is only the X magnetization which is in phase at (F) that is stored, and that at (N) it is only the in-phase proton magnetization which is observed in an X-decoupled experiment. The dependence of the signal intensity on the spin system involved, its J values and the lengths of the delays can then be calculated by modifying the formula of Sørensen and Ernst (49); this formula (equation [5.1]) gives the magnitude of the observable magnetization σ_f in an S-observed INEPT sequence for a spin system $I_N S$.

$$\sigma_f \alpha \sin(\pi J\Delta_1)\sin(\pi J\Delta_2)\cos^{N-1}(\pi J\Delta_2)S_x \qquad .....[5.1]$$

Where S_x = operator for in-phase x magnetization of nucleus S.

For two successive polarization transfer steps this equation becomes,

$$\sigma_f \alpha \sin^2(\pi J\Delta_1)\sin^2(\pi J\Delta_2)\cos^{2N-2}(\pi J\Delta_2)S_x \qquad .....[5.2]$$

Equation [5.2] may be checked by comparison with the results of a density matrix computation; a comparison of this type is shown in Figure 5.9 for a spin system consisting of two protons and one S nucleus. In this simulation the lengths of the delays (A) to (C) and (L) to (N) are fixed at 1/2J and the delays (E) to (F) and (I) to (N) are varied as Δ_2. As expected the maximum signal is seen at Δ_2 = 1/8J, and a null is seen at Δ_2 = 1/4J. The good agreement of equation [5.2] with the density matrix calculation confirm that this formula can be used for optimization of the sequence.

FIGURE 5.9

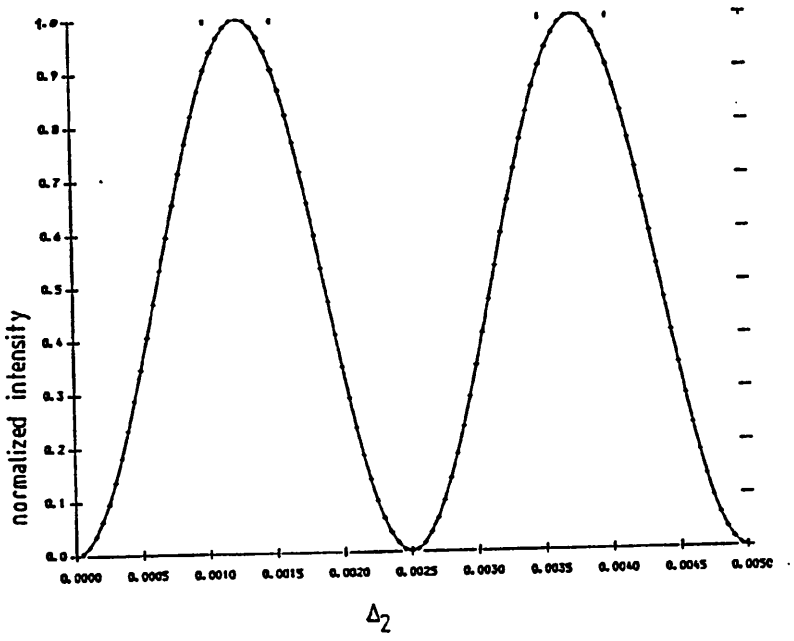

Comparison of formula 5.2 (crosses) with density matrix calculation (solid line) for the optimization of the NEMESIS pulse sequence. A three spin system AX_2, has been used and the intensities of the X detected signals have been normalized with respect to the maximum obtainable yield of the experiment. Both coupling constants are 100 Hz.

5.2 (D) Suppression of Non-Satellite Signals

The aim of the suppression scheme incorporated into the sequence at (G) is to reduce the intensity of the proton signals detected at (N) which arise from any coherence pathway other than double polarization transfer. This has two effects: firstly, it reduces the dynamic range of the signal, allowing better digitization of the satellite peaks, and secondly, it reduces the level of stability required of the spectrometer in order to obtain artifact-free spectra. The delay (G) to (H) has to be short in order to prevent significant T_1 relaxation of the enhanced X spin population difference. Since a residual proton signal at (N) will arise from any net proton coherence at (H); this should be minimized in order to gain the dynamic range advantage. The main component of the signal at (N) which originates from this coherence should have a constant phase so that it can be accurately removed by the phase cycling scheme.

The unwanted signal at (N) may be reduced by randomization of the residual coherence at (H); this can be arranged by making the phase of coherence vary between different regions of the sample. By making this phase a rapidly varying function of position in the sample the sum of the coherence over the whole of the sample may be greatly reduced. This apparent randomization may be achieved by the use of proton irradiation and field gradients. Randomization by proton irradiation is achieved by making use of inhomogeneities in the coil supplying the irradiation; variation in the R.F. field strength over the sample results in different regions of the sample experiencing different pulse amplitudes. It is found experimentally that, for the relatively short irradiation pulses of the NEMESIS sequence, suppression is most efficiently achieved if coherent

irradiation is used. By not using rapid phase changes, this 'randomization' scheme avoids the formation of rotary echoes and so makes best use of the spacial inhomogeneity of the RF field. This should be contrasted with the approach of ref. (81) in which randomization is used as a means of spectral editing. This reference claims that the use of random 90° phase changes results in 'spherical randomization' of proton spins due to spacial inhomogeneity of the RF field, and results in a cancellation of ^{13}C magnetization from selected spin systems. It has been shown (82) that for the long periods of irradiation used in this application, spacial inhomogeneity is not necessary to achieve this type of randomization.

The use of field gradients in addition to proton irradiation can provide an extra level of suppression. In combining the two suppression techniques care must be taken to avoid echo formation. A period of proton irradiation included between two field gradient pulses may act as an apparent 180° pulse over some region of the sample; in this case an echo may be formed if the two field gradients are applied in the same direction. The use of field gradients applied about different axes has been reported in ref. (83) in order to suppress broad water proton signals in experiments carried out <u>in vivo</u>. Here each field gradient is used only once and a selective 90° pulse is applied to the water resonances between gradient pulses; a suppression ratio of 1000:1 is obtained for a 64 transient experiment. In the NEMESIS experiment the only field gradient which is available on the spectrometer used is parallel to the z axis. Using the field gradient pulse, it is found that a delay of 8×10^{-3} seconds is sufficient to obtain a reduction in intensity of a water proton signal by an order of magnitude. Longer field gradient pulses may be used to obtain higher

levels of suppression but for samples containing low concentrations of lock material any gain in randomization may be outweighed by reduced efficiency of the phase cycling due to lock instability.

It was found experimentally that best suppression was obtained by applying the field gradient pulse before the proton irradiation; coherent irradiation was then applied about the x axis for 0.04 seconds and then about the y axis for 0.06 seconds. In a single transient acquisition, preceded by four 'steady state' transients this suppression scheme achieved a suppression ratio of the order of 1000:1, a 60 dB reduction in the dynamic range of the signal can therefore be achieved for experiments run in protonated solvents. Additional levels of suppression are achieved by phase cycling, as described below.

The main requirement of the phase cycling scheme for the NEMESIS experiment is to distinguish transverse magnetization originating from the double polarization transfer pathway from any residual magnetization which has survived the proton suppression scheme. Since the second polarization transfer step starts from in-phase X-spin magnetization, initial X-spin coherence can also give rise to observable proton magnetization, unlike the case in the experiment of Bodenhausen and Ruben (12). In order to suppress such signals, phase cycling must be incorporated to ensure that only magnetization originating from the first polarization transfer step is acquired. The appropriate phase cycling can be achieved by applying a phase shift of 180° to the phases of the first proton pulse and the first 90°(X) pulse in alternate blocks of 8 transients, while keeping constant the relative phase of the receiver reference. It will be shown in section 5.6 that this phase cycling does not remove any signals originating from X spin T_1 relaxation during the delay (G) to (H), but since this delay is short in the basic NEMESIS sequence such signals do not cause any observable

effects in the spectra obtained. A similar phase alternation is applied to the two pulses involved in the second polarization step, a 180° phase shift being applied to alternant blocks of 32 transients.

Additional levels of phase cycling are provided to eliminate any signals originating from pulse imperfections. The receiver reference phase and the phases of the final two proton pulses have an additional level of phase cycling; their phases are incremented by 90° on each transient so that the detected signal takes all four possible phases; this has the effect of suppressing zero frequency artifacts in t_2. The full phase cycling scheme for the experiment is shown in Table 5.5.

Table 5.5

$\phi_1 = 0_8 2_8$

$\phi_2 = 1$

$\phi_3 = 0,2$

$\phi_4 = 1_{16} 3_{16} + 0_{32} 2_{32} + 0123$

$\phi_5 = 0_{32} 2_{32} + \text{'phase'}$

$\phi_6 = 1_{16} 3_{16}$

Acquisition = 0123

(The convention of ref. (4) has been used that $\phi_1 = 0_8 2_8$ means that the phase of ϕ_1 is 0 (the $\dot{x}$ axis) in the first eight transients and 2 (the $-\dot{x}$ axis) in the next eight transients.)

During the acquisition of the first and second data sets the parameter 'phase' is set to 0 and 1 respectively.

The combination of phase cycling and randomization can achieve a high level of suppression of unwanted proton signals. The systematic component of the residual signal which survives the suppression sequence is removed by the phase cycling; using that described above, a suppression ratio of 10000, can be obtained in a 64 transient experiment on a sample of 90% water, with four steady state transients used before the start of the experiment. On longer acquisitions a corresponding increase in the suppression ratio is not seen, the level of suppression then becoming dependent on the stability of the machine over the duration of the experiment.

Figure 5.10 shows an expansion of the amide region of a spectrum obtained in 12 hours from a 50 mM solution of gramicidin S in 60/40 methanol/methanol-d_4. The full spectrum is shown in Figure 5.11 together with a projection onto the proton frequency axis. Comparison of this spectrum with the conventional one-dimensional proton spectrum shown in Figure 5.12 illustrates the reduction in dynamic range which the NEMESIS sequence provides. Suppression of the methanol proton signals in the indirect detection experiment was by a factor of ~30000. The signal-to-noise ratio of the slowly exchanging amide protons in this spectrum is 30:1 indicating no significant loss of sensitivity and no dynamic range problems (for comparison of this sensitivity with that obtained in a non-exchanging deuterated solvent see section 5.4). The level of suppression obtained allowed spectra to be run in H_2O; a spectrum obtained from 140 mg of bacitracin in 0.9 g of water (90% H_2O, 10% D_2O) is shown in Figure 5.13.

Table 5.6

^{1}H and ^{15}N chemical shifts for Gramicidin S in methanol at 30°C

Residue	$\delta^{1}H$		$\delta^{15}N$	
	expt.(a)	lit.(b)	expt.(c)	lit.(d)
Val	7.83	7.73	93.04	118.07
Leu	9.02	8.80	101.68	127.33
Orn	8.79	8.70	101.38	125.93
Phe	8.91	8.90	102.95	127.03

(a) At 30°C internally referenced to methanol peak. See Figure 5.6.

(b) Reference 79, assignments made at 22°C, no attempt has been made at temperature correction.

(c) Externally referenced to $^{15}NH_4NO_3$ in DMSO-d_6.

(d) Reference 80, referenced to NH_3 at 22°C and temperature corrected to 30°C.

Caption to Figure 5.10

Amide region of a proton-nitrogen shift correlation spectrum of Gramicidin S obtained from a 50 mM solution in 60:40 methanol:methanol-D_4. ^{15}N 'WALTZ-16' decoupling was applied during t_2. A 64 ms acquisition time was used per transient; for both values of the 'phase' parameter 256 transients were acquired for each of 64 t_1 increments. The repetition time of the experiment was 1.3 seconds giving a total acquisition time of 12 hours. The spectrum was processed with a line broadening of 10 Hz in f_2 and 3 Hz in f_1. Assignments of the resonances in this spectrum are shown in Table 5.6.

FIGURE 5.10

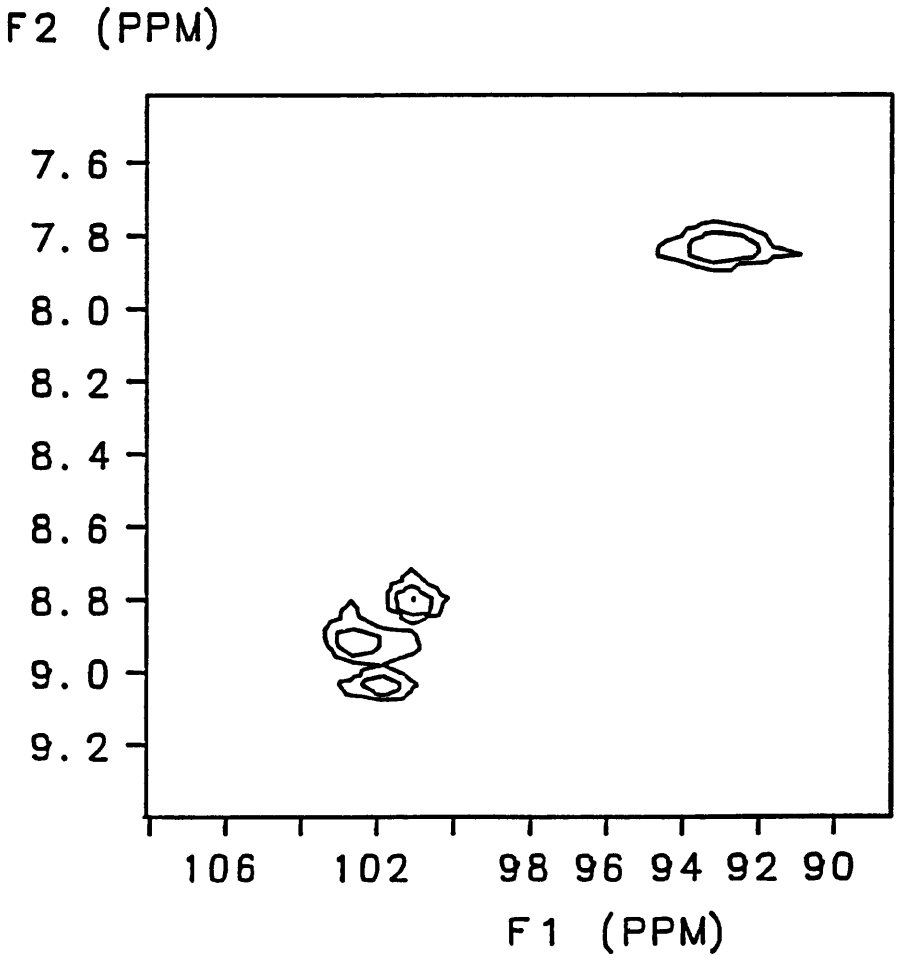

FIGURE 5.11

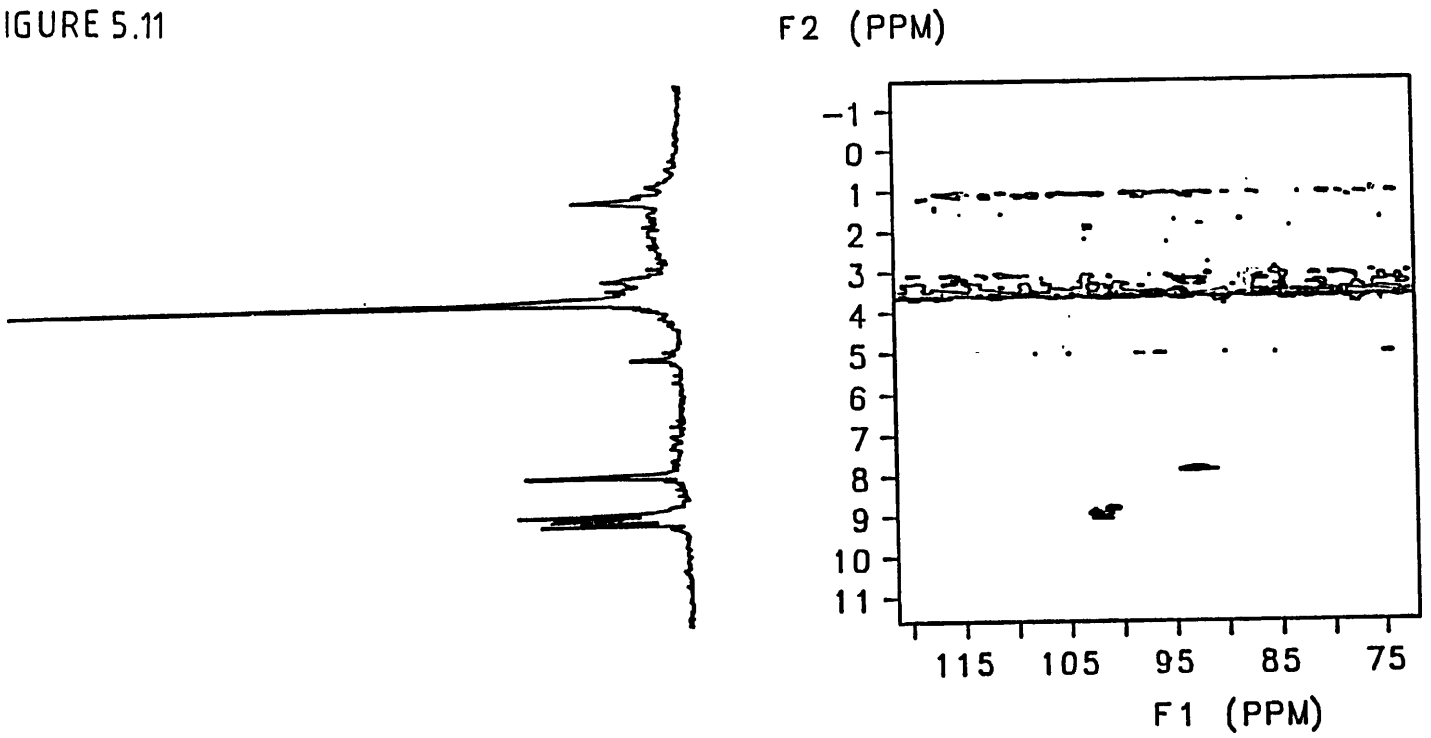

Right, full spectrum of figure 5.10, the solvent peaks in this spectrum are suppressed by a factor of around 30000.

Left, maximum value projection of the two-dimensional spectrum.

FIGURE 5.12

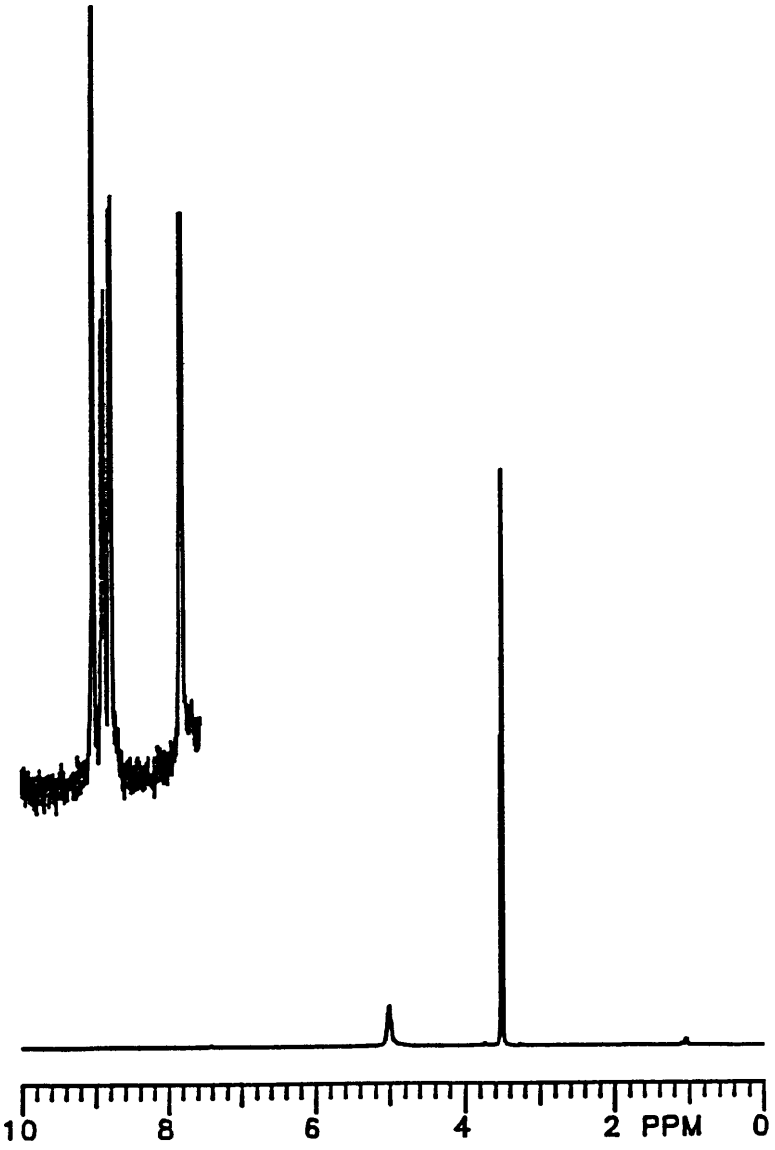

One-dimensional proton spectrum of the sample used in figures 5.10 and 5.11. The inset shows the amide proton region of this spectrum with the vertical scale enlarged by a factor of 1000.

FIGURE 5.13

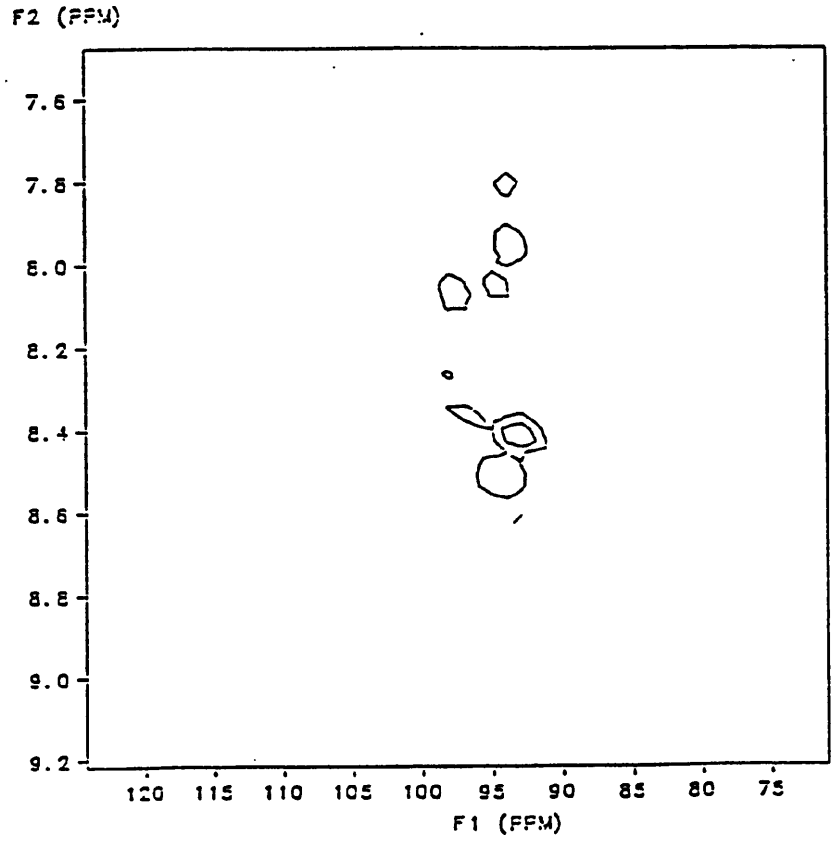

^{15}N-^{1}H Shift correlation spectrum of the slowly exchanging amide protons of bacitracin. The sample contained 0.143 g of bacitracin (Sigma, ref.84) in 0.818 g water (10% D_2O, pH~3). For each of 32 t_1 increments 128 transients were acquired, 64 for each value of the 'phase' parameter. The total acquisition time of this experiment was 90 minutes.

5.3 Comparison of Results with those from H.M.Q. Experiments

In addition to suppression considerations, the NEMESIS experiment has a number of advantages over H.M.Q. Firstly, in the basic H.M.Q. experiment evolution during t_1 is under the chemical shifts of both nuclei involved in the multiple quantum coherence; this results in a spectrum in which proton chemical shifts are correlated with the multiple quantum frequency. Reprocessing of the data (26) is necessary if a direct shift correlation spectrum is required or if the zero and double quantum spectra are to be co-added to improve sensitivity (section 5.1). A further drawback of this form of spectrum is the fact that optimization of the spectral width in f_1 requires some initial knowledge of the way in which the chemical shifts of the two species are correlated. The inclusion of a 180° proton pulse at the mid-point of t_1 can give the desired form of spectrum and allow phase sensitive spectra to be obtained, but results in greater suppression problems (18). In the NEMESIS experiment, evolution during t_1 is under X nucleus chemical shifts alone, therefore producing a direct shift correlation spectrum without further modification or data manipulation.

The use of proton decoupling during t_1 of the NEMESIS experiment removes the effects of both heteronuclear and proton-proton homonuclear couplings from the f_1 dimension. Proton decoupling during t_1 is not possible in the basic version of the H.M.Q. experiment since this would mix the multiple quantum transitions; spectra produced by the H.M.Q. sequence may therefore show multiplet structure in f_1 arising from homonuclear couplings. Due to the properties of M.Q.C. discussed earlier, heteronuclear couplings between the spins involved in the

multiple quantum coherences are not seen in f_1, long-range heteronuclear couplings may be unresolved in this dimension.

Proton irradiation during t_1 may be incorporated into a modified form of the H.M.Q. experiment (85,86). By refocussing the effects of chemical shifts during the preparation period it can be arranged that the density operator of the heteronuclear spin system at the start of t_1 is $H_x Y_y$, so that proton irradiation about the x axis of the proton rotating frame spin-locks the H_x component. Evolution during t_1 is therefore free of the effects of proton chemical shifts and of proton-proton couplings. This variant on the H.M.Q. experiment has been used as the basis of a technique by which resolved X nucleus spectra may be obtained in an inhomogenous field; in this application improved suppression of non-satellite peaks is claimed by the following mechanism. Proton magnetizations of non-satellite signals are represented by the density operator I_y at the start of t_1, proton irradiation applied along the x axis has the effect of dephasing this magnetization due to inhomogeneities in the radio frequency field. This dephasing is claimed to reduce the intensity of the non-satellite signals, but it should be pointed out that since the period of irradiation is short and variable the level of suppression achieved in this experiment should not be expected to be high.

The spectra of Figures 5.8 and 5.14 illustrate a comparison of the use of H.M.Q. and NEMESIS techniques for obtaining ^1H-^{15}N correlation spectra of gramicidin S; both spectra were obtained from 80 mM solutions in DMSO-d_6. The sensitivity of these experiments will be dealt with in section 5.4 and will not be considered here. Spectrum 5.14 shows the result of a 12.5 hr H.M.Q. experiment, 2400 transients were acquired for each of 64 increments, the acquisition time per

FIGURE 5.14

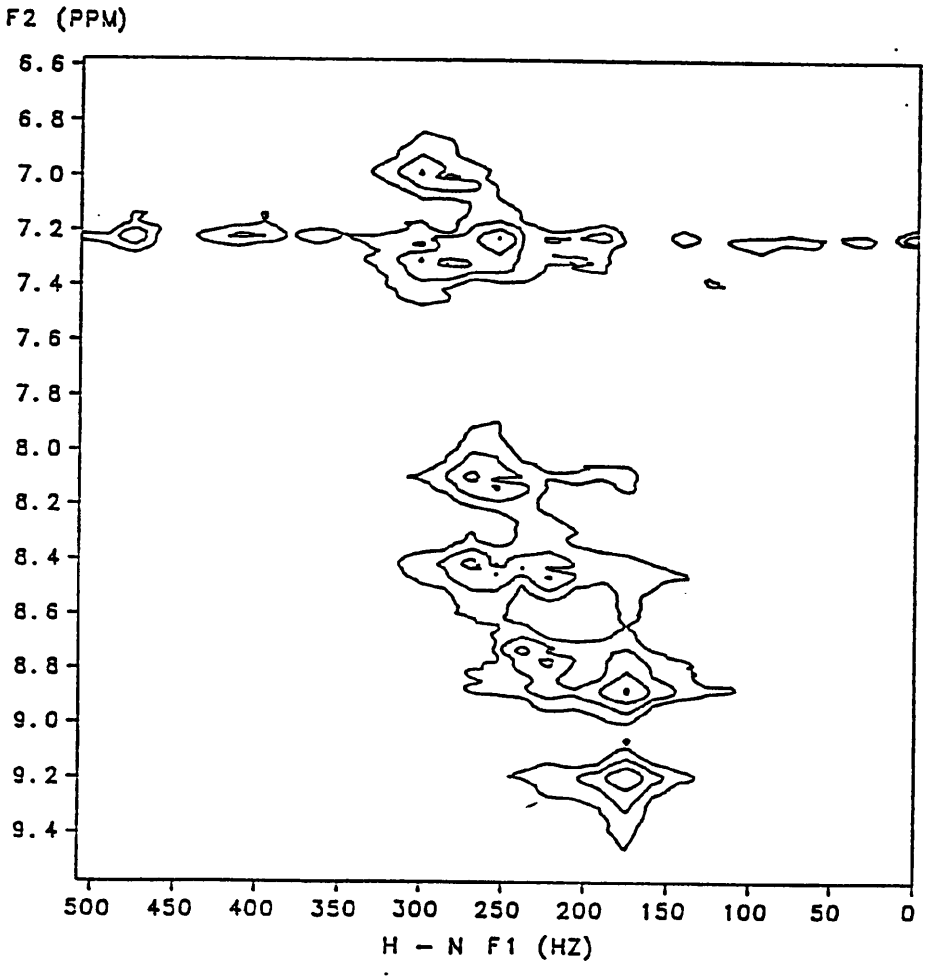

Indirect detection spectrum obtained from an 80 mM solution of Gramicidin S in DMSO-d_6 using the three pulse version of the HMQ technique (see Table 5.7). The total acquisition time was 12.5 hours, no ^{15}N decoupling was applied during t_2.

transient was 0.142 sec. The delay, D1, between successive transients was optimized according to equation [2.67] for the 60° proton pulse used and for a proton T_1 of 0.4 sec. The simplest, three pulse, version of the H.M.Q. experiment was used with the phase cycling of Table 5.7, and no decoupling was applied during t_2. The effects of homonuclear couplings in both dimensions can clearly be seen on the peaks in the range 8.0 to 8.8 ppm in f_2.

Table 5.7

For sequence

$90°_{\phi_1}(^1H)$ (1/2J) $90°_{\phi_2}(^{15}N)$ t_1 $90°_{\phi_3}(^1H)$ Acquire

$\phi_1 = 0_8 1_8 2_8 3_8$

$\phi_2 = 0_8 1_8 2_8 3_8 - 1230$

$\phi_3 = 0$

Acq = -(1230)

The poor suppression in this spectrum illustrates the problems associated with this type of experiment when carried out on a spectrometer of poor pulse reproducibility (Chapter 4). The aromatic protons of phenylalinine, which overlap the valine amide protons in the region of 7.2 ppm in f_2, are a particular problem. This sharp resonance provides suppression problems for two reasons. Firstly, the narrow linewidth means that a high level of phase stability is required in order to achieve the required accuracy of subtraction. Secondly, the T_1 of these aromatic peaks is longer than the delay between successive transients; the feed-through of magnetization from one transient to the next is therefore possible and may reduce the efficiency of the

phase cycling. In order to reduce the effects of feed-through a second H.M.Q. experiment was performed in which a field gradient pulse was included at the start of the delay D1. The fact that the level of suppression in this experiment was no greater than that of spectrum 5.14 suggests that instrumental instability makes the greater contribution to of spurious peaks.

The spectrum of Figure 5.8 shown earlier was obtained using the NEMESIS pulse sequence. For both of the values of 'phase' used 128 t_1 increments were used in an experiment lasting 10 hours. Suppression of the aromatic protons in this spectrum is in excess of 10^4:1, the only artifact from the aromatic protons can be seen at 96.9 (2150 Hz) ppm in f_1. Due to the high level of suppression in this spectrum ^{15}N decoupling can be applied without any risk of the satellite peaks being confused with residual parent peaks. Figure 5.15 was obtained in this way by applying 'WALTZ-16' (87) decoupling to the ^{15}N nuclei during acquisition of the proton signals. In order to prevent damage to the X nuclues transmitter of the spectrometer its duty cycle was restricted to <5%; the experiment was carried out with an acquisition time of 0.064 s, with a total time between successive transients of 1.284 s. For each t_1 increment 128 transients were acquired; the remaining parameters are the same as used to obtain Figure 5.8.

Caption to Figure 5.15

Proton observed ^{15}N correlation spectrum of gramicidin S. A 90 mM sample in DMSO-d_6 was used in a 12 hour acquisition, ^{15}N 'WALTZ' decoupling was applied during t_2. An idea of the sensitivity of the technique can be obtained from the traces through the spectrum at the ^{15}N chemical shifts indicated.

FIGURE 5.15

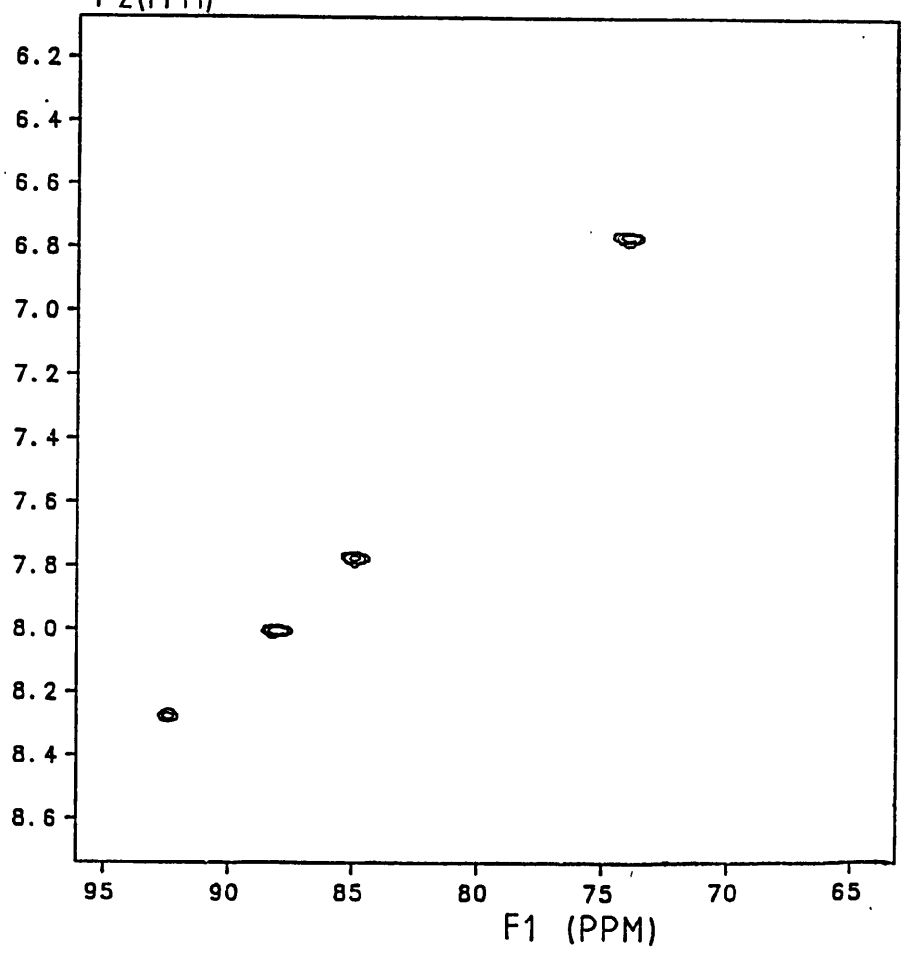
F2(PPM)
6.2
6.4
6.6
6.8
7.0
7.2
7.4
7.6
7.8
8.0
8.2
8.4
8.6
95
90
85
80
75
70
65
F1 (PPM)

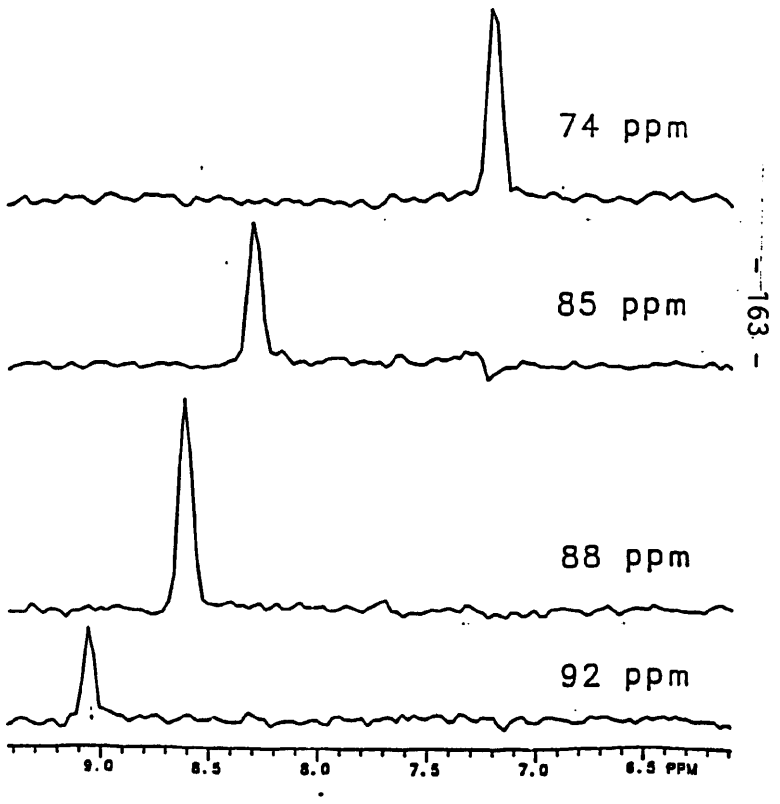
74 ppm
85 ppm
88 ppm
92 ppm
9.0
8.5
8.0
7.5
7.0
6.5 PPM

A related approach to aid suppression in proton detected heteronuclear shift correlation experiments has been used by Brühwiler and Wagner (88); the pulse sequence for their experiment is shown in Figure 5.16. Antiphase proton magnetization at (C) is converted into longitudinal spin order, I_zS_z before a field gradient pulse is applied at (D). After a delay τ_1 during which the spectrometer is allowed to stabilize, heteronuclear two spin order is regenerated by the pulses applied to both nuclei. Magnetization from protons not coupled to X nuclei is in phase along the y axis at (C), so that the $90°_y$ pulse has no effect on this magnetization. The effect of the homospoil pulse is to randomize this in-phase magnetization, extra suppression is therefore achieved by J filtration. The rest of the experiment is the standard H.M.Q. sequence, a 180° proton pulse being required at the mid-point of t_1 if shift correlation spectra are to be obtained. Since the experiment relies on the generation of two spin-order, additional suppression by proton irradiation at (D) is not possible. Ref. (88) does not give any details of the level of suppression possible using this pulse sequence nor does it present any standard correlation spectra obtained by its use. It does however present spectra obtained using the sequence of Figure 5.16 as the initial excitation sequence of a relay experiment. The combination of indirect detection methods with relay experiments will be discussed in section 5.6.

FIGURE 5.16

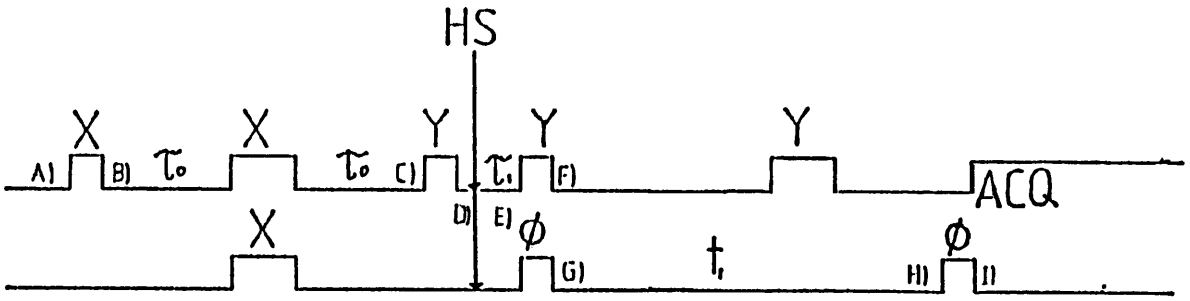

Pulse sequence for the correlation experiment of Brühwiler and Wagner (88).
The narrow pulses have rotation angles of 90°, the wide pulses 180°.
HS indicates the application of a field gradient (homospoil pulse).

5.4 Sensitivity

Equation [2.73] of section 2.4 may be used to predict the sensitivity expected in the detection of a nucleus by N.M.R. The relative sensitivities of proton detection and carbon detection for the same sample concentration can be expressed in the form:

$$\frac{(S/N)^{1}H}{(S/N)^{13}C} = \left[\frac{V_s(^{1}H)}{V_s(^{13}C)}\right] \cdot \left[\frac{t_{90(^{13}C)}}{t_{90(^{1}H)}}\right] \cdot \left[\frac{P_{13_C}}{P_{1_H}}\right]^{\frac{1}{2}} \cdot \left[\frac{\gamma^{1}H}{\gamma_{13C}}\right]^{2} \cdot \left[\frac{LW_{13_C}}{LW_{1_H}}\right]^{\frac{1}{2}} \quad \ldots[5.3]$$

where V_s is the sample volume, t_{90} the 90° pulse width at power P and LW is the linewidth. Substituting the following values leads to the predicted sensitivity ratio for the spectrometer used in this experimental work.

$$\frac{t_{90(^{13}C)}}{t_{90(^{1}H)}} = 1.9 \qquad \left[\frac{P_{13_C}}{P_{1_H}}\right]^{\frac{1}{2}} = 1.8$$

$$\frac{(S/N)^{1}H}{(S/N)^{13}C} = 55 \cdot \frac{\left[LW_{13_C}\right]^{\frac{1}{2}}}{\left[LW_{1_H}\right]^{\frac{1}{2}}} \cdot \frac{V_s(^{1}H)}{V_s(^{13}C)} \quad \ldots\ldots[5.4]$$

The MEASURED sensitivity of the spectrometer for protons is 209:1 for the methy TRIPLET of a 0.1% solution of ethylbenzene, the linewidth is 0.18 Hz. For ^{13}C the MEASURED sensitivity is 230 :1 for a 60% solution of C_6D_6 in dioxane, linewidth 3·5 Hz. The active volume of the proton detection coil is estimated as 0.10 cm^3 and contains 1.4×10^{-6} moles of ethylbenzene.

For the ^{13}C experiment the active volume is estimated as 1.15 cm^3 and contains 5.26 x 10^{-4} moles of C_6D_6. Taking into account the number of equivalent nuclei in each molecule, the multiplet structure of the resonances and their linewidths, the signal-to-noise ratio expected for a sample containing one mole of protons is 5.7 x 10^7 for a 1 Hz linewidth; for a mole of ^{13}C the signal-to-noise ratio is expected to be 2.5 x 10^6 for a 1 Hz linewidth. The measured sensitivity advantage of protons over ^{13}C is therefore of the order of 23. The discrepancy between this value and that predicted above is probably due to the approximations involved in the derivation of equation [2.73] and problems in estimating the active volumes of the detection coils. Assuming that the error is an over-estimation of proton sensitivity (proximity and inhomogeneity effects being more important at the higher frequency) a factor of 0.42 should be included in equation [2.73] for application to the proton probe used.

The sensitivity advantage of proton detected indirect observation over unaided ^{13}C observation is expected to be of the order of 30 for identical linewidths and an equal number of transients accumulated. A further gain in sensitivity will result from the repetition rate advantage of the indirect detection experiment; however this advantage is also available for the INEPT experiment since both experiments start from proton polarization. The sensitivity advantage of indirect detection over INEPT enhanced detection is

$$\frac{(S/N)_{ind}}{(S/N)_{INEPT}} = \left[\frac{V_{s(ind)}}{V_{s(INEPT)}}\right] \left[\frac{t_{90(^{13}C)}}{t_{90(^{1}H)}}\right] \left[\frac{P1_{^{13}C}}{P1_{^{1}H}}\right]^{\frac{1}{2}} \left[\frac{LW_{(^{13}C)}}{LW_{(^{1}H)}}\right]^{\frac{1}{2}} \left[\frac{\gamma 1_H}{\gamma 1_{^{13}C}}\right] \times 0.42$$

.....[5.5]

For the values given above this predicts a maximum enhancement of $5.5(LW^{13}C/LW^{1}H)^{\frac{1}{2}}.V_{s(ind)}/V_{s(INEPT)}$ over ^{13}C detected INEPT for proton acquired ^{13}C indirect detection.

For the application of both sequences to ^{15}N the sensitivity advantage of indirect detection in the spectrometer used can be found using the following values:

$$\frac{t_{90(^{15}N)}}{t_{90(^{1}H)}} = 2.8 \qquad \frac{P15_N}{P1_H}^{\frac{1}{2}} = 1.8$$

$$\frac{(S/N)_{indirect}}{(S/N)_{INEPT}} = 21.\frac{\left(LW15_N\right)^{\frac{1}{2}}}{\left(LW1_H\right)^{\frac{1}{2}}} \qquad .....[5.6]$$

Proton linewidths and multiplet widths are generally larger than those of ^{15}N and so the value 21 represents the maximum gain which may be expected.

This value will be further modified by the yields of the two experiments. The yields of the pulse sequences involved were measured using isotopically enriched samples. Comparison of the unenhanced signal with an INEPT enhanced signal gives a yield of 80% for this sequence. The yields of H.M.Q. and NEMESIS were found by comparison of the satellite signal intensities in a conventional spectrum with those obtained in one-dimensional versions of the indirect detection experiments. Under well-optimized conditions the yield of the H.M.Q. experiment was found to be 89%, whereas that of NEMESIS was 79%; under less well-optimized conditions the yields of both pulse sequences were around 65%. ~~The yields of the two-dimensional versions of both sequences will be further reduced since~~

~~the regeneration of observable proton magnetization is modulated in t_1 by the chemical shifts involved.~~ In practice, when a long total acquisition time is used, the yields of both sequences are found to be around 60%. This may reflect the relative unimportance of inhomogeneity of the R.F. field produced by a large X irradiation coil when used with a small proton coil. Taking the yields into account the maximum advantage of indirect detection over INEPT for our experimental system is expected to be 13.

The predicted enhancement may be checked against the sensitivity of the spectra shown in Figures 5.15 and 5.17. First the sensitivity of proton detection in the indirect experiment may be compared with that of the standard sensitivity sample. The gramicidin sample contained an effective concentration of 6.7×10^{-4} M of the sites of interest, the width of the detected multiplets is 15 Hz due to the unresolved homonuclear coupling and each of the doublets has a signal-to-noise ratio of 50:1. The active volume of the proton detection coil in this experiment is estimated to be 0.10 cm^3, it therefore contains 6.7×10^{-8} moles of the ^{15}N-^{1}H groups. A total of 512 transients were acquired for each of 64 t_1 increments, giving a total number of transients of 32768. The signal-to-noise ratio expected from a sample containing one mole of the sites of interest in a one transient experiment is 1.60×10^7 for a 1 Hz linewidth. This value is 28% of the signal-to-noise ratio of the standard sensitivity sample, the yield of the two-dimensional experiment being lower than that measured for the one-dimensional experiment.

The spectrum shown in Figure 5.17 was obtained by acquiring 20000 transients in an INEPT experiment using an 80 mM solution of gramicidin. The ^{15}N linewidth is 2 Hz and the signal-to-noise ratio

is 20:1, the active volume of the ^{15}N detection coil is 0.227 cm^3, it therefore contains 1.34×10^{-7} moles of the ^{15}N-^{1}H sites. The expected sensitivity for a one transient experiment applied to a sample containing one mole of the sites of interest is 1.49×10^{6} for a 1 Hz linewidth. The sensitivity advantage of indirect detection in this case is 10.7 for identical linewidths and no repetition rate advantage.

When instrumental considerations have been taken into account, the sensitivity advantage of indirect detection experiments over a direct detection INEPT experiment is found to have a maximum expected value of around 11 for ^{15}N; this will be reduced in practice due to the linewidths of the proton resonances being greater than those of the ^{15}N resonances. Despite these losses the sensitivity of the indirect detection experiment is quite high. The measured sensitivity advantage is $\sim 80\%$ of that predicted using equation [5.6] once the yields have been taken into account; this discrepancy arises from the approximations involved in the derivation of equation [2.73] and from the errors involved in the experimental measurements.

FIGURE 5.17

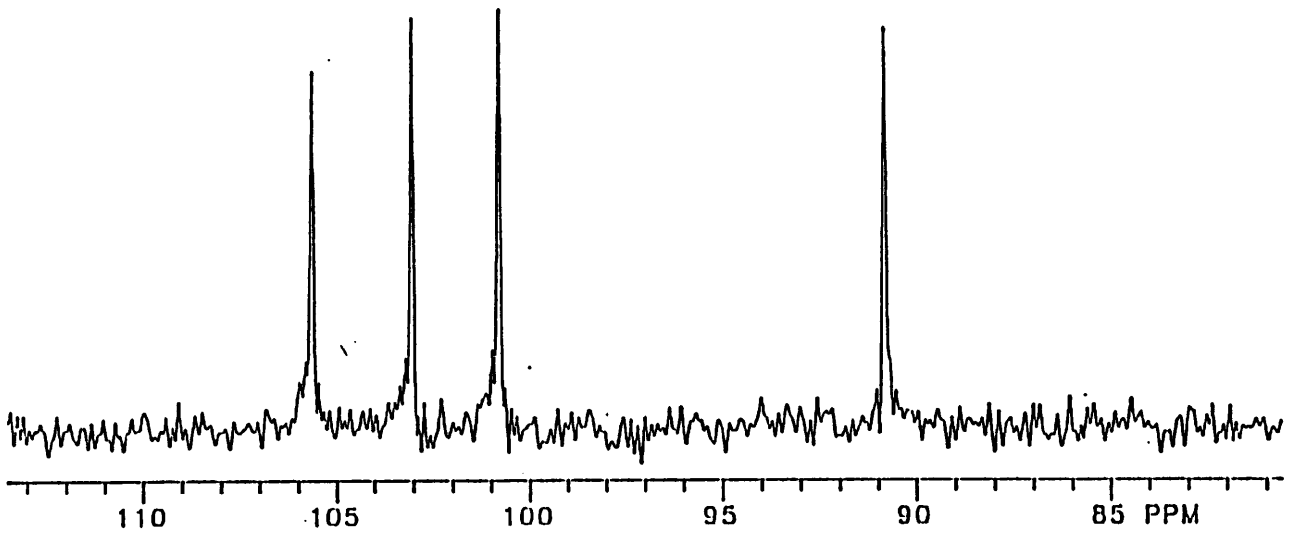

INEPT enhanced ^{15}N spectrum obtained from an 80 mM solution of Gramicidin S in DMSO-d_6. 20000 transients were acquired in an experiment lasting 8 hours.

In this application, where we are mainly concerned with the $^{15}N-^{1}H$ two spin systems of amides, the ratio of the signal intensity to the thermal noise level in spectra obtained using the NEMESIS experiment is the same as that available using the H.M.Q. experiment. For applications to larger spin systems, such as XH_2 and XH_3, the H.M.Q. experiment will have an extra sensitivity advantage due to the fact that the multiple quantum coherence can be created and detected via all of the protons in the spin system. For an XH_n spin system an extra sensitivity advantage of n would therefore be expected; for the corresponding NEMESIS experiment this increase in sensitivity would not be seen. Since NEMESIS spectra do not suffer from the suppression problems associated with H.M.Q. spectra, the signal-to-artifact ratio is far greater in spectra obtained using the polarization transfer based sequence. The elimination of artifacts and the reduced dynamic range of the detected signal are the main advantages of this new method of obtaining indirect detection spectra; in addition the NEMESIS pulse sequence can easily be modified to yield extra information; modifications of this type are described in the following sections.

5.5 Heteronuclear Relay Spectroscopy with Proton Detection

One approach to overcoming the problem of overlap in proton spectra of large molecules is the use of heteronuclear probes. Correlation of a proton signal with an assignable, resolved signal of a heteronucleus in a heteronuclear two-dimensional shift correlation experiment can allow assignment of the proton resonance. The correlation experiment may consist of a single one-bond coherence transfer, or it may involve a proton-proton relay step in order to correlate signals from distant nuclei. In the conventional experiment the signal acquired is that of the heteronucleus, proton chemical shifts being obtained in f_1. An indirect observation experiment used in this application has the advantage of providing greater resolution in the proton dimension (f_2) (89).

Proton detected relayed transfer can be carried out by including a mixing period t_m followed by a 90° proton pulse at the end of a conventional H.M.Q. experiment (89); alternatively a series of pulses may be added to the end of the H.M.Q. experiment in order to transfer magnetization by the homonuclear Hartman-Hahn mechanism (90). The inclusion of extra proton pulses in the basic H.M.Q. experiment leads to increased suppression problems; these may be reduced by the inclusion of a BIRD sequence at the start of the experiment (as discussed in section 5.1) or by use of the relay version of the experiment of ref. (88). The NEMESIS pulse sequence may easily be extended to give relayed detection spectra, the pulse sequence for this experiment is shown in Figure 5.18. The application of a NEMESIS-relay experiment to gramicidin S is shown in Figure 5.19;

FIGURE 5.18

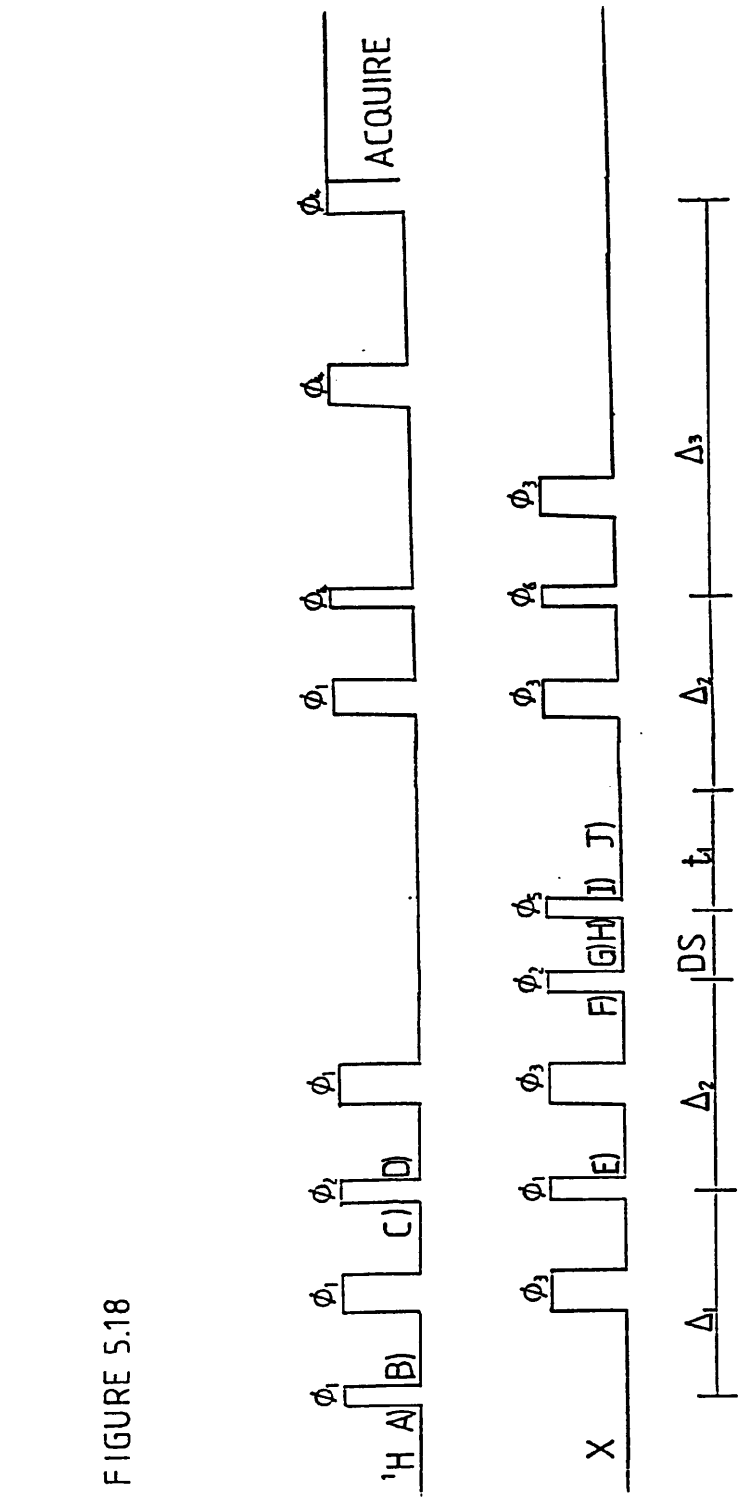

Pulse sequence for the NEMESIS-Relay experiment. The narrow pulses are 90° pulses, the wide pulses 180°. The delay between the last 180° (X) and 180° (H) allows refocussing with respect to the one-bond hetronuclear coupling.

the amide nitrogen chemical shifts are correlated with the shifts of the amide protons as in spectra 5.2 and 5.9, but here three of the resonances show additional correlations to the alpha protons of the amino acid residues. The fourth residue does not exhibit a resolved coupling between the amide proton and the alpha proton and so the corresponding peak is missing from spectrum 5.19. For comparison with this spectrum Figure 5.20 shows a one-dimensional spectrum of gramicidin. An obvious extension of this sequence would be an extended heteronuclear relay experiment analogous to that of Field and Messerle (91).

FIGURE 5.19

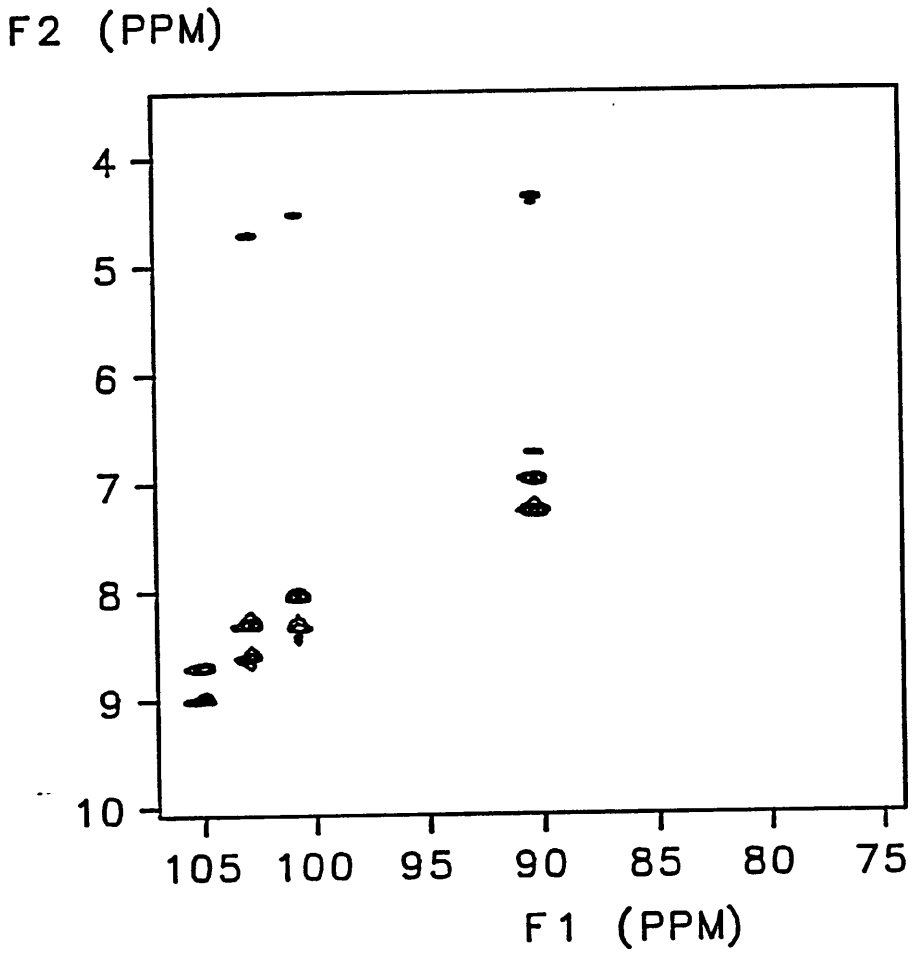

Spectrum obtained using the NEMESIS-relay pulse sequence of figure 5.18. The same sample was used as in figures 5.8, 5.14, and 5.17; the relay delay was fixed at 4.4×10^{-2} seconds, the spectrum was run at 50°C. The relay experiment correlates the α proton chemical shifts with the corresponding amide ^{15}N chemical shift. The spectrum is shown in absolute value mode.

FIGURE 5.20

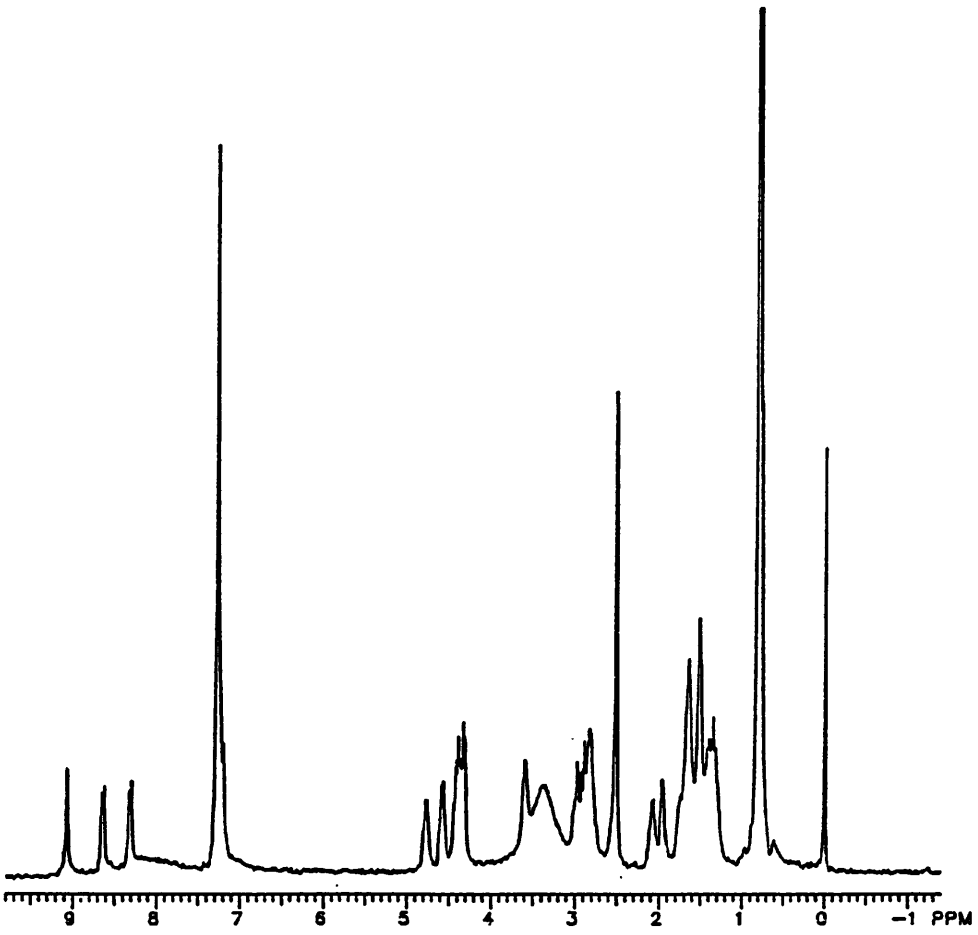

One-dimensional proton spectrum of gramicidin S, obtained from a 48 mM solution in DMSO-d_6 at 30°C.

5.6 T_1 Measurements by Indirect Detection

5.6 (A) Introduction

Due to the low sensitivity of low γ nuclei the measurement of their spin-lattice relaxation times can be very time consuming. In an inversion recovery experiment (39) the total signal acquired for each relaxation delay has a sensitivity which is less than the maximum available in a normal one-dimensional experiment. The sensitivity therefore decreases as the relaxation delay is increased, and considerable time averaging is required if good sensitivity is to be obtained in spectra acquired using a long relaxation delay. The repetition rate of a standard T_1 experiment is determined by the relaxation parameters of the nucleus under study, and it is therefore necessary to estimate T_1 before its value can be measured. Under-estimation of T_1 results in a decreased signal intensity in each transient acquired and in a systematic error in the measured T_1, whereas over-estimation of T_1 results in a repetition rate for the experiment which is less than the optimum; in either case the sensitivity of the experiment is less than the maximum obtainable.

The sensitivity of T_1 measurements can be improved by arranging that the first step of the experiment is a polarization transfer from protons. Not only does this provide an enhancement due to the population considerations of equation [1.4], but it also makes the repetition rate of the experiment dependent on the T_1 values of the protons, which are often shorter than the T_1 values of the low γ nuclei. Due to the high sensitivity and natural abundance of protons, their T_1 values can easily be measured and so optimization of the repetition rate can be achieved. This approach has been used in references (8,92);

a similar result can be obtained by using a modified form of the NEMESIS pulse sequence described below.

5.6 (B) T_1 Measurement using NEMESIS

If a one-dimensional version of the NEMESIS experiment is carried out with a value of DS of the same order of magnitude as $T_1(X)$, the spin-lattice relaxation time of the low γ nucleus X, significant relaxation will occur before the second polarization transfer. This relaxation of X nucleus polarization may be monitored, and the value of $T_1(X)$ found, by recording spectra for various values of DS. Proton saturation is maintained during DS in order to ensure proton signal suppression and to give relaxation under conditions of proton saturation; the relaxation process observed is therefore from the initial INEPT enhanced z magnetization to the NOE enhanced z magnetization. If both of these magnetizations have the same sign then the maximum change in intensity possible during the experiment will be small, leading to a low expected accuracy for the T_1 value obtained.

To obtain a greater range of intensity values, and so a higher accuracy of the value of $T_1(X)$, it should be arranged that the INEPT enhanced z magnetization has the opposite sign to the NOE enhanced z magnetization. This can be achieved by using the appropriate phase of the X nucleus pulse at (F), -y in the case of a positive NOE and y in the case of a negative NOE. For a negative γ nucleus the situation at (G) is then described by the operator bX_z, where b is a multiplier (equation [2.20]) indicating INEPT enhanced magnatization; this term relaxes back to the negative NOE enhanced intensity; for a positive γ the situation at (G) is described by the operator $-bX_z$ which relaxes to the positive NOE enhanced value. A relaxation measurement of this type is shown in Figure 5.21.

FIGURE 5.21

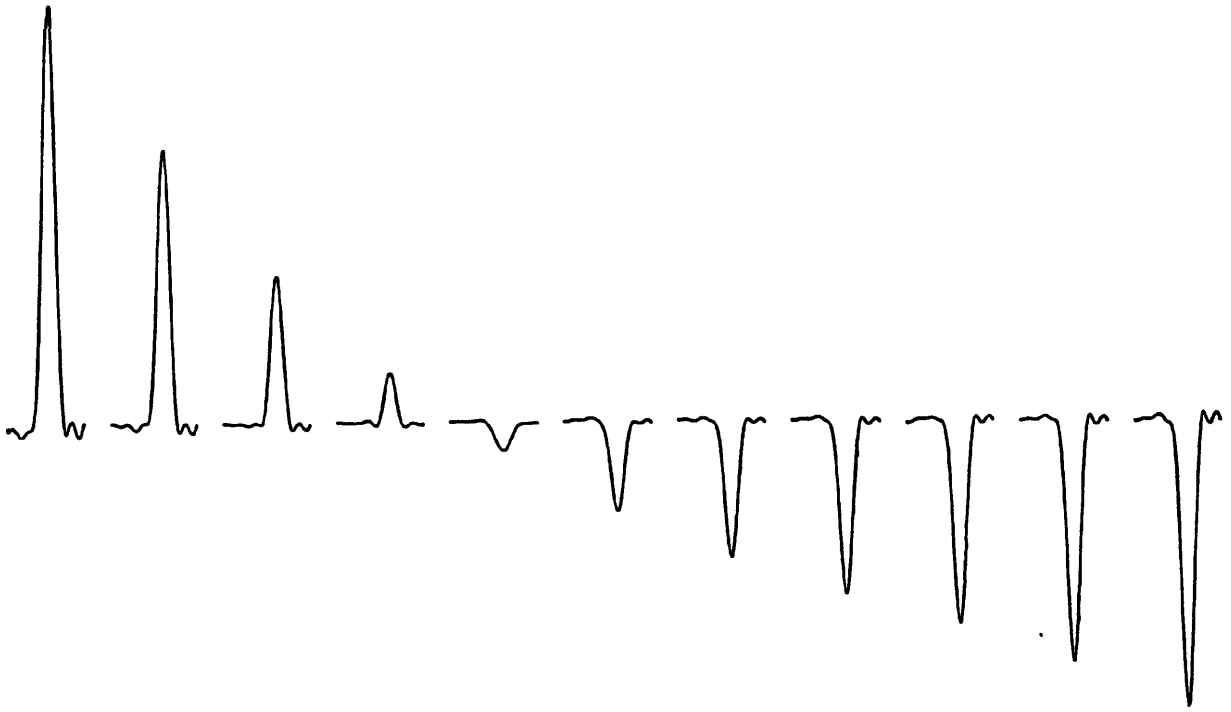

Indirect measurement of ^{15}N T_1 values using a one-dimensional version of NEMESIS. The sample used was ^{15}N enriched Boc-*Gly-OMe in DMSO-d_6. Using DS values of 0.1, 1, 2, 3, 4, 5, 6, 7, 8, 10, 15 s the ^{15}N T_1 value is found to be 2.9 seconds.

Problems may occur in this experiment if perfect selection of the double polarization transfer pathway is not achieved; coherence from other pathways may then give rise to observable proton magnetization at (N) and so lead to a misleading value of $T_1(X)$. Coherence originating from relaxation during DS can be removed by using a modified form of the phase cycling (Table 5.8, Figure 5.22) which eliminates any signals which do not originate from the first polarization transfer step. This phase cycling also removes the NOE enhanced X nucleus magnetization and so the observed signal tends to zero for long values of DS; there is therefore a sensitivity loss compared with the previous experiment. A T_1 measurement of this type, for the sample used in Figure 5.21, is shown in Figure 5.23. In this case the T_1 values obtained from both of the indirect methods agree to within 4% of the directly measured value. These T_1 measurements may give unreliable results in the case of larger spin-systems such as CH_2 and CH_3, this will be discussed below.

Table 5.8

$$\phi_1 = 0_8 2_8$$
$$\phi_2 = 1$$
$$\phi_3 = 0,2$$
$$\phi_4 = 1_{16} 3_{16} + 0_{32} 2_{32} + 0123$$

FIGURE 5.22

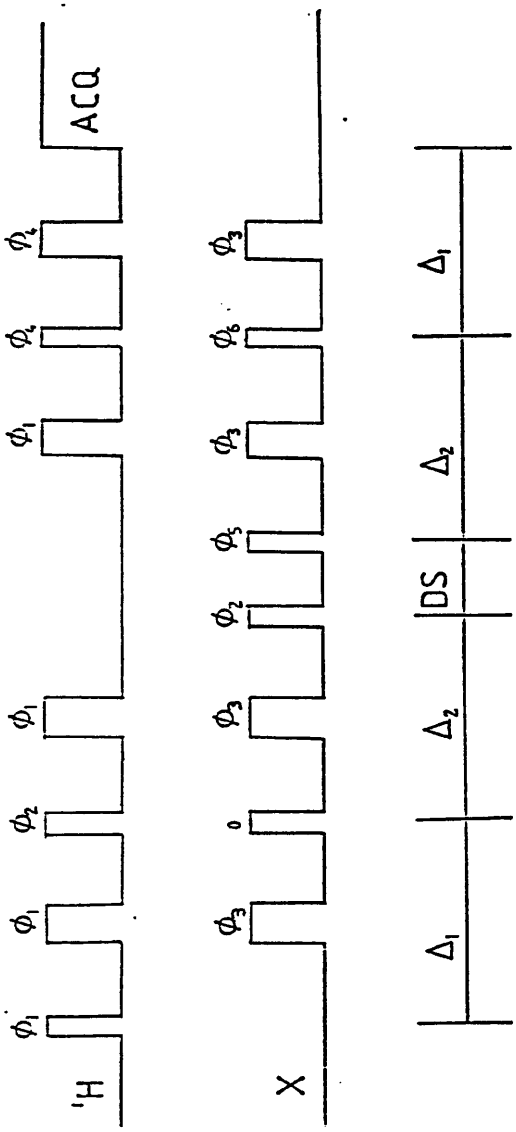

Modified indirect detection pulse sequence for the measurement of T_1 values. The phase cycling for this experiment is shown in Table 5.8.

FIGURE 5.23

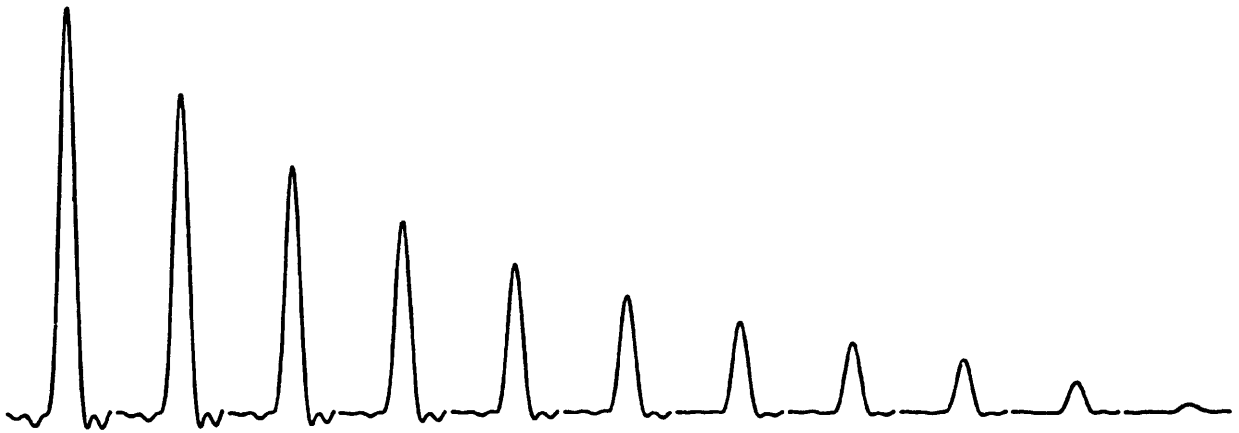

Indirect measurement of ^{15}N T_1 for the same sample and same experimental conditions as figure 5.21 but using the sequence of figure 5.22.

5.6 (C) T_1 Measurement using DEPT Based Sequences

A very similar approach to that described above has recently been reported in references (93) and (94). These sequences make use of the DEPT polarization transfer sequence (95) in place of the INEPT sequences used in NEMESIS. The pulse sequence for these techniques is shown in Figure 5.24. From (A) to (F) this is a DEPT experiment; the 90° pulse at (F) flips the enhanced X nucleus magnetization onto the z axis, just as in the INEPT based experiment. After the saturation delay the 90° pulse at (H) regenerates X spin transverse magnetization which is then transferred to the protons by a reverse DEPT sequence, (I) to (N). It has been suggested (94) that the accuracy of the results obtained by this sequence may be reduced due to the survival of multiple quantum terms. For a spin system I_1I_2S, in an I acquired S indirect detected experiment, the density matrix components involving S_z are given by:

$$\sigma_G = \pm S_z \pm 4 I_{1x} I_{2x} S_z \qquad \text{.....[5.7]}$$

Ref. (94) claims that the zero quantum component of the second term survives the saturation/randomization scheme and can give rise to observable proton magnetization at (N). This effect is blamed for the poor agreement between the results obtained using the DEPT-inverse DEPT indirect T_1 experiment and those obtained using a conventional inversion recovery experiment for CH_2 and CH_3 systems. The mechanism of the DEPT sequence is dealt with in references (95,49) and will not be given here, but the origin of the terms in equation [5.7] can be seen in the S_x terms of formula 11 of ref. (49); in order to see how this term (or any other zero quantum term) can

FIGURE 5.24

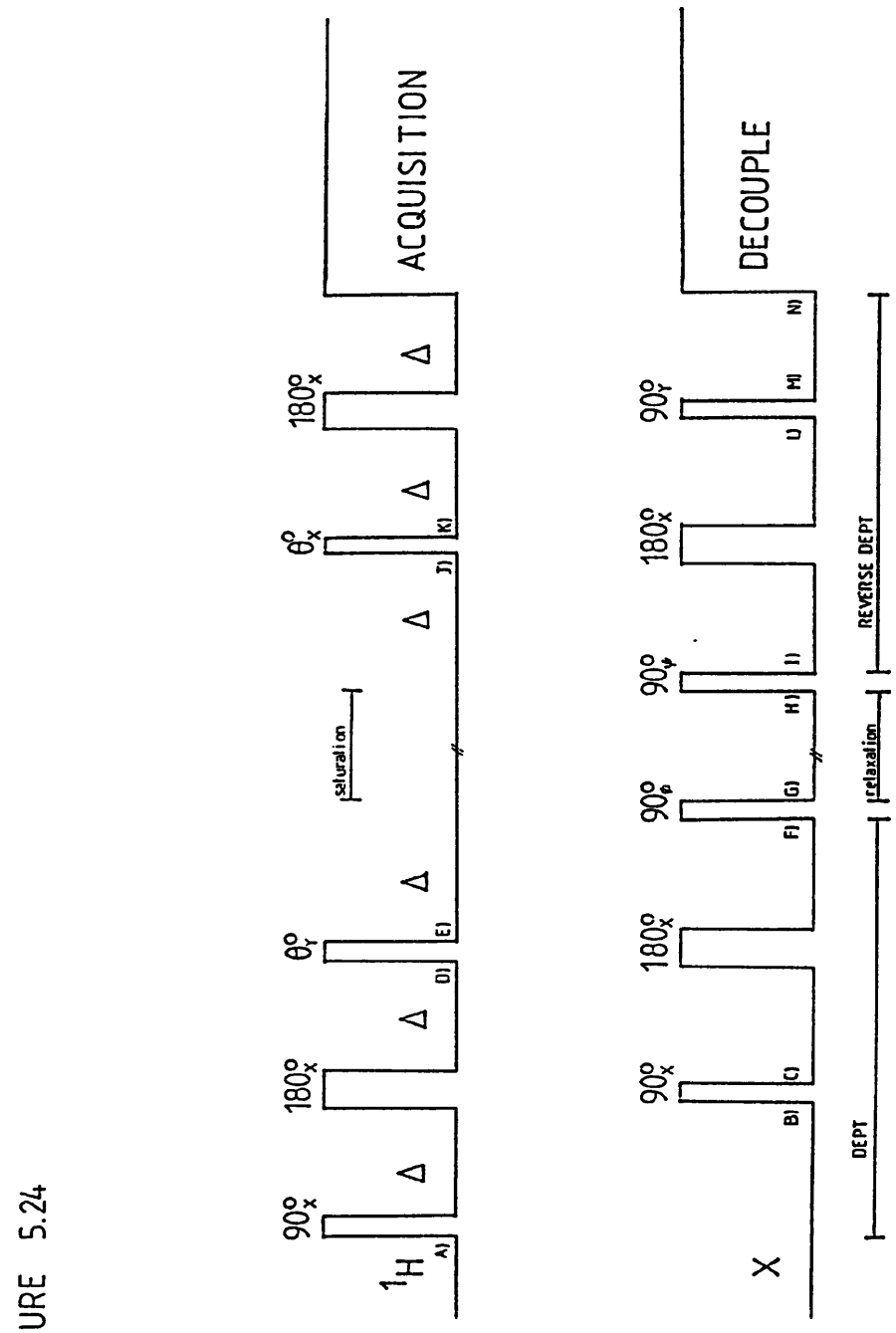

Pulse sequence for the indirect measurement of T_1 values using a DEPT based sequence.

lead to observable magnetization it is necessary only to consider the second polarization transfer step of the experiment.

In the following product operator description of the reverse DEPT experiment the effects of chemical shifts will not be considered since these should be refocussed. At (H) the relevant zero quantum term can be expressed as:

$$(H)\quad \tfrac{1}{2}S_z\{2I_{1x}I_{2x}+2I_{1y}I_{2y}+2I_{1y}I_{2x}-2I_{1x}I_{2y}\}$$

$$\downarrow\ 90°_x(S)$$

$$(I)\quad -\tfrac{1}{2}S_y\{2I_{1x}I_{2x}+2I_{1y}I_{2y}+2I_{1y}I_{2x}-2I_{1x}I_{2y}\}$$

$$\downarrow\ 2\pi J\Delta I_zS_z$$

(No evolution of M.Q.C. under the scalar coupling)

$$(J)\quad -\tfrac{1}{2}S_y\{2I_{1x}I_{2x}+2I_{1y}I_{2y}+2I_{1y}I_{2x}-2I_{1x}I_{2y}\}$$

$$\downarrow\ \theta_x(I)$$

$$(K)\quad -\tfrac{1}{2}S_y\{\underset{(1)}{2I_{1x}I_{2x}}+\underset{(2)}{2I_{1y}I_{2y}}\cos^2\theta+\underset{(3)}{2I_{1y}I_{2z}}\cos\theta\sin\theta$$

$$+\underset{(4)}{2I_{1z}I_{2y}}\cos\theta\sin\theta+\underset{(5)}{2I_{1z}I_{2z}}\sin^2\theta+\underset{(6)}{2I_{1y}I_{2x}}\cos\theta$$

$$+\underset{(7)}{2I_{1z}I_{2x}}\sin\theta-\underset{(8)}{2I_{1x}I_{2y}}\cos\theta-\underset{(9)}{2I_{1x}I_{2z}}\sin\theta\}$$

$$\downarrow\ 2\pi J\Delta I_zS_z$$

(L) The multiple quantum terms (1), (2), (6) and (8) do not evolve under the scalar coupling.

(K) $2\pi J\Delta I_z S_z$ (L)

(3) ⟶ $\frac{1}{2}S_x I_{1y}\cos\theta\sin\theta$ (3)'

(4) ⟶ $\frac{1}{2}S_x I_{2y}\cos\theta\sin\theta$ (4)'

(5) ⟶ Terms only in I_{1z}, I_{2z} and S_y

(7) ⟶ $\frac{1}{2}S_x I_{2x}\sin\theta$ (7)'

(9) ⟶ $\frac{1}{2}S_x I_{1x}\sin\theta$ (9)'

$90°_y(S)$

(3)' ⟶ $-\frac{1}{2}S_z I_{1y}\cos\theta\sin\theta$

(4)' ⟶ $-\frac{1}{2}S_z I_{2y}\cos\theta\sin\theta$

(7)' ⟶ $-\frac{1}{2}S_z I_{2x}\sin\theta$

(9)' ⟶ $-\frac{1}{2}S_z I_{1x}\sin\theta$

These terms can all give rise to observable I spin magnetization at (N). Since the pathways which produce these terms have the same changes in coherence order at (H), (J) and (L) as the desired pathway it is not possible to remove the unwanted signals by phase cycling.

For the reverse INEPT experiment the situation after the 90°(S) pulse is:

$$-\frac{1}{2}S_y\{2I_{1x}I_{2x}+2I_{1y}I_{2y}+2I_{1y}I_{2x}-2I_{1x}I_{2y}\}$$

between (I) and (K) there is no evolution since the effects of chemical shifts are refocussed, and scalar couplings have no effect on the

nuclei involved in a multiple quantum transition. As the S pulse at (K) is applied about the y axis this has no effect on the spin system, the product operator description of the system at (L) is therefore the same as that at (I). The final 90° pulse may be applied about either the x or the y axis.

$$\xrightarrow{90°_x} -\frac{1}{2}S_y\{2I_{1x}I_{2x}+2I_{1z}I_{2z}+2I_{1z}I_{2x}-2I_{1x}I_{2z}\}$$

$$\xrightarrow{90°_y} -\frac{1}{2}S_y\{2I_{1z}I_{2z}+2I_{1y}I_{2y}-2I_{1y}I_{2z}+2I_{1z}I_{2y}\}$$

The reverse INEPT experiment only gives rise to multiple quantum terms at (N), no observable I spin magnetization being produced. Thus provided that the effects of pulse imperfections are removed by phase cycling, and the phase cycling of Table 5.8 is used, the term in $I_{1x}I_{2x}S_z$ is not expected to affect the results obtained for the NEMESIS experiment. The application of the NEMESIS experiment to the measurement of the T_1 values of ^{13}C in the CH_2 and CH_3 groups of ethanol is illustrated in Figure 5.25; the results of corresponding inversion recovery experiment are shown in Figure 5.26. For the CH_3 group the T_1 value obtained from the NEMESIS experiment is within ~3% of that obtained for the conventional experiment (T_1(NEMESIS) = 6.5 S, T_1(inversion recovery) = 6.7 S)). For the CH_2 group the NEMESIS experiment gives a T_1 value of 7.3 S, the inversion recovery experiment gives a value of 9.5 S. These results would indicate that, in agreement with ref. (93) misleading values are obtained when indirect experiments are used to measure the T_1 value of CH_2 carbons. The origin of this problem has not yet been found but it is thought that it may arise from the difficulty in maintaining saturation of proton transitions during DS.

FIGURE 5.25

Indirect measurement of ^{13}C T_1 values for ethanol using a one-dimensional version of the NEMESIS pulse sequence. The DS values used were 0.1, 4.0, 8.0, 12.0, 16.0, 20.0, 50.0 s; 64 transients were acquired for each DS value. The T_1 values obtained were 7.3 s for the quartet and 6.5 s for the triplet.

FIGURE 5.26

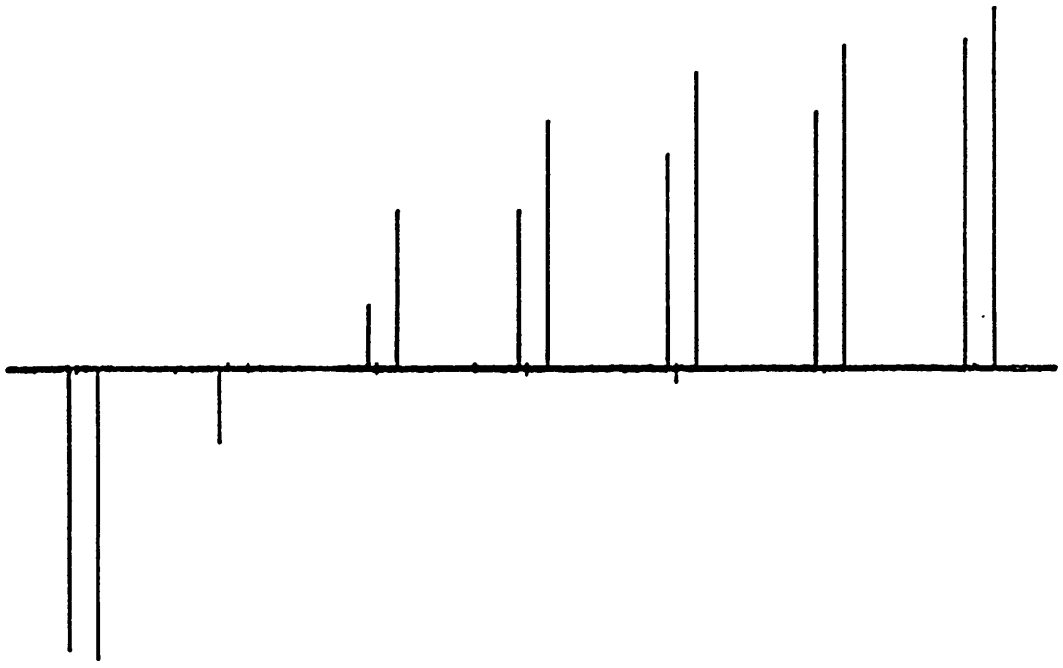

Inversion recovery experiment on the sample used for figure 5.25; the same DS values were used in both experiments. Eight transients were acquired for each DS value. T_1 values of 6.7 s and 9.5 s were obtained for the quartet and triplet respectively.

5.7 Long-Range Correlation Experiments

References (19) and (20) describe a modification of the H.M.Q. experiment to achieve correlation via a long-range coupling; the pulse sequence for this experiment is shown in Figure 5.5, it can be considered as a low-pass J filtered H.M.Q. experiment. The delay Δ_1 is optimized for a one-bond coupling and the phase ϕ of the first X nucleus pulse is alternated on successive blocks of two transients with no corresponding alternation of the receiver phase; this removes the effects of any multiple quantum coherence created between directly coupled nuclei. The delay Δ_2 is adjusted for the long-range coupling ^nJ, to minimize losses from homonuclear couplings and relaxation the optimum value of Δ_2 will be less than $1/2^nJ$. This experiment has two possible applications; it may be used to establish assignments for unprotonated X nuclei, as a more sensitive alternative to the H,C-COLOC experiment, or it can be used as a means of removing ambiguity in the assignment of protonated carbons.

In the first of these applications, the total length of the equivalent NEMESIS sequence would have to be of the order of $2/^nJ$; this sequence would therefore suffer from increased losses due to X nucleus relaxation and so would be of limited use. In the second application an asymmetric form of the NEMESIS sequence may be of use; the following discussion will be limited to this application. A long-range correlation experiment may be used in cases where overlapping proton signals prevent the one-bond correlation experiment from providing unambiguous assignment of X nucleus resonances. In this application the X nucleus of interest shows both one-bond and long-range couplings; use may be made of the one-bond coupling in order to provide the sequence with an

easily optimized and relatively short first polarization transfer step. To obtain the correlation information the second polarization transfer step is optimized for the long-range coupling.

The full sequence is therefore asymmetric and has a total length (excluding the t_1 delay) of $(1/^1J)+(1/^nJ)$, making it slightly longer than the corresponding H.M.Q. sequence (which has a total length of $1/^nJ$). This does not however mean that its yield will be less than that of the long-range H.M.Q. since the total time during which the coherence is associated with proton transitions is only $(1/2^1J)+(1/2^nJ)$ in a NEMESIS experiment, whereas it is the full $1/^nJ$ in the H.M.Q. experiment. Thus in the case where the proton T_1 is considerably less than that of the X nucleus, or where there are extensive homonuclear couplings, the NEMESIS experiment will have the higher yield. The yields of both techniques will be modified due to the one-bond coupling. In the polarization transfer sequence, failure to suppress the one-bond polarization transfer pathway in the second stage of the experiment will result in a sharing of the signal among both long-range and short-range coupling partners. One-bond heteronuclear couplings should not give rise to extra peaks in the long-range H.M.Q. experiment but may cause signal losses due to the generation of proton magnetization which is in antiphase with respect to an unresolved homonuclear coupling.

In this application NEMESIS should give better suppression of unwanted signals than the corresponding H.M.Q. experiment. The low value of the long-range coupling constants prevents the use of BIRD sequence element to achieve J filtration to suppress non-satellite signals in H.M.Q. experiments; suppression in this experiment is therefore dependent on phase cycling alone. The use of a randomization delay

in the polarization transfer sequence allows suppression of non-satellite peaks irrespective of the size of the coupling constant involved in the system under study. A higher level of suppression should therefore be possible in these experiments than in the corresponding H.M.Q. experiment. This is particularly important in the case of small long-range coupling constants since, in a spectrum coupled in f_2, the satellite signals will be close to the position of any residual parent peaks.

An example of the use of an asymmetric NEMESIS experiment is shown in Figure 5.27, the spectrum was run on a sample of ^{15}N enriched Boc-*Gly-OMe in DMSO-d_6. The first two delays of the sequence were set to 5.56 msec, the last two delays were set to 55.6 msec. The doublet corresponding to the one-bond coupling is seen at around 8 ppm, the peak at 4 ppm indicates a two-bond transfer to the glycine methyline protons ($^2J(^{15}N\text{-}C\text{-}H)$ for glycine is 0.5 Hz (95). The equivalent one-dimensional experiment is shown in the lower spectrum of Figure 5.28; the upper spectrum shows the result of a H.M.Q. experiment optimized for a scalar coupling of 20 Hz. The presence of amine peaks, from a *GLY-OMe impurity, at ~6.6 ppm in the H.M.Q. spectrum illustrates the poorer suppression of this experiment.

FIGURE 5.27

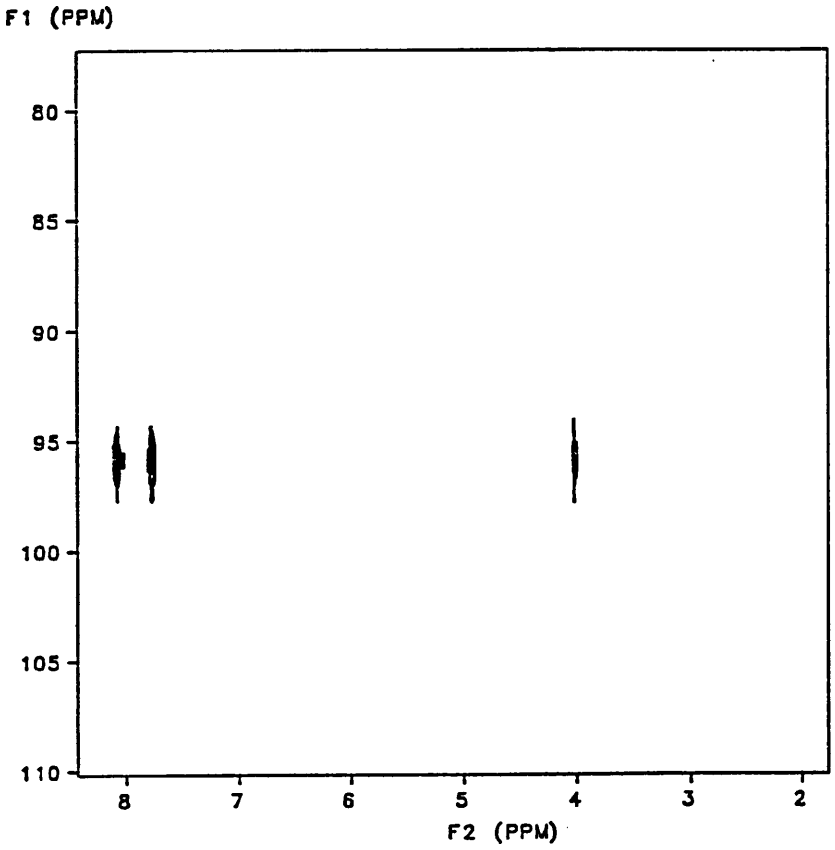

Long-range version of MEMESIS experiment carried out on Boc-*Gly-OMe; 64 transients were acquired per 'phase' value for each of 32 t_1 increments. One-bond correlation peaks are at 8 ppm, two-bond correlation peaks at 4 ppm. The spectrum is shown in absolute value mode.

FIGURE 5.28

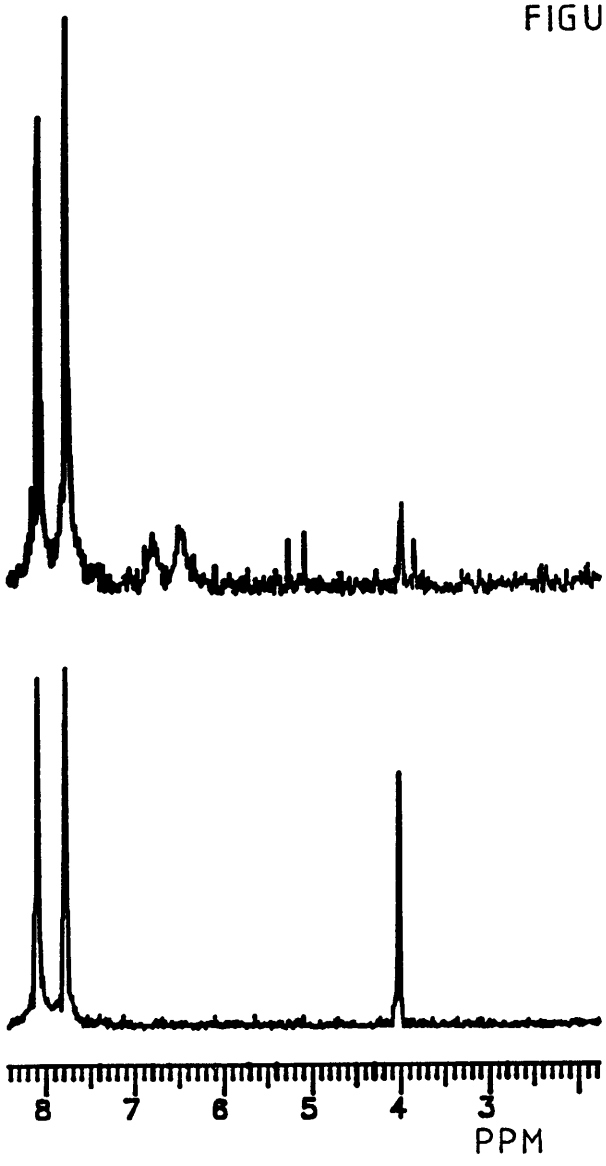

One-dimensional long-range experiments carried out on the same sample as figure 5.27. The upper trace shows the result of carrying out a HMQ experiment, the lower a NEMESIS experiment, 128 transients were acquired in each case. Both spectra are presented in absolute intensity.

The NEMESIS experiment provides a means by which indirect detection experiments can be carried out in protonated solvents without introducing any dynamic range problems. The suppression obtainable using this technique is far better than that available from existing indirect detection experiments, while the sensitivity of the technique is of the same order as that obtainable using H.M.Q. The high level of suppression is also useful in the relay and long-range versions of the experiment. T_1 measurements by the modified sequence appear to work well for two spin heteronuclear systems but at present give misleading results for larger spin systems. The cause of the error in measurement of T_1's of CH_2 carbons has not yet been found but it is believed not to be the mechanism proposed in ref. (93).

CHAPTER 6

DISCUSSION

This thesis has introduced new pulse sequences aimed at improving sensitivity in N.M.R. The sequences of Chapter 3 provide an enhancement of sensitivity for carbon correlation experiments; at the same time they illustrate the way in which polarization transfer can be used to improve the sensitivity of existing sequences. Chapter 5 demonstrated the sensitivity advantage which is observed for indirect detection experiments and compared it with that which is expected in theory. The calculation of the expected advantage takes into consideration various losses which have not been accounted for in previous treatments (31), the sensitivity advantage is therefore lower than that given elsewhere. Even taking these considerations into account, the predicted signal-to-noise ratios only agree with those measured experimentally to within a factor of two for each species; more simple treatments based only on the relative magnitudes of the magnetogyric ratios are expected to have little significance.

For the Varian XL-300 used, the maximum expected sensitivity advantage over direct detected INEPT enhancement is ~11 for ^{15}N. While this value is less than that predicted in references (21,22,31) it still represents a useful sensitivity gain; at the same time the indirect method provides correlation information which is not available in spectra obtained by INEPT.

Due to the higher static magnetic field strength and improved coil design, the proton signal-to-noise ratio for a modern 400 MHz instrument is around four times better than that obtained on the instrument used in this study. The limit of detection of these instruments is therefore very much lower than that for the spectrometer used here; a spectrum can be obtained from 9.5 mg of gramicidin-S in an unprotonated solvent

in 2.8 hours (96). Of course the sensitivity of the corresponding INEPT experiment will also increase at higher fields but under well optimized conditions the sensitivity of an indirect detection experiment should always be greater than that of direct detection. To carry out indirect detection experiments ordinary heteronuclear probes may be used, but to make the best of the available signal-to-noise ratio a probe is required which has the correct geometry for indirect detection. This must be able to provide a good signal-to-noise ratio for proton detection while at the same time being able to irradiate the X nucleus. Such probes are now becoming available commercially (96,97).

To obtain a useful sensitivity advantage, previously reported experiments require a very high level of radio frequency stability if clean spectra are to be obtained. While this may be available on the latest generation of N.M.R. machines, which have been designed with indirect detection experiments in mind, for older machines the results are unacceptable. The NEMESIS pulse sequence reduces the stability requirement, making this type of technique available to spectrometers of poor R.F. stability. Changes in the relative phase of the decoupler output with respect to the decoupler L.O. will reduce the yield of both experiments, so too will variations in pulse amplitude. In the case of H.M.Q. such irreproducibilities will reduce the efficiency of the phase cycling and result in the presence of artifacts in the spectrum; these will not be seen in a NEMESIS experiment. Phase shifts in the transmitter will not result in any suppression problems in either experiment; systematic drifts in the phase of the transmitter with respect to the decoupler should not seriously affect the yield of either

experiment provided that the time scale of the drift is long compared to the duration of the sequence. Random transmitter phase changes, or variations in transmitter pulse amplitudes, during the pulse sequence will have an effect on the yield. Further developments in R.F. stability should be of little benefit to NEMESIS but may improve the quality of the results obtainable from the H.M.Q. type of sequence.

The NEMESIS experiment overcomes the dynamic range problems associated with the use of indirect detection for samples made up in protonated solvents, this may give the experiment an advantage over H.M.Q. even in the case of good R.F. stability. The suppression possible on a single transient experiment is almost an order of magnitude greater than that claimed (96) for the BIRD-H.M.Q. experiment (32), which is currently the most widely advocated form of the H.M.Q. experiment. In a NEMESIS experiment this suppression ratio is achieved for all resonances in the spectrum; this differs from the suppression available in the BIRD-H.M.Q. experiment which is dependent on the T_1 of the resonance to be suppressed. While the pulse sequence for NEMESIS is longer than that for H.M.Q. it should be remembered that for the signals of interest the time during which the coherence pathways are associated with proton transitions is the same in both of the experiments. The extra length of the NEMESIS experiment is associated with X nucleus transitions, extra losses due to relaxation are therefore small and are out-weighed by the gain in suppression. This extra level of suppression is particularly important in the relay and long-range versions of the experiment.

The quality of spectra obtained from the NEMESIS sequence may be improved by increasing suppression still further; suppression by at least an extra order of magnitude would be required in order to obtain clean spectra in the presence of overlapping solvent peaks. Suppression of this order may also help find the origin of the problem associated with the indirect measurement of T_1 values of carbons in CH_2 groups. In designing new suppression schemes care must be taken to avoid the repetition of identical pulses or field gradients; such a repetition would introduce the risk of producing echo effects which would reduce the efficiency of the suppression scheme. It may be that suppression can be improved by using more than one field gradient; by applying gradients about all three Cartesian axes a high level of randomization of coherence may be possible.

APPENDICES

APPENDIX A

Angular momentum operators for spin $\frac{1}{2}$ particles.

The z component of classical angular momentum $\underline{l}$ may be expressed in terms of the components of linear motion P_x, P_y,

$$\hat{l}_z = xP_y - yP_x$$

Substituting the operators for P_y and P_x leads to the operator for $\hat{l}_z$,

$$\hat{l}_z = -i\hbar\, x\frac{\delta}{\delta y} - y\frac{\delta}{\delta x}$$

Corresponding definitions exist for the operators for $\hat{l}_x$ and $\hat{l}_y$; the three operators satisfy the commutation rules,

$$\left[\hat{l}_i, \hat{l}_j\right] = i\hbar\, \hat{l}_k \qquad \text{where i, j and k are cyclic permutations of x, y and z.}$$

Since the components of $\underline{\hat{l}}$ do not commute, only one component is defined; by convention this is $\hat{l}_z$.

$\underline{\hat{l}}$ and $\hat{l}_z$ do not commute, but $\hat{l}^2$ does commute with $\hat{l}_z$ and so the magnitude of the angular momentum is defined. For a spin $\frac{1}{2}$ nucleus $\hat{l}^2$ has the eigenvalue $\frac{1}{2}\left(1 + \frac{1}{2}\right)\hbar^2$ which implies the matrix representation,

$$l^2 = \frac{3}{4}\hbar^2\begin{bmatrix}1 & 0\\ 0 & 1\end{bmatrix}$$

In the eigenbasis of the $\hat{l}_z$ operator. This will act on an α state $\begin{bmatrix}1\\0\end{bmatrix}$ or a β state $\begin{bmatrix}0\\1\end{bmatrix}$ to give the value $\frac{3}{4}\hbar^2$.

For $\hat{l}_z$ the matrix representation is $\frac{\hbar}{2}\begin{bmatrix}1 & 0\\ 0 & -1\end{bmatrix} = \hbar\, I_z$

Similarly, $\hat{l}_x = \frac{\hbar}{2}\begin{bmatrix} 0 & 1 \\ 1 & 0 \end{bmatrix} = \hbar I_x$, $\hat{l}_y = \frac{\hbar}{2}\begin{bmatrix} 0 & -i \\ i & 0 \end{bmatrix} = \hbar I_y$

Where I_x, I_y and I_z are the Pauli spin matrices (44) for spin angular momentum about the x, y and z axes respectively. The operator $e^{-i\psi I_d}$ (where d = x, y, z) generates a rotation of ψ radians about the d axis. For example, the transformation of an operator Ω with respect to $e^{i\pi I_x}$ will cause a rotation of Ω about the x axis, the rotation angle is π radians. For $\Omega = I_y$ it can be seen that,

$$e^{-i\pi I_x} \; I_y \; e^{i\pi I_x} = -I_y$$

This is an example of a similarity transform (98).

Two other operators, the 'shift operators', may be defined

$$\hat{l}^+ = \hat{l}_x + i\hat{l}_y$$

$$\hat{l}^- = \hat{l}_x - i\hat{l}_y$$

The corresponding Pauli matrices are,

$$I^- = \begin{bmatrix} 0 & 0 \\ 1 & 0 \end{bmatrix} \qquad I^+ = \begin{bmatrix} 0 & 1 \\ 0 & 0 \end{bmatrix}$$

$\hat{l}^+$ and $\hat{l}^-$ have the effect of raising or lowering the z component of angular momentum of a state by one unit and are termed the raising and lowering operators respectively. Since the magnitude of l_z is limited, in that its magnitude may not exceed l, there must exist maximum and minimum values of l_z. The action of the shift operators on these states is shown below,

$$l^+|l, l_z max\rangle = 0$$

$$l^-|l, l_z max\rangle = 0$$

The action of the shift operators on the spin states (α and β) of a spin-$\frac{1}{2}$ nucleus can be seen by considering the product of the Pauli matrix with the spin state matrix.

$$I^+|\beta\rangle = \hbar|\alpha\rangle \quad \underset{\hat{I}^+}{\begin{bmatrix}0 & 1\\ 0 & 0\end{bmatrix}} \underset{\beta}{\begin{bmatrix}0\\ 1\end{bmatrix}} = \underset{\alpha}{\begin{bmatrix}1\\ 0\end{bmatrix}}$$

$$I^-|\beta\rangle = 0 \quad \underset{\hat{I}^-}{\begin{bmatrix}0 & 0\\ 1 & 0\end{bmatrix}} \underset{\beta}{\begin{bmatrix}0\\ 1\end{bmatrix}} = \begin{bmatrix}0\\ 0\end{bmatrix}$$

$$I^+|\alpha\rangle = 0 \quad \underset{\hat{I}^+}{\begin{bmatrix}0 & 1\\ 0 & 0\end{bmatrix}} \underset{\alpha}{\begin{bmatrix}1\\ 0\end{bmatrix}} = \begin{bmatrix}0\\ 0\end{bmatrix}$$

$$I^-|\alpha\rangle = \hbar|\beta\rangle \quad \underset{\hat{I}^-}{\begin{bmatrix}0 & 0\\ 1 & 0\end{bmatrix}} \underset{\alpha}{\begin{bmatrix}1\\ 0\end{bmatrix}} = \underset{\beta}{\begin{bmatrix}0\\ 1\end{bmatrix}}$$

APPENDIX B

The enclosed FORTRAN program (rear cover) simulates the action of N.M.R. pulse sequences by density matrix calculation. The subroutine HAM reads in the data specifying the spin system, and constructs the matrix representation, H, of the free-precession Hamiltonian in the product basis. This Hamiltonian includes terms for the chemical shifts and scalar coupling (equation [2.14]). So that the X approximation may be applied each nucleus is given an isotope number in the input data; if the X approximation is used, the off-diagonal matrix elements of H are set to zero for scalar couplings between nuclei of differing isotope numbers. Diagonalization of H is carried out by a NAG routine called by the subroutine DIAG. The eigenvectors of this matrix are used in transformations between the product basis and the free-precission eigenbasis; the eigenvalues are used to calculate the resonance frequencies of transitions in the final spectrum, these frequencies are contained in the array ENE.

The subroutine BASIS expands spin operators into the product basis of all nuclei other than those of a selected isotope number. In this way selective and non-selective operators can easily be created for the spin system. The action of this subroutine is to take the operator appropriate to each nucleus and to expand it into the relevant product basis, the sum of these expanded operators then describes the operator for the system of nuclei, I_s (99). The operator for an N spin system is given by $I_s = \Pi_m^N 1_{(m-1)} I_m 1_{(N-m)}$, where 1_p is a unit matrix of size p, and I_m is the spin operator for the m^{th} nucleus.

The subroutine BASIS is used to set up the polarization at the start of the experiment, the operator I_z being expanded into the appropriate product basis. Similarly the operators I_x and I_y are expanded into the appropriate basis for the construction of pulses.

EFFECT carries out the action of an element of a pulse sequence. It first constructs the Hamiltonian which is effective during the pulse sequence element; for a period of free precession this will simply be the Hamiltonian H, for a pulse the Hamiltonian must include terms in $\gamma B_1 I_s$. In addition to the duration of the pulse sequence element, four parameters may be passed to the subroutine effect, two operators I_s and I_s' and the corresponding values γB_1 and $\gamma B_1'$. It is therefore possible to simulate the simultaneous application of different pulses to two different groups of nuclei. The full Hamiltonian is then diagonalized and the appropriate exponential operator constructed (see Chapter 2). To simulate evolution under the Hamiltonian the matrix representing the spin system is then transformed by the exponential operator.

The subroutine EFFECT is used several times in order to build up the pulse sequence, the form of the resulting spectrum can be found by examining the matrix representation of the spin system after the last application of EFFECT. To find the intensity of a particular observable the relevant spin operator, I_x, I_y or I_p is expanded into the product basis of the observed nuclear species to give the matrix OBS. Both OBS and SYS are then transformed into the free-precession basis and passed to the subroutine RES. Multiplication and corresponding elements in OBS and SYS gives a matrix containing the intensities of observable transitions in the spectrum; elements with the

same frequency are combined and the intensities and frequencies of the transitions are output.

For the simulation of NEMESIS, BASIS is used initially to expand I_z into the proton product basis; no X spin polarization is initialized, so no phase cycling to remove this is needed. After the first polarization transfer step the subroutine PBYP simulates a randomization scheme. All elements of the array MOSK are set to zero except for those corresponding to the desired orders of coherence; multiplication of the corresponding elements of the two arrays therefore retains the desired elements of SYS while setting the others to zero. A second polarization step, back to the I spins, is then simulated. For each increment in the delay TTIME (which corresponds to the refocussing delay of an INEPT sequence) a full simulation of the sequence is carried out and the total I spin signal found using the subroutine PBYP; in addition the intensity expected from equation [5.2] is calculated by subroutine PREDMG. At the end of the simulation the two sets of intensities are each normalized and the resulting intensities plotted by the subroutine PLOUT.

APPENDIX C

The PASCAL source codes for the main pulse sequences used in this thesis are shown on the following pages.

The parameters for the HICCUP sequence (Hydrogen-Intensified Carbon CoUPlings) are as follows:

JCH the value of the heteronuclear one-bond scalar coupling constant.

PP the proton 90° pulse width.

CHN a parameter set according to the multiplicity of the site of interest.

JCC the value of the homonuclear scalar coupling constant.

HMSD duration of the homospoil delay at the start of each transient.

MULT a parameter used to scale the initial delay of the polarization sequence.

For the X nucleus calibration sequence:

PP the proton 90° pulse width.

J the value of the heteronuclear scalar coupling constant.

TPF parameter which determines the form of calibration curve obtained.

For the NEMESIS sequence (NMR Enhanced Measurement Entailing Successive INEPT Sequences):

BP randomization pulse.

PP1 proton 90° pulse width.

HMSD duration of homospoil delay in randomization sequence.

D3, D4, D5, D6 delays for evolution under scalar coupling.

PHASE parameter to allow generation of phase sensitive spectra.

```
"HICCUP"
PROCEDURE PULSESEQUENCE;
VAR PS,PP,TAU,MULT,JCH,JCC,CHN,HMSD,DL1,DL2,DL3:REAL;
BEGIN
GETVAL(JCH,'JCH    ');
GETVAL(PP,'PP     ');
GETVAL(CHN,'CHN    ');
GETVAL(JCC,'JCC    ');
GETVAL(HMSD,'HMSD   ');
GETVAL(MULT,'MULT   ');
DL1:=MULT*(0.25/JCH)-ROF1-ROF2;
PS:=3.0*PW;
IF (TRUNC(CHN)=0) THEN DL2:=0.3/JCH;
IF (TRUNC(CHN)=1) THEN DL2:=0.5/JCH;
IF (TRUNC(CHN)=2) THEN DL2:=0.25/JCH;
IF (TRUNC(CHN)=3) THEN DL2:=0.17/JCH;
DL2:=DL2-ROF2;
TAU:=(0.25/JCC)-ROF1-ROF2;
HLV(CT,V1);
HLV(V1,V1);
HLV(V1,V3);
MOD4(V3,V3);
DBL(V1,V1);
ADD(OPH,V1,V2);
MOD2(CT,V4);
DBL(V4,V4);
ADD(V4,V1,V1);
STATUS(A);
PULSE(PS,ZERO);
PULSE(PS,ONE);
HSDELAY(HMSD);
DECPHASE(V1);
DELAY(D1);
DECPULSE(PP,V1);
DELAY(DL1);
SIMPULSE(2.0*PW,2.0*PP,V3,OPH,ROF1,ROF2);
DELAY(DL1);
SIMPULSE(PW,PP,V2,ONE,ROF1,ROF2);
DELAY(DL2);
STATUS(B);
DELAY(TAU-DL2);
PULSE(2.0*PW,V2);
DELAY(TAU);
PULSE(PW,V2);
STATUS(C);
DECPHASE(ZERO);
END;
```

```
"SEQUENCE FOR THE CALIBRATION OF X NUCLEUS
COIL"
PROCEDURE PULSESEQUENCE;
VAR D3,J,PP,TPF:REAL;
BEGIN
    GETVAL(PP,'PP     ');
    GETVAL(J,'J      ');
    GETVAL(TPF,'TPF    ');
"TPF = 1 GIVES 1-COS(2*THETA) DEPENDENCE
  NULL AT THETA = 180 DEGREES
 TPF = 2 GIVES COS(THETA)-COS(3*THETA) DEPENDENCE
  CHANGE OF SIGN AT THETA = 90 DEGREES"
    D3:=(0.5/J);
SUB(ZERO,OPH,V10);
MOD4(V10,V10);
HLV(CT,V1);
HLV(V1,V1);
DBL(V1,V1);
MOD4(V1,V1);
    STATUS(A);
    DELAY(D1);
    STATUS(B);
      DECPULSE(PP,V10);
      DELAY(D3-ROF2);
PULSE(PW,ZERO);
DECPULSE(2.0*PP,ZERO);
PULSE(TPF*PW,V1);
     DELAY(D3-ROF1);
     DECPHASE(ZERO);
ADD(OPH,V1,OPH);
MOD4(OPH,OPH);
    STATUS(C);
END;
```

```
"NEMESIS"
PROCEDURE PULSESEQUENCE;
VAR ZP,PP1,D3,D4,D5,D6,BP,HMSD,PHASE:REAL;
BEGIN
GETVAL(BP,'BP     ');
GETVAL(PP1,'PP1    ');
GETVAL(HMSD,'HMSD   ');
GETVAL(D3,'D3     ');
GETVAL(D4,'D4     ');
GETVAL(D5,'D5     ');
GETVAL(D6,'D6     ');
GETVAL(PHASE,'PHASE ');
ZP:=0.0;
D3:=D3-2.0*ROF1-2.0*ROF2;
D4:=D4-2.0*ROF1-2.0*ROF2;
D5:=D5-2.0*ROF1-2.0*ROF2;
D6:=D6-2.0*ROF1-2.0*ROF2;
STATUS(A);
DECPHASE(ZERO);
HLV(CT,V1);
HLV(V1,V1);
HLV(V1,V3);
MOD2(V1,V1);
DBL(V1,V1);
MOD4(V1,V1);
ADD(ONE,V1,V2);
MOD2(CT,V6);
DBL(V6,V6);
HLV(V3,V5);
HLV(V5,V4);
MOD2(V3,V3);
DBL(V3,V3);
MOD2(V5,V5);
DBL(V5,V5);
ADD(V5,ONE,V5);
MOD2(V4,V7);
DBL(V7,V7);
ADD(V7,V5,V4);
ADD(V4,OPH,V4);
ADD(ONE,V7,V8);
MOD4(V1,V1);
MOD4(V2,V2);
MOD4(V6,V6);
MOD4(V3,V3);
MOD4(V7,V7);
MOD4(V4,V4);
MOD4(V8,V8);
MOD4(V5,V5);
DELAY(D1);
SIMPULSE(ZP,PP1,ONE,V1,ROF1,ROF2);
DELAY(D3/2.0);
SIMPULSE(2.0*PW,2.0*PP1,V6,V1,ROF1,ROF2);
DELAY(D3/2.0);
SIMPULSE(PW,PP1,V1,ONE,ROF1,ROF2);
DELAY(D4/2.0);
SIMPULSE(2.0*PW,2.0*PP1,V6,V3,ROF1,ROF2);
DELAY(D4/2.0);
SIMPULSE(PW,ZP,ONE,ONE,ROF1,ROF2);
"RANDOMISATION DELAY"
HSDELAY(HMSD);
DECPULSE(BP,ZERO);
DECPULSE(1.5*BP,ONE);
DECPHASE(ZERO);
IF TRUNC(PHASE)=1 THEN SIMPULSE(PW,ZP,V7,ONE,ROF1,ROF2)
 ELSE SIMPULSE(PW,ZP,V8,ONE,ROF1,ROF2);
STATUS(B);
DECPULSE(D2,ZERO);
STATUS(A);
DECPHASE(ZERO);
DELAY(D5/2.0);
SIMPULSE(2.0*PW,2.0*PP1,V6,V3,ROF1,ROF2);
DELAY(D5/2.0);
SIMPULSE(PW,PP1,V5,V4,ROF1,ROF2);
DELAY(D6/2.0);
SIMPULSE(2.0*PW,2.0*PP1,V6,V4,ROF1,ROF2);
DELAY(D6/2.0+ROF1);
DECPHASE(ZERO);
STATUS(C);
END;
```

REFERENCES

1. F. Bloch, W.W. Hansen, and M. Packard, Phys.Rev., 69, 127 (1946)
2. E.M. Purcell, H.C. Torrey, and R.V. Pound, Phys.Rev., 69, 37 (1946)
3. R.R. Ernst and W.A. Anderson, Rev.Sci.Instrum., 37, 93 (1966)
4. G.A. Morris, Magn.Reson.Chem., 24, 371 (1986)
5. G.A. Morris and R. Freeman, J.Am.Chem.Soc., 101, 760 (1979)
6. G.A. Morris, in 'Topics in Carbon-13 NMR Spectroscopy', Vol.4, Ed. G.C. Levy, Wiley, 1984
7. D.M. Doddrell, D.T. Pegg, and M.R. Bendall, J.Magn.Reson., 48, 323 (1982)
8. J. Kowalewski and G.A. Morris, J.Magn.Reson., 47, 311 (1982)
9. O.W. Sørensen, R. Freeman, T. Frenkiel, T.H. Mareci, and R. Schuck, J.Magn.Reson., 46, 180 (1982)
10. J. Jeener, Ampere International Summer School, Basko Polje, Yugoslavia, 1971
11. A. Bax, 'Two-Dimensional Nuclear Magnetic Resonance in Liquids', Delft University Press (1982)
12. G. Bodenhausen and D.J. Ruben, Chem.Phys.Lett., 69, 185 (1980)
13. L. Mueller, J.Am.Chem.Soc., 101, 4481 (1979)
14. A. Minoretti, W.P. Aue, M. Reinhold, and R.R. Ernst, J.Magn.Reson., 40, 175 (1980)
15. A.G. Redfield, Chem.Phys.Lett., 69, 537 (1983)
16. M.F. Roberts, D.A. Vidusek, and G. Bodenhausen, FEBS Letters, 117, 311 (1980)
17. D.A. Vidusek, M.F. Roberts, and G. Bodenhausen, J.Am.Chem.Soc., 104, 5452 (1982)
18. V. Sklenář and A. Bax, J.Magn.Reson., 71, 379 (1987)
19. M.F. Summers, L.G. Marzilli, and A. Bax, J.Am.Chem.Soc., 108, 4285 (1986)
20. A. Bax and M.F. Summers, J.Am.Chem.Soc., 108, 2093 (1986)
21. R. Benn and C. Brevard, J.Am.Chem.Soc., 108, 5622 (1986)

22. D. Live, I.M. Armitage, D.C. Dalgarno, and D. Cowburn, J.Am.Chem.Soc., 107, 1775 (1985)

23. D.H. Live, C.L. Kojiro, D. Cowburn, and J.L. Markley, J.Am.Chem.Soc., 107, 3043 (1985)

24. J.D. Otvos, H.R. Engeseth, and S. Wehrli, J.Magn.Reson., 61, 579 (1985)

25. M.H. Frey, G. Wagner, M. Vašák, O.W. Sørensen, D. Neuhaus, E. Wörgötter, J.H.R. Kägi, R.R. Ernst, and K. Wüthrich, J.Am.Chem.Soc., 107, 6847 (1985)

26. A. Bax, R.H. Griffey, and B.L. Hawkins, J.Magn.Reson., 55, 301 (1983)

27. A. Bax, R.H. Griffey, and B.L. Hawkins, J.Am.Chem.Soc., 105, 7188 (1983)

28. R.H. Griffey, C.D. Poulter, A. Bax, B.L. Hawkins, Z. Yamaizumi, and S. Nishimura, Proc.Natl.Acad.Sci.USA, 80, 5895 (1983)

29. M.J. Bogusky, P. Tsang, and S.J. Opella, Biochem.and Biophys. Res.Comm., 127, 540 (1985)

30. G. Ortiz-Polo, R. Krishnamoorthi, J.L. Markley, D.H. Live, D.G. Davis, and D. Cowburn, J.Magn.Reson., 68, 303 (1986)

31. D.H. Live, D.G. Davis, W.C. Agosta, and D. Cowburn, J.Am.Chem.Soc., 106, 6104 (1984)

32. A. Bax and S. Subramanian, J.Magn.Reson., 67, 565 (1986)

33. R.H. Griffey, A.G. Redfield, R.E. Loomis, and F.W. Dahlquist, Biochemistry, 24, 817 (1985)

34. U. Hahn, R. Desai-Hahn, and H. Rüterjans, Eur.J.Biochem., 146, 705 (1985)

35. L. Mueller, R.A. Schiksnis, and S.J. Opella, J.Magn.Reson., 66, 379 (1986)

36. H. Kessler, W. Bermel, and C. Griesinger, J.Magn.Reson., 62, 573 (1985)

37. A. Abragam, 'The Principles of Nuclear Magnetism', Oxford University Press (1962)

38. O.W. Sørensen, G.W. Eich, M.H. Levitt, G. Bodenhausen, and R.R. Ernst, Prog.in NMR Spect., 16, 163 (1983)

39. R.K. Harris, 'Nuclear Magnetic Resonance Spectroscopy', Pitman (1983)

40. A. Bax, R. Freeman, and G.A. Morris, J.Magn.Reson., 42, 164 (1981)

41. J. Keeler and D. Neuhaus, J.Magn.Reson., 63, 454 (1985)

42. H.D.W. Hill and R.E. Richards, J.Sci.Instrum., 1, 977 (1968)

43. D.I. Hoult and R.E. Richards, J.Magn.Reson., 24, 71 (1976)

44. R.R. Ernst, G. Bodenhausen, and A. Wokaun, 'Principles of Nuclear Magnetic Resonance in One and Two Dimensions', Oxford (1987)

45. W.P. Aue, P. Bachmann, A. Wokaun, and R.R. Ernst, J.Magn.Reson., 29, 523 (1978)

46. D.P. Burum and R.R. Ernst, J.Magn.Reson., 39, 163 (1980)

47. D.M. Doddrell, H. Bergen, D. Thomas, D.T. Pegg, and M.R. Bendall, J.Magn.Reson., 40, 591 (1980)

48. P.H. Bolton, J.Magn.Reson., 41, 287 (1980)

49. O.W. Sørensen and R.R. Ernst, J.Magn.Reson., 51, 477 (1983)

50. K.V. Schenker and W. von Philipsborn, J.Magn.Reson., 61, 294 (1985)

51. G. Bodenhausen, H. Kogler, and R.R. Ernst, J.Magn.Reson., 58, 370 (1984)

52. A. Bax, R. Freeman, and S.P. Kempsell, J.Am.Chem.Soc., 102, 4849 (1980)

53. A. Bax, R. Freeman, and S.P. Kempsell, J.Magn.Reson., 41, 349 (1980)

54. A. Bax, R. Freeman, T.A. Frenkiel, and M.H. Levitt, J.Magn.Reson., 43, 478 (1981)

55. A. Bax, R. Freeman, and T.A. Frenkiel, J.Am.Chem.Soc., 103, 2102 (1981)

56. S.W. Sparks and P.D. Ellis, J.Magn.Reson., 62, 1 (1985)

57. C.S. Schneider and K.H. Pook, J.Chem.Soc., Perkin Trans., 877 (1986)

58. K.S. Lee and G.A. Morris, J.Magn.Reson., 70, 332 (1986)

59. H. Kessler, W. Bermel, C. Griesinger, P. Hertl, E. Streich, and A. Rieker, J.Org.Chem., 51, 596 (1986)

60. H. Kessler, C. Griesinger, J. Zarbock, and H.R. Loosli, J.Magn.Reson., 57, 331 (1984)

61. G.A. Morris and M.J. Toohey, J.Magn.Reson., 63, 629 (1985)

62. H. Kogler, O.W. Sørensen, G. Bodenhausen, and R.R. Ernst, J.Magn.Reson., 55, 157 (1983)

63. K.S. Lee and G.A. Morris, Magn.Reson.Chem., 25, 176 (1987)

64. D.L. Turner, Molec.Phys., 44, 1051 (1981)

65. D.J. States, R.A. Haberkorn, and D.J. Ruben, J.Magn.Reson., 48, 286 (1982)

66. A. Bax, R. Freeman, and G.A. Morris, J.Magn.Reson., 43, 333 (1981)

67. R. Freeman, T.H. Mareci, and G.A. Morris, J.Magn.Reson., 42, 341 (1981)

68. N.C. Nielsen, H. Bildsøe, H.J. Jakobsen, and O.W. Sørensen, J.Magn.Reson., 66, 456 (1986)

69. M. Bergmann and L. Zervas, Bergichte der Deutschen Chem.Gesellsch, 65, 1192 (1932)

70. A. Vogel, 'Vogel's Textbook of Practical Organic Chemistry', Longman (1978)

71. M.D. Sauzade and S.K. Kan, Advances in Electronics and Electron Physics, 34, 1 (1973)

72. J.C. Lindon and A.G. Ferrige, Prog.NMR Spect., 14, 27 (1980)

73. W.P. Aue, E. Bartholdi, and R.R. Ernst, J.Chem.Phys., 64, 2229 (1976)

74. R.H. Griffey, D. Davis, Z. Yamaizumi, S. Nishimura, A. Bax, B. Hawkins, and C.D. Poulter, J.Biol.Chem., 260, 9734 (1985)

75. D.R. Davis, R.H. Griffey, Z. Yamaizumi, S. Nishimura, and C.D. Poulter, J.Biol.Chem., 261, 3584 (1986)

76. P. Plateau and M. Gueron, J.Am.Chem.Soc., 104, 7310 (1982)

77. M.R. Bendall, D.T. Pegg, and D.M. Doddrell, J.Magn.Reson., 45, 8 (1981)

78. D. Neuhaus, J. Keeler, and R. Freeman, J.Magn.Reson., 61, 553 (1985)

79. E.M. Krauss and S.I. Chan, J.Am.Chem.Soc., 104, 6953 (1982)

80. D.H. Live, D.G. Davis, W.C. Agosta, and D. Cowburn, J.Am.Chem.Soc., 106, 1939 (1984)

81. D.T. Pegg, M.R. Bendall, and D.M. Doddrell, J.Magn.Reson., 49, 32 (1982)

82. R.E.D. McClung and B.K. John, J.Magn.Reson., 59, 20 (1984)

83. D.M. Doddrell, G.J. Galloway, W.M. Brooks, J. Field, J.M. Bulsing, M.G. Irving, and H. Baddeley, J.Magn.Reson., 70, 176 (1986)

84. I.D. Campbell, C.M. Dobson, G. Jeminet, and R.J.F. Williams, FEBS Letters, 49, 115 (1974)

85. M. Gochin, D.P. Weitekamp, and A. Pines, J.Magn.Reson., 63, 431 (1985)

86. M. Gochin and A. Pines, J.Am.Chem.Soc., 107, 7193 (1985)

87. A.J. Shaka, J.Keeler, T. Frenkiel, and R. Freeman, J.Magn.Reson., 52, 335 (1983)

88. D. Brühwiler and G. Wagner, J.Magn.Reson., 69, 546 (1986)

89. P.H. Bolton, J.Magn.Reson., 62, 143 (1985)

90. L. Lerner and A. Bax, J.Magn.Reson., 69, 375 (1986)

91. L.D. Field and B.A. Messerle, J.Magn.Reson., 66, 483 (1986)

92. D. Marion, C. Garbay-Jaureguiberry, and B.P. Roques, J.Am.Chem.Soc., 104, 5573 (1982)

93. V. Sklenář, D. Torchia, and A. Bax, J.Magn.Reson., 73, 375 (1987)

94. L.E. Kay, T.L. Jue, B. Bangerter, and P.C. Demou, J.Magn.Reson., 73, 558 (1987)

95. V.F. Bystrov, Prog.N.M.R. Spect., 10, 41 (1976)

96. Varian trade literature (1987)

97. Bruker trade literature (1987)

98. P.L. Corio, 'The Structure of High Resolution N.M.R. Spectra', Academic Press (1966)

99. P.D. Buckley, K.W. Jolley, and D.N. Pinder, Prog.N.M.R. Spect., 10, 1 (1975)